Anal. Methods Environ. Chem. J. 7 (2) (2024) 5-17

AMECJ

Research Article, Issue 2
Analytical Methods in Environmental Chemistry Journal
Journal home page: www.amecj.com/ir

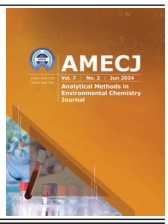

Adsorption of methylene blue into modified mesoporous silica from palm oil boiler ash

Shinta Ayu Kusumaningtyas[a], Dwi Siswanta[a], and Adhitasari Suratman[a,*]
[a] *Department of Chemistry, Faculty of Mathematics and Natural Sciences, Universitas Gadjah Mada, Sekip Utara, Yogyakarta 55281, Indonesia*

ARTICLE INFO:
Received 2 March 2024
Revised form 25 Apr 2024
Accepted 22 May 2024
Available online 29 Jun 2024

Keywords:
Modified mesoporous silica
Adsorption
Palm oil boiler ash
Methyl ester sulfonate
Methylene blue
UV-Vis spectrophotometer

ABSTRACT
The adsorption of methylene blue dye on modified mesoporous silica based on palm oil boiler ash (MS-POBA) as an adsorbent with a methyl ester sulfonate (MES) was investigated. MS-POBA and MES as a template improved the adsorption capacity of methylene blue by increasing the pore size of boiler ash silica. The characteristics of the material were determined using FTIR, XRD, BET, and SEM-EDX analyzers. The adsorption of methylene blue on the MS-POBA adsorbent was determined using a UV-Vis spectrophotometer. The MES as a template pasted to MS-POBA, could be increased surface area, pore diameter, and volume. In optimized conditions, pH, the adsorbent mass, the adsorption time, the methylene blue concentration, the adsorption capacity, and recovery were obtained at 7.0, 0.03 g, 45 minutes, 20 mg L^{-1}, 15.578 mg g^{-1}, and 96.9%, respectively. The adsorption of methylene blue on boiler ash silica with an MES template follows the pseudo-second-order kinetic model with a value of $R^2 = 0.999$ and Langmuir isotherm adsorption model.

1. Introduction

Indonesia has a large distribution of palm oil-producing factories that sustainably produce palm oil, including the Sumatra and Kalimantan provinces [1]. For this reason, it is necessary to utilize waste properly and optimally from palm oil mills as well as solid waste in the form of biomass, namely empty fruit bunches, fiber, and shells. Several potential uses exist for palm oil waste biomass in Indonesia [2]. The fibers and shells as solid waste are commonly applied as boiler fuel to create heat and mechanical power in palm oil processing. The problem that arises is the residual combustion in the boiler in the form of shell ash, which is disposed of as solid waste and causes disruption to the environment and health. Boiler ash contains 40.60% SiO_2, 19.60% CaO, and 3.71% Al_2O_3 [3]. The potential of boiler ash to produce silica (SiO_2) depends on the number of silica and the application for industry, such as catalysts, adsorbents, and filter media. Silica has different pore sizes, surface areas, particle sizes, and pore volumes. The addition of a template can modify the pore size of silica [4]. Mesoporous silica synthesis is carried out by adding an organic compound, one being a surfactant, and then the calcination process is carried out to remove the surfactant [5]. Mesoporous silica can be used in adsorption because it has high thermal stability, large pore volume, small pore diameter distribution, and high surface area [6]. Templates are structure-directing agents used to create hollow porous structures, where the gap in silica will be filled by the template, then after the template is removed, it allows for the formation of hollow

*Corresponding Author: Adhitasari Suratman
Email: adhitasari@ugm.ac.id
https://doi.org/10.24200/amecj.v7.i02.269

particles with newly created pores [7]. MES anionic surfactant was added as a template because it has several advantages: economical use, low toxicity, and rapid biodegradability [8]. MES is an environmentally friendly green surfactant, comes from renewable materials, can be decomposed naturally, is made from vegetable oil, is relatively stable at reservoir temperatures, has relatively low adsorption on reservoir rocks, and can be produced economically [9]. The alkyl chain length, the degree of surfactant ionization, and the ratio of co-structure-directing agent (CSDA) and surfactant contribute to the measurement of silica pores. MES is an anionic surfactant with a long alkyl surfactant chain that is important in determining the size of micelles and mesopores [10]. Industries that produce wastewater, such as textiles, paper, plastic, printing, food, and cosmetics, can cause environmental problems. One of them, serious attention, is to be focused on the removal/separation of the coloring components from wastewater. The available methods for removing dyes from wastewater are adsorption, membrane separation, coagulation, electrochemical processes, reverse osmosis, chemical oxidation, and aerobic and anaerobic microbial degradation of dye components [11]. In this research, the adsorption method was chosen because adsorption effectively reduces negative environmental due to pollutants such as metals, dyes, and organic substances. It is environmentally friendly, simple, and relatively inexpensive [12]. Environmental impact, economic profit, and adsorption efficiency are the main parameters when selecting adsorbents. Various adsorbents derived from agricultural residues and industrial wastes have been used to remove various hazardous components from wastewater. Synthesis of modified adsorbent has been widely carried out to match the substance to be separated so that the adsorption process is more effective and efficient in its use [13,14,15]. However, the intensive power requirements, the evolution of toxic by-products, and the high cost make most methods less feasible in large-scale plants for removing dye components from wastewater [16]. Dye waste can cause harmful effects and can also endanger health if the waste is immediately disposed of without any prior processing. Methylene blue is widely found in wastewater. Methylene blue is a cationic dye with a heterocyclic aromatic chemical compound structure. Methylene blue dye influences the environment due to its highly toxic effects and is carcinogenic [17]. Methylene blue is allowed in the water at a 5–10 mg L^{-1} concentration. The Declare of the Environment Minister of the Republic of Indonesia (KEP-51/MENLH/10/1995) concerns the quality standards of industrial wastewater [18]. Also, nanotechnology methods were used to remove organic materials from different samples [19-21]. Methylene blue is a hazardous waste. One of the waste treatments in the aquatic environment is by adsorption using solid waste from palm oil mills, namely burning coconut shells, which produce boiler ash.

Increasing the pore size of boiler ash silica using the MES template was investigated. This research prepared mesoporous silica from palm oil boiler ash (MS-POBA) as an adsorbent through a simple method of microemulsion polymerization. Initially, MES as a templating agent was added during the synthesis of mesoporous silica, MES is kept in a silica framework and then calcinated to be removed. MS-POBA will provide an active site to improve the adsorption performance of methylene blue dye. Adsorption data will be explained based on the physicochemical properties of MS-POBA and methylene blue dye at equilibrium.

2. Material and Methods

2.1. Materials

The material used in this study was the boiler ash of the palm oil factory. Also, the reagents such as HCl (Merck, 6 M, CAS No.: 7647-01-0), NaOH (Merck, 6 M, CAS No.: 1310-73-2), Methyl Ester Sulfonate (MES, Sigma Aldrich, CAS No. 93348-22-2), 3-Aminopropyl Trimethoxysilane (APMS, Sigma Aldrich, CAS No.: 13822-56-5), and methylene blue dye (Merck, CAS No. 61-73-4) were prepared.

2.2. Instrument

The instruments include Fourier Transform Infrared Spectrophotometer (FTIR, 8201PC Shimadzu), X-Ray Diffraction (XRD, Bruker D8 Advance ECO), Brunaur, Emmet, and Teller (BET, Gemini VII Version 5.03 Serial 2037), Scanning Electron Microscopy-Energy Dispersive X-Ray (SEM-EDX, JEOL JSM-6510LA), and UV-Vis Spectrophotometer (Thermo Scientific Orion Aquamate 8100) were used. Also, a set of glassware, analytical balance, pH meter, filter paper and Whatman 42, 250 mesh sieve, porcelain cup, magnetic stirrer, hotplate, measuring flask, glass stirrer, thermometer, a set of tools for reflux, oven (Kirin KBO-190RAW), and furnace (Fisher Isotemp Muffle Furnace Model 184) were used.

2.3. Synthesis of Adsorbent

2.3.1.Boiler ash purification

Boiler ash from the palm oil factory was weighed, and 6 M HCl was added. The mixture was boiled at 110 °C for 3 hours and then was allowed to stand until it cooled down. The boiler ash was filtered using a vacuum filter and washed with distilled water until the neutral pH. The boiler ash was dried in an oven and then heated using a furnace. The boiler ash is cooled and weighed.

2.3.2.Extraction of Silica with NaOH

The purified ash was weighed at as much as 10 g and put into a beaker, and then 60 mL of NaOH 6 M was added. The mixture was heated while stirring, carried out with a stirrer until half of the initial volume evaporated. Then, it was allowed to stand at room temperature until it cooled down. The mixture was filtered with Whatman paper, taking a sodium silicate solution as a filtrate. The HCl (2 M) was added to the filtrate drop by drop until the pH was neutral and a white gel was formed. The sol-gel that has been formed is allowed to stand for 18 hours, or process aging was carried out so that the gel becomes mature and stiff. The solid precipitation product was washed with distilled water and filtered using a vacuum filter, then dried in an oven before the calcination process at a temperature of 500 °C.

2.3.3. Synthesis of MS-POBA

The synthesis of MS-POBA with a mesoporous structure was carried out by preparing solution A containing 0.98 g MES as a template, then adding 90 mL of distilled water and 9 mL of 0.1 M HCl. The solution was stirred at 40 °C for 1 hour. Solution B, which contained 2.4 g of silica, 5 mL of methanol, and 1.67 mL of APMS, was dissolved in 5 mL of methanol. Then, solution B was added to solution A, accompanied by stirring for 1 hour. Solutions A and B were refluxed at 70 °C for 5 hours. The solid precipitation product is washed with distilled water, then the solution is filtered, and the residue is rewashed with distilled water until the pH is neutral. After being neutral, the residue was dried in an oven at 90 °C for 12 hours. Then, it was calcined at 550, 750, and 950 °C to determine the optimum temperature.

2.4. Adsorption procedure

As Figure 1, the optimum pH condition was measured by preparing methylene blue solution with a concentration of 20 mg L^{-1} and then adjusting the pH solution to 4, 5, 6, 7, and 8. Each solution was added 0.05 g MS-POBA with and without the MES template, then stirred for 60 minutes. Then, it was filtered to separate the adsorbent and filtrate. The filtrate's absorbance was measured using a UV-Vis Spectrophotometer to determine the adsorption capacity of methylene blue into MS-POBA. The optimum mass of the adsorbent was carried out by adding methylene blue solution with a concentration of 20 mg L^{-1}, and the acidity level of the methylene blue solution was adjusted to the optimum pH. Then, MS-POBA with and without the MES template was added with masses of 0.01, 0.02, 0.03, 0.04, and 0.05 g. The stirring was carried out for 60 minutes, and then the mixture was filtered to separate the residue and the filtrate. The absorbance of the filtrate was measured using a UV-Vis Spectrophotometer and the adsorption capacity of methylene blue can be determined. Also, the adsorption contact time was determined by preparing 20 mg L^{-1} of methylene blue solution and MS-POBA with optimum mass by procedure.

The acidity level of the solution is adjusted at the optimum pH. The absorbance of the solution was measured with various contact times of 5, 15, 30, 45, 60, and 75 minutes. Furthermore, the adsorption capacity was obtained at each contact time. Determination of optimum Methylene Blue Concentration using the same procedure above at optimum pH, absorbent mass, and contact time was carried out. The initial Methylene Blue concentrations in the solution were 5, 10, 15, 20, 25, and 30 mg L^{-1}.

3. Result and Discussion

Due to the synthesis of the silica with the MES template, the boiler ash from the palm oil factory was purified using HCl to remove metal oxides and then extracted with NaOH. Using the sol-gel method, HCl was added to produce silica powder with Equation 1. Also, the silica structure is the interaction between sulfate ion, APMS, and silica which is shown in Figure 2. The interaction between MES, APMS, and silica sulfate ions shows that $–SO_3^-$ groups from MES and $–NH_3^+$ groups from APMS are involved in intermolecular interactions, determining the silica material's porous nature (Fig. 2).

$$SiO_{2(s)} + 2NaOH_{(aq)} \rightarrow Na_2SiO_{3\,(aq)} + H_2O_{(l)}$$
$$Na_2SiO_{3\,(aq)} + 2HCl_{(aq)} \rightarrow H_2SiO_{3(l)} + 2NaCl_{(aq)}$$
$$H_2SiO_{3(l)} \rightarrow SiO_2.H_2O_{(s)}$$

(Eq.1)

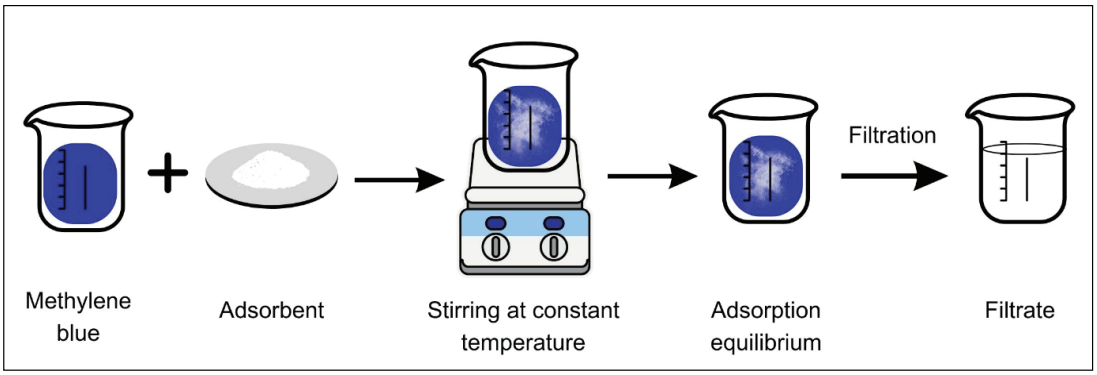

Fig. 1. Illustration of the adsorption mechanism

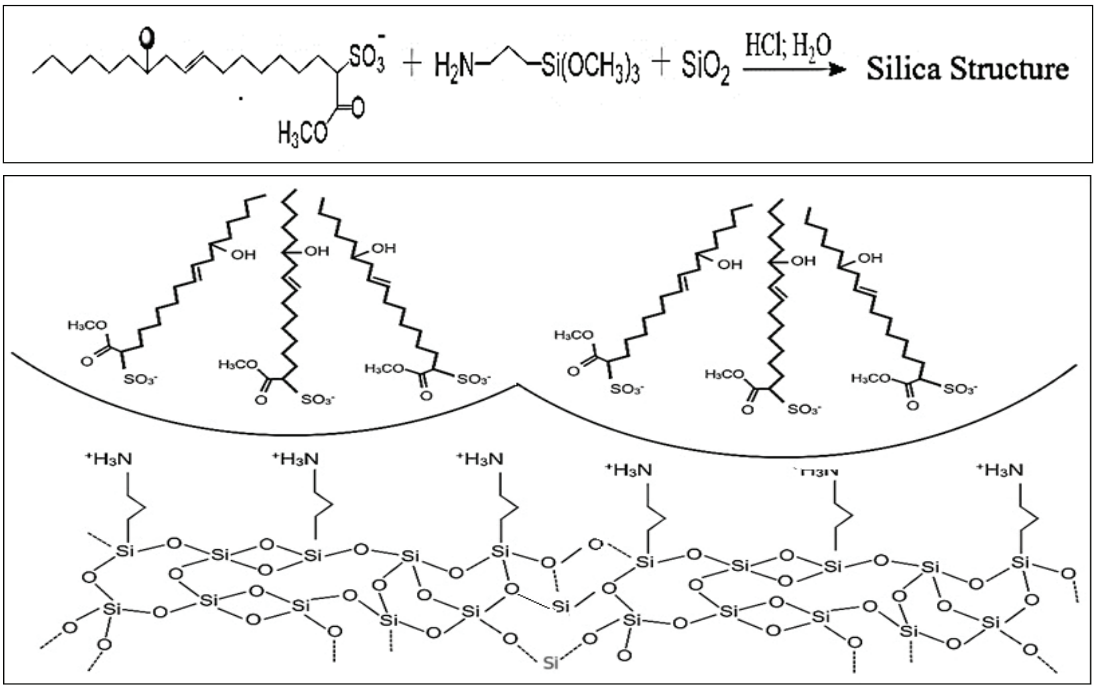

Fig. 2. Schematic of interaction between sulfate ion, APMS, and silica network

3.1. FT-IR Data

Fourier Transform Infra-Red (FT-IR) characterization aims to find out the functional groups of material. Infrared spectra of silica material without a template and modified silica with an MES template can be seen in Figure 3 and Table 1. MS-POBA has specific characters Si-OH and Si–O–Si, and MES have specific characters in the sulfonate group. The formation of a sulfonate group (S=O) is indicated by the peak of the wave number 1219–128 cm^{-1} [10]. Through the calcination process, MES is lost, and then modified mesoporous silica is formed. The absence of absorption at a wavenumber of 1226 cm^{-1} indicates the loss of sulfonate groups due to the calcination process.

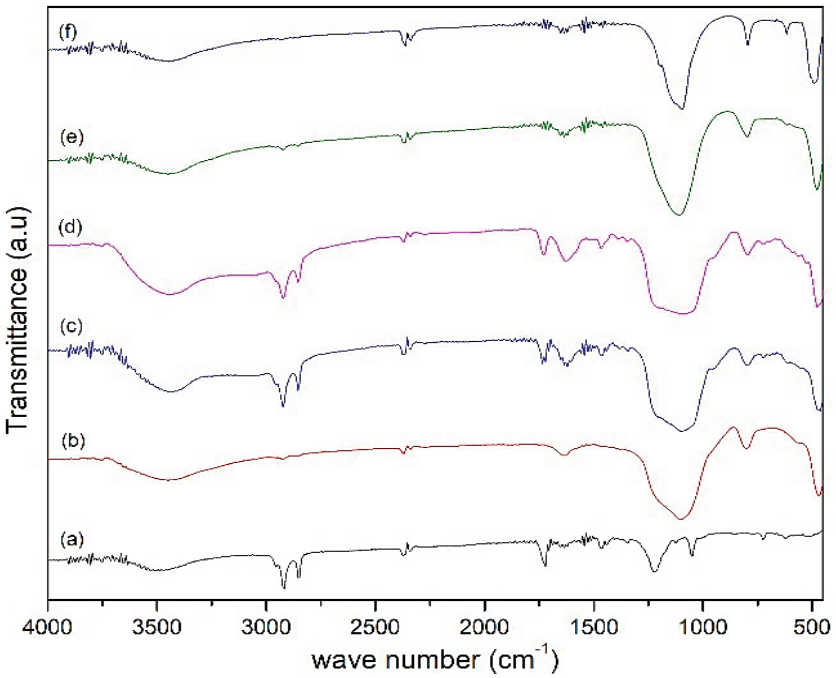

Fig. 3. FT-IR spectra of a) MES, b) MS-POBA, c) MS-POBA with MES template without calcination, d) MS-POBA with MES template (calcination temperature of 550 °C), e) MS-POBA with MES template (calcination temperature of 750 °C), f) MS-POBA with MES template (calcination temperature of 950 °C)

Table 1. Functional group and wave numbers by FTIR

Wave number	Functional groups
802	Si−O symmetric
1103	Si−O asymmetric
957	S=O symmetric
1211	S=O asymmetric
1620	N−H bending
2916−2854	C−H stretching
1620	O−H bending
3449−3749	O−H stretching

3.2. X-Ray Diffraction (XRD) Data

XRD was used to determine the phase on silica of the MS-POBA and MS-POBA with the MES template. Figure 4 (a) is a silica material without adding a template, showing the dominant form of a single phase in quartz (SiO_2) at $2\theta = 23.08^{o}$, and the material is amorphous silica. Figure 4 (c) and (d) are mesoporous silica materials with the addition of MES and the calcination temperature of 750 ºC and 950 ºC. This mesoporous silica was tall and sharp, indicating that the structure was crystalline. Higher temperatures can result in the growth of larger crystals. The adsorption of methylene blue in this research used an amorphous material that calcinated at a temperature of 550 °C.

3.3. Brunaur, Emmet, and Teller (BET) Data

Figure 5 shows the graph of the nitrogen adsorption-desorption isotherm of MS-POBA and MS-POBA using a MES template. According to the IUPAC classification, the pattern shows a Type IV isotherm that has a hysteresis loop in the middle region. This indicated the type of adsorption from the mesoporous category. Table 2 shows the characteristics of the MS-POBA surface. The addition of an MES template affects porosity and causes an increase in surface area, pore diameter, and volume.

3.4. Optimized of adsorption parameters

3.4.1.Effect of pH

Figure 6 shows the optimal pH at pH 7, indicated by an increase in adsorption capacity to pH 7 and decreases after that. The adsorbent surfaces of MS-POBA with MES template can undergo protonation under acidic conditions, producing a charge more positive. The more positive charge can reduce the surface ability of the adsorbent to interact with cationic methylene blue. The electrostatic attraction between methylene blue and the adsorbent surface can be reduced, resulting in a lower adsorption capacity. The higher the pH, the more adsorption capacity increases because more adsorbents are deprotonated to be negatively charged, so methylene blue is more electrostatically adsorbed and optimally at pH 7.

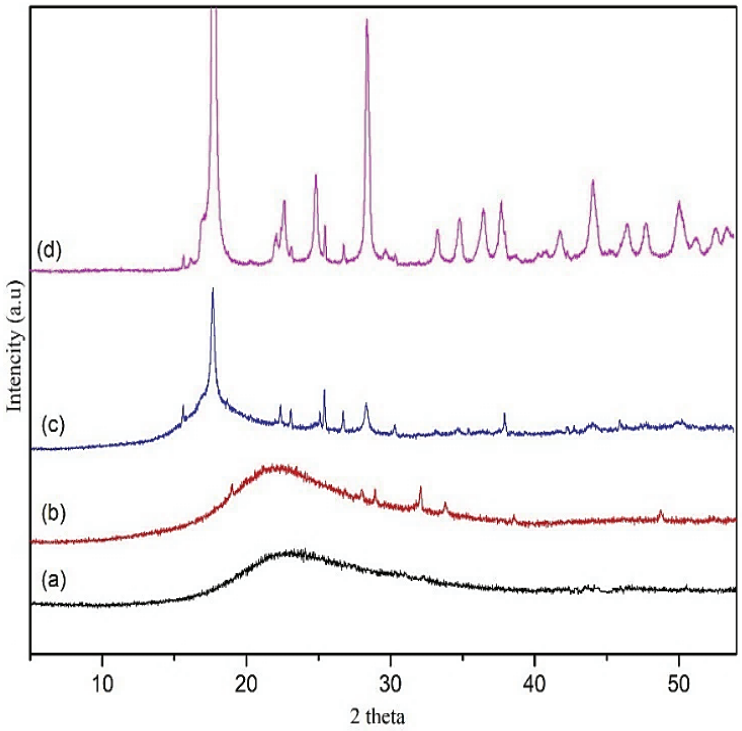

Fig. 4. The diffractogram of MS-POBA
a) without template, b) calcination temperature of 550 °C, c) 750 °C and d) 950 °C

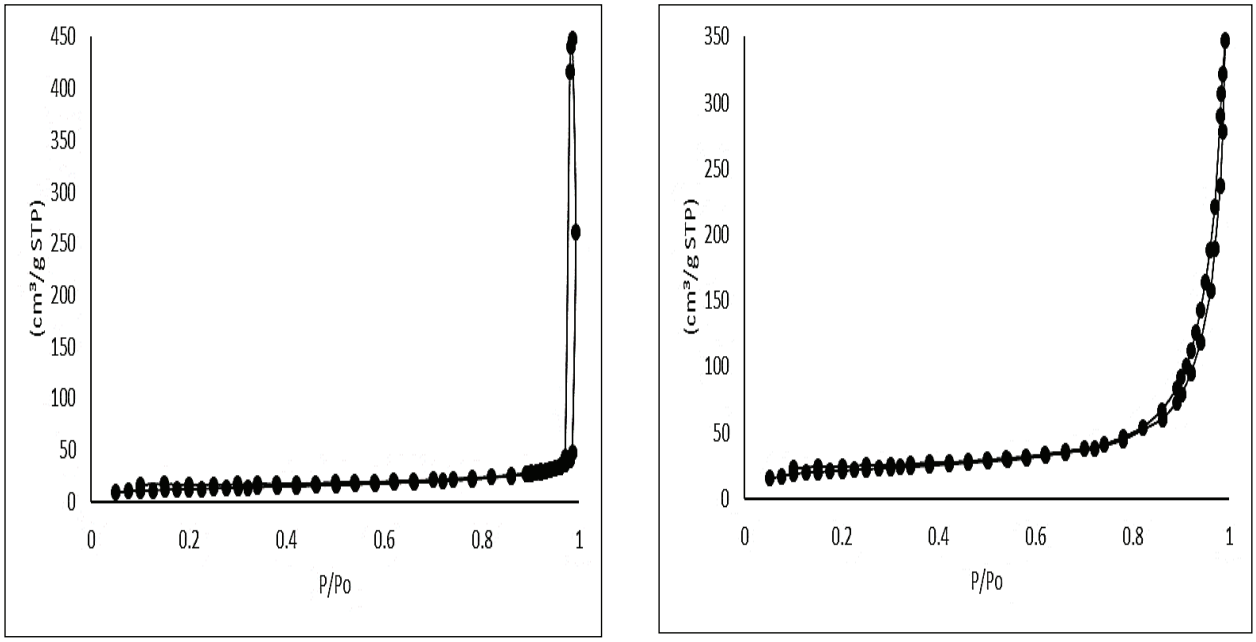

(a (b

Fig. 5. Graph of Nitrogen Adsorption-Desorption Isotherm a) MS-POBA and b) MS-POBA with MES template

Table 2. The Surface Characters of MS-POBA

Sample	Surface Area ($m^2 g^{-1}$)	Pore Diameter (nm)	Pore Volume ($cc g^{-1}$)
MS-POBA	41.033	4.180	0.250
MS-POBA with MES	71.014	7.923	0.524

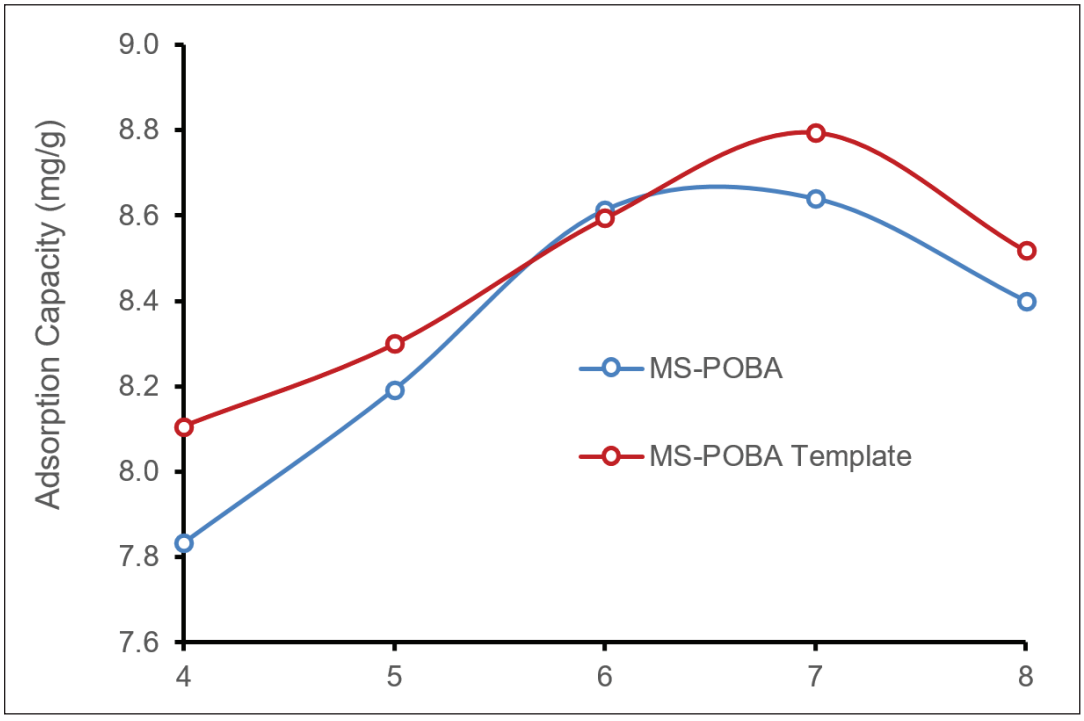

Fig. 6. Determination of optimum pH on methylene blue adsorption

3.4.2.Effect of adsorbent mass and contact time

Figure 7a shows an increased methylene blue mass that was adsorbed in MS-POBA and MS-POBA with the MES template and an increased adsorbent mass. The optimal mass of MS-POBA and MS-POBA with MES templates is 0.04 g and 0.03 g, respectively. However, the figure shows no significant difference in methylene blue adsorbed into MS-POBA and MS-POBA with the MES template. Figure 7b shows an increase in the adsorption capacity of methylene blue, along with an increase in contact time between adsorbent and adsorbate. Methylene blue adsorption capacity reached a contact time of 60 minutes on MS-POBA and 45 minutes on MS-POBA with the MES template. The equilibrium between the adsorbent and adsorbate will be reached when the number of active sites on the adsorbent has been exhausted. Tables 3 and 4 show the calculation results of the methylene blue adsorption kinetics model by MS-POBA and MS-POBA with the MES template. Both follow the pseudo-second-order adsorption kinetics model, which is indicated by the linearity value (R^2), which is close to 1, namely 0.998 of MS-POBA and 0.999 of MS-POBA with MES template.

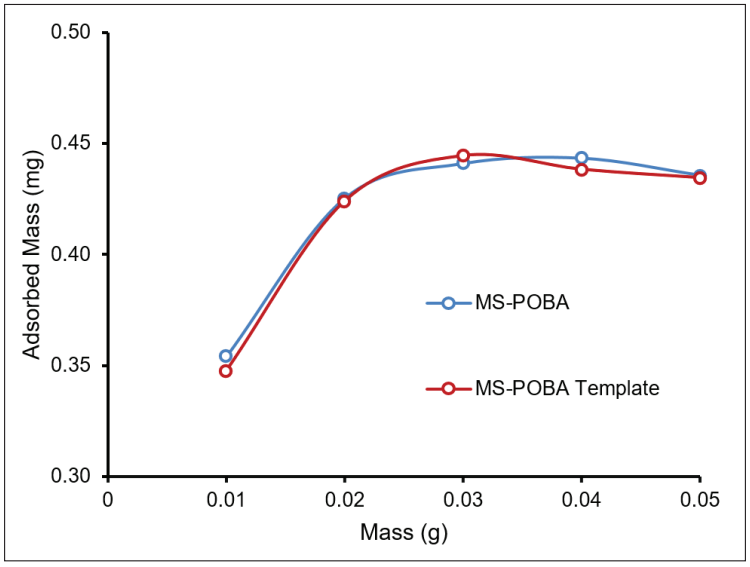

Fig.7a. Determination of optimum adsorbent mass

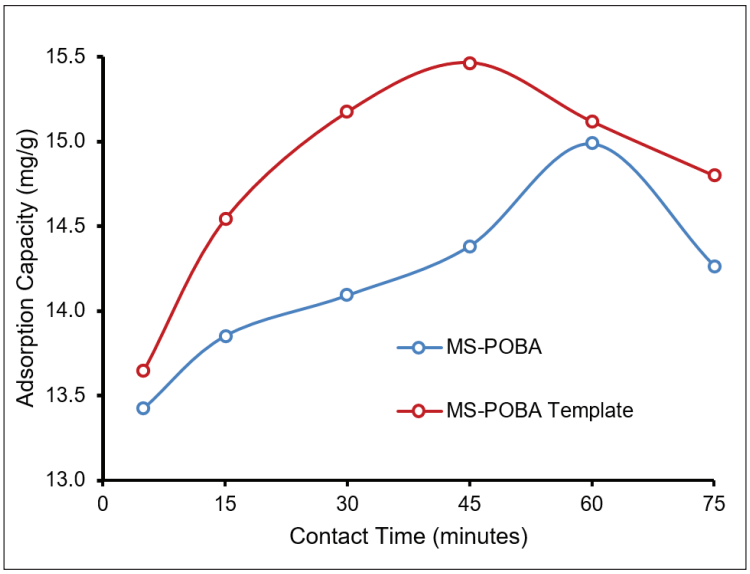

Fig.7b. Determination of optimum contact time

Table 3. The pseudo-first-order and pseudo-second-order kinetic model of methylene blue adsorption on MS-POBA

Model	Parameter	Result
Pseudo-first-order	R^2	0.209
	K (/minutes)	0.058
	q_e (mg g^{-1})	2.397
Pseudo-second-order	R^2	0.998
	K (g mg^{-1} min^{-1})	0.111
	q_e (mg g^{-1})	14.619

Table 4. The pseudo-first-order and pseudo-second-order kinetic model of methylene blue adsorption on MS-POBA with MES template

Model	Parameter	Result
Pseudo first-order	R^2	0.242
	K (/minutes)	0.012
	q_e (mg g^{-1})	1.130
Pseudo second-order	R^2	0.999
	K (g mg^{-1} min^{-1})	1.706
	q_e (mg g^{-1})	15.150

3.4.3. The optimum initial concentration of methylene blue

Figure 8 illustrates a direct correlation between the adsorption capacity and the concentration of methylene blue. As the concentration of the adsorbate in the solution rises, there is a proportional increase in the adsorption on the surface of the adsorbent, consequently leading to higher adsorption capacity. The optimum initial concentration of methylene blue obtained on the MS-POBA is 25 mg L^{-1}, and on the MS-POBA with MES template is 20 mg L^{-1}. After reaching equilibrium, the adsorption capacity is constant while the concentration of methylene blue in the solution increases. Based on Figure 8, the adsorption capacity is 15.396 mg g^{-1} on MS-POBA and 15.578 mg g^{-1} on MS-POBA / MES template, where it can be concluded that MS-POBA with the template has a slightly higher adsorption capacity compared to MS-POBA without templates. Tables 5 and 6 show the adsorption isotherm model of MS-POBA with and without template. The closest linearity to 1 is the Langmuir isotherm model with an R^2 value of 0.870 for MS-POBA and R^2 of 0.999 for MS-POBA /MES template, so it can be concluded that methylene blue adsorption in this study followed the Langmuir Isotherm model. The Langmuir Isotherm model is suitable for use in this study because the Langmuir Isotherm model assumes that no interaction between adsorbed molecules each other, and the adsorption occurs in a single layer of adsorbed molecules on the surface of the adsorbent.

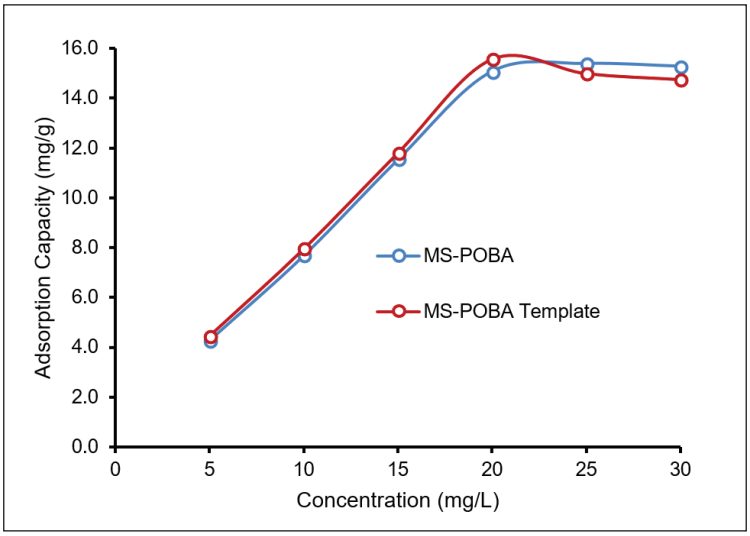

Fig. 8. Determination of optimum initial concentration of methylene blue

Table 5. The adsorption isotherm model of MS-POBA

Parameter	Results
Isotherm Langmuir	
R^2	0.870
K_L (L mol^{-1})	2.665
q_m (mg g^{-1})	17.211
Isotherm Freundlich	
R^2	0.653
K_f (L mol^{-1})	9.550
N	1.894

Table 6. The adsorption isotherm model of MS-POBA with MES template

Parameter	Result
Isotherm Langmuir	
R^2	0.242
K_L (L mol^{-1})	0.012
q_m (mg g^{-1})	1.130
Isotherm Freundlich	
R^2	0.999
K_f (L mol^{-1})	1.706
n	15.150

3.4.4.Scanning Electron Microscope–Energy Dispersive X-Ray (SEM-EDX) Data

The surface morphology and characteristics of the MS-POBA with MES template before and after methylene blue adsorption are shown in Figure 9. The adsorbent before adsorption shows an irregular particle distribution and irregular cavities between particles, hence having a significant number of pores that provide the place for the absorption of Methylene blue molecules. After the adsorption of the methylene blue process, Figure 9b illustrates morphological changes in the SEM image of silica

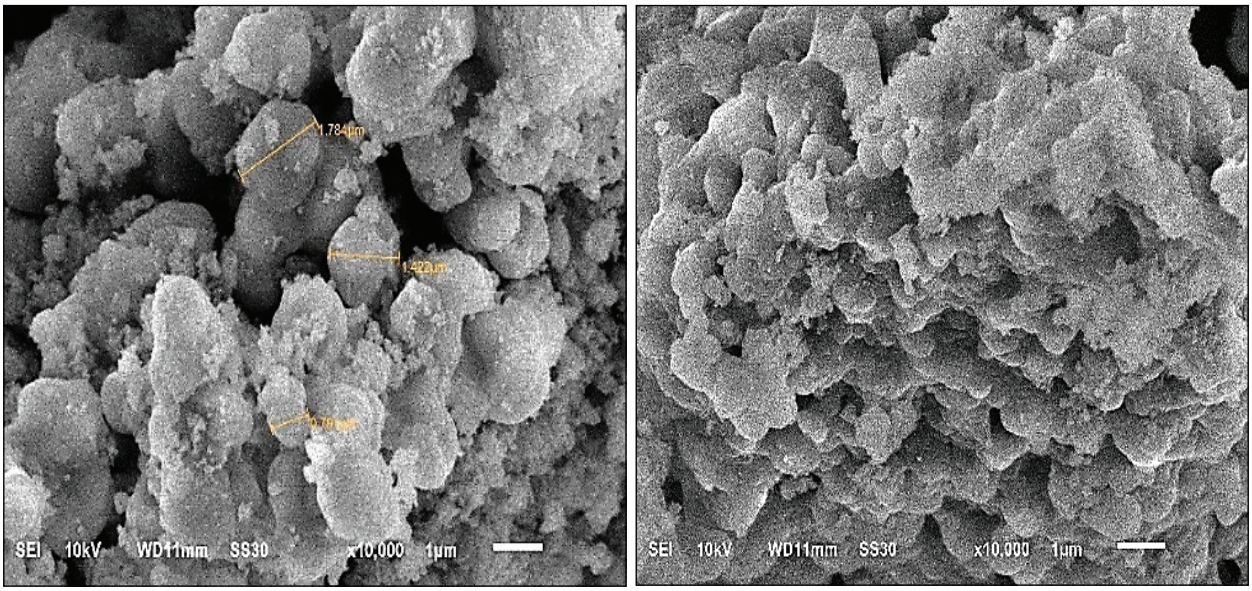

Fig. 9. SEM image of MS-POBA with MES template
(a: left) before adsorption and (b: right) after adsorption of methylene blue dye magnification 10.000 x

Table 7. Composition of MS-POBA with MES template before and after adsorption

Element	weight%	
	Before adsorption	After adsorption
C	6.71	4.34
O	51.91	45.48
Na	1.23	1.24
Al	1.16	1.20
Si	39.00	47.74

mesopores, showing that methylene blue molecules have partially filled the silica material's pores. This fact suggests that Methylene blue molecules are absorbed on the surface of the adsorbent.

As Table 7, the MS-POBA MES template contains several elements: C, O, Na, Al, and Si before adsorption. EDX is used to confirm the presence of Si and O in SiO_2. The adsorption process of methylene blue dye on the MS-POBA MES template changes the composition of the percentage elements contained.

4. Conclusion

In conclusion, this work demonstrated the synthesis of large pore mesoporous silica nanoparticles with an anionic surfactant as the template. The silica surface area, pore diameter, and pore volume of silica on MS-POBA with MES template are 71.014 $m^2 g^{-1}$, 7.923 nm, and 0.524 cc g^{-1}, respectively. The optimum conditions for adsorption of methylene blue dye by the MS-POBA adsorbent with MES template are obtained at pH 7, adsorbent mass 0.03 g, adsorption time of 45 minutes, and methylene blue concentration of 20 mg L^{-1} with adsorption capacity of 15.578 mg g^{-1}. The recovery (%) obtained in this study is 96.9%. The adsorption of methylene blue dye by MS-POBA with an MES template follows a pseudo-second-order kinetic model with a value of R^2 = 0.999 and a constant adsorption rate of 1.706 g mg^{-1} min^{-1}. The adsorption process follows the Langmuir Isotherm model.

5. References

[1] E. Hambali, M. Rivai, The potential of palm oil waste biomass in indonesia in 2020 and 2030, IOP Conf. Ser.: Earth Environ. Sci., 65 (2017) 012050. https://doi.org/10.1088/1755-1315/65/1/012050

[2] M.N. Amalia, K.P. Tresna, E. Ernah, Utilization of palm oil waste as bioenergy, J. Environ. Sustain., 3 (2019) 48-66. https://doi.org/10.22515/sustinere.jes.v3i1.77

[3] Y. Zarina, A.M.M. Al Bakri, H. Kamarudin, I. Khairul Nizar, AR Sandu, P. Vizureanu, A.R. Razak, Chemical and physical characterization of boiler ash from palm oil industry Wate for geopolymer composite, Rev. Chim. (Bucharest), 64 (2013) 1408-1412. https://www.researchgate.net/publication/264081382

[4] S. Dash. S. Mishra. S. Patel. B.K. Mishra. Organically modified silica: Synthesis and applications due to its surface interaction with organic molecules, Adv. Colloid Interface Sci., 140 (2008) 77-94. https://doi.org/10.1016/j.cis.2007.12.006

[5] N. Rameli, K. Jumbri, R.A. Wahab, A. Ramli, F. Huyop, Synthesis and characterization of mesoporous silica nanoparticles using ionic liquids as a template, J. Phys.: Conf. Ser., 1123 (2018) 012068. https://doi.org/10.1088/1742-6596/1123/1/012068

[6] J. Wang, C. Zhang, Y. Bai, Q. Li, X. Yang, Synthesis of mesoporous silica with ionic liquid surfactant as template, Mater. Lett., 291 (2021) 129556. https://doi.org/10.1016/j.matlet.2021.129556

[7] S. Kumar, M.M. Malik, R. Purohit, Synthesis methods of mesoporous silica materials, Mater. Today: proc., 4 (2017) 350-357. https://doi.org/10.1016/j.matpr.2017.01.032

[8] N. Tobori, T. Kakui, Methyl ester sulfonate, biobased surfactants, second ed. AOCS press, (2021) 303-324. https://doi.org/10.1016/B978-0-12-812705-6.00009-5

[9] Z.A. Maurad, Z.A. Maurad, L.C. Abdullah, MS Anuar, NNAK Shah, Z. Idris, Preparation, characterization, morphological and particle properties of crystallized palm-based methyl ester sulphonates (MES) powder, Molecules, 25 (2020) 2629. https://doi.org/10.3390/molecules25112629

[10] C. Gao, Formation mechanism of anionic surfactant-templated mesoporous silica, Chem. Mater.,18 (2006) 3904-3914. https://doi.org/10.1021/CM061107+

[11] A. Amina, D.K. Hakim, Z.B. Hassina, Textile dyes removal from wastewater using recent promising composite: A review, Alger. J. Chem. Eng., 02 (2021) 49-65. http://dx.doi.org/10.5281/zenodo.5451775

[12] Y. Kuang, X. Zhang, S. Zhou, Adsorption of methylene blue in water onto activated carbon by surfactant modification, Water (Switzerland), 12 (2020) 1–19. https://doi.org/10.3390/w12020587

[13] C. Jamshidzadeh, A new analytical method based on bismuth oxide-fullerene nanoparticles and photocatalytic oxidation technique for toluene removal from workplace air, Anal. Methods Environ. Chem. J., 2 (01) (2019) 73-86. https://doi.org/10.24200/amecj.v2.i01.55

[14] S. Teimoori, New extraction of toluene from water samples based on nano-carbon structure before determination by gas chromatography, Int. J. Environ. Sci. Technol., 20 (2023) 6589-6608. https://doi.org/10.1007/s13762-023-04906-9

[15] S. Teimoori, A.H. Hassani, M. Panahi, N. Mansouri, An immobilization of aminopropyl trimethoxysilane-phenanthrene carbaldehyde on graphene oxide for toluene extraction and separation in water samples, Chemosphere, 316 (2023) 3137800. https://doi.org/10.1016/j.chemosphere.2023.137800

[16] P.O. Oladoye, T.O. Ajiboye, E.O. Omotola, O.J. Oyewola, Methylene blue dye: Toxicity and potential elimination technology from wastewater, Results Eng., 16 (2022) 100678. https://doi.org/10.1016/j.rineng.2022.100678

[17] J.J. Salazar-Rabago, R. Leyva-Ramos, J. Rivera-Utrilla, R. Ocampo-Perez, F.J.

Cerino-Cordova, Biosorption mechanism of Methylene Blue from aqueous solution onto White Pine (Pinus durangensis) sawdust: Effect of operating conditions, Sustain. Environ. Res., 27 (2017) 32–40. https://doi.org/10.1016/j.serj.2016.11.009

[18] Keputusan Menteri Negara Lingkungan Hidup Republik Indonesia Nomor: KEP-51/MENLH/10/1995, tentang Baku Mutu Limbah Cair bagi Kegiatan Industri. Jakarta, 1995. https://faolex.fao.org/docs/pdf/ins27432.pdf

[19] C. Jamshidzadeh, A new method for removal of hazardous toluene vapor from air based on ionic liquid-phase adsorbent, Int. J. Environ. Sci. Technol., 16 (2019) 2797-2808. https://doi.org/10.1007/s13762-018-1975-5

[20] A. Faghihi-Zarandi, J. Rakhtshah, BB. Yarahmadi, A rapid removal of xylene vapor from environmental air based on bismuth oxide coupled to heterogeneous graphene/graphene oxide by UV photo-catalectic degradation-adsorption procedure, J. Environ. Chem. Eng., 8 (2020) 104193. https://doi.org/10.1016/j.jece.2020.104193

[21] R. Ashouri, S.A. Hajiseyed Mirzahosseini, Synthesis of carbon quantum dots from olive stones for efficient adsorption of benzene from the ambient air, J. Nanostructures, 11 (2021) 480-497. https://doi.org/10.22052/JNS.2021.03.007

Anal. Methods Environ. Chem. J. 7 (2) (2024) 18-28

AMECJ

Research Article, Issue 2
Analytical Methods in Environmental Chemistry Journal
Journal home page: www.amecj.com/ir

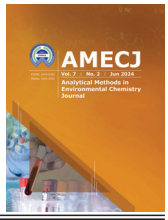

Direct analysis of hexavalent chromium in water samples by UV-Vis spectrophotometry: Effects of pH and the presence of foreign ions

Rayane Nadjet Fassi [a], and Chahrazed Boukhalfa [a,*]

[a] *Laboratory of Pollution and Water Treatment, Chemistry Department, University Brothers Mentouri Constantine 1, Constantine, Algeria*

ARTICLE INFO:

Received 10 Feb 2024
Revised form 14 Apr 2024
Accepted 17 May 2024
Available online 30 Jun 2024

Keywords:
Analytical method
Chromium (VI)
UV-Vis spectroscopy
Water samples

ABSTRACT

The present study aims to characterize the direct UV-Vis spectrophotometric analysis of hexavalent chromium (CrVI) in aqueous solution. The effects of pH and the presence of different ions are evaluated. The results obtained show that at pH ≤ 6, Cr(VI) analysis must be carried out at 350 nm. The Beer-Lambert law is respected for a concentration lower than 100mg Cr(VI) L^{-1}. At pH ≥ 8, the analysis must be performed at 372 nm. In this case, the linearity range of the standard curve does not exceed the concentration of 25 mg Cr(VI) L^{-1}. In the pH range 6 <pH < 8, the direct Cr(VI) analysis cannot be performed. Whatever the pH of the solutions, the presence of acetate, oxalate, citrate, and tartrate with a concentration ten times higher than that of Cr(VI), has no effect. At pH 2, only the presence of Fe(II) and Fe(III) ions prevents the direct determination of Cr(VI) ions. In the presence of metallic ions [Mn(II), Co(II), Ni(II), Cu(II), Zn(II), Cd(II)), Cr(VI)] analysis must be carried out at pH 2. At higher pH, these ions have a significant effect.

1. Introduction

Metal speciation is crucial to characterize their behavior and effects. Two forms of the same metal can be very different. Various methods are developed for toxic metal speciation in various samples [1, 2]. Chromium is one of the known toxic metals. It can exist in different oxidation states, ranging from the divalent to the hexavalent state. Generally, in water, chromium can be found as trivalent (Cr(III)) or hexavalent (Cr(VI)). The hexavalent form (Cr(VI)) is characterized by a high oxidative potential and a high solubility. It is considered to be the most toxic form of chromium. Cr(VI) forms species mainly with oxo or hydroxo ligands, which are readily absorbed from the gastrointestinal tract due to their high ability to diffuse across all types of cell membranes [3]. It is suggested that Cr(VI) exclusively impairs cellular energy production, disrupts the homeostatic metabolism of carbohydrate, protein, and lipid pathways; deregulates metabolically related enzymes, and impairs the structural and functional integrity of the liver and kidneys [4]. Potassium dichromate ($K_2Cr_2O_7$) and sodium chromate (Na_2CrO_4) are two hexavalent chromium salts widely used in industrial processes such as metallurgy, chromium plating, chemical industry, textile manufacturing, wood preservation, photography and photoengraving [5]. The main method used to analyze Cr(VI) in water is the 1,5-diphenylcarbazide method, which has been proposed for a long time [6]. This method is based on the formation, under acidic conditions of a red-violet

*Corresponding Author: Chahrazed Boukhalfa
Email: Chahrazed_boukhalfa@yahoo.com
https://doi.org/10.24200/amecj.v7.i02.278

color complex characterized by a UV-visible absorption band at 540 nm [7, 8]. However, it can only be used for low concentrations (< 0.3 mg L^{-1}), and dilution is often required. Consequently, several researchers have been interested in the direct determination of Cr(VI) ions in water using the UV-Vis spectrophotometric properties of Cr(VI) solutions. In a method developed for natural water, the concentration of Cr(VI) at pH 9 was determined by measuring the height of the absorption peak at 372 nm [9]. The Cr(VI) species were quantified by direct determination of Cr(VI) at 371nm at different pH values [10]. The direct multi-wavelength determination of Cr(VI) in natural waters, and urban and industrial effluents has given results comparable to those of the diphenylcarbazide method [11]. From the comparison of the dilution effect on the determination of Cr(VI) ions by the direct method and the diphenylcarbazide method, it has been suggested that the direct method is recommended for the quantification of Cr(VI) at concentrations higher than 1mg. L^{-1} [12]. Concerning the effect of the presence of foreign ions, it has been found that the presence of major ions such as Na^+, K^+, NO_3^- and Cl^-, does not affect the direct determination of Cr(VI) ions at 363 nm up to a concentration greater than 1000 mg L^{-1}. The tolerated concentration limit was 200 mg L^{-1} in the case of SO_4^{2-} and CO_3^{2-}, 100 mg L^{-1} in the case of $Al^{3+,}$ and 15 mg L^{-1} in the case of Mg^{2+} [13], experiments were carried out in the pH range 5-7. Recently, some methods such as isopropyl 2-[(isopropoxycarbothiolyl) disulfanyl ethane thioate, amino bimodal mesoporous silica nanoparticles, task-specific ionic liquid, and acetylcysteine based on dispersive liquid-liquid microextraction were used for chromium determination in different samples [14-19]. Also, the Raman analysis showed that the pH range 2-6 can be used for Cr(VI) [20]. The present study aims to optimize the direct determination of Cr(VI) in the presence of transition metals (Mn(II), Fe(II), Fe(III), Co(II), Ni(II), Cu(II), Zn(II) and Cd(II)) and organic anions (oxalate, citrate, acetate, and tartrate).

2. Material and methods

2.1. Instrumental

Quantitative analysis of UV-visible spectrophotometry relies on the Beer-Lambert law which establishes a relation between the absorption of light by a substance and its concentration in a solution. The Beer-Lambert law is valid in the case of monochromatic light, diluted solutions, and in the absence of interferences from reflection, scattering, or fluorescence. In the present study, analyses were performed using Shimadzu 1610, UV-Vis spectrophotometer. A quartz cell was used for all analyses.

2.2. Reagents

All chemical reagents used in this study are of analytical grade and have not been purified. All solutions were prepared in distilled water. The Cr (VI) solutions were prepared from potassium dichromate (ChemischeFabrick (Germany) CAS No:7778-50-9) and potassium chromate (Sigma-Aldrich (United States) CAS No:7789-00-6). Transition metals were used as chloride or nitrate salts. Iron (III) chloride (CAS No: 7705-08-0), manganese (II) chloride (CAS No: 7791-18-6), cadmium (II) nitrate (CAS No: 10022-68-1), and zinc (II) nitrate (CAS N°: 10196-18-6) were purchased from BIOCHEM (France). Nickel (II) chloride (CAS No: 7791-20-0) and cobalt (II) chloride (CAS No: 7791-13-1), were purchased from MERCK (Germany). Copper (II) chloride (CAS No: 10125-13-0) and iron (II) chloride (CAS No:13478-10-9) were purchased from NORMAPUR (Spain) and Sigma-Aldrich (United States) respectively. Organic ions were used as their potassium, sodium, or ammonium salts. Ammonium acetate (CAS No:8013-60-4), ammonium oxalate (H_2O, CAS No:6009-70-7), and potassium sodium tartrate (CAS No: 6381-59-5) were purchased from Thermo Scientific Chemicals (United States), NORMAPUR (Spain) and MERCK (Germany) respectively. Potassium citrate (CAS No: 6100-05-6) and sodium acetate (CAS No: 127-09-3) were purchased from BIOCHEM (France). Hydrochloric acid (CAS No:7647-01-0) and sodium hydroxide (CAS No: 1310-73-2) were purchased from BIOCHEM (France) and NORMAPUR (Spain) respectively.

2.3. Procedure

Cr(VI) stock solutions were prepared in distilled water. Cr(VI) solutions with various concentrations were obtained by dilution in distilled water. After pH adjustment using HCl (0.1M) or NaOH (0.1M), the absorbance of each prepared solution was measured (Figure 1). The same procedure was repeated in the presence of the foreign ions using Cr(VI) solution with a concentration of 10 mg L^{-1} and various foreign ions concentrations. Stock solutions of 20 mg L^{-1} in the case of cations and 200 mg L^{-1} in the case of anions were prepared and used. All the experiments were performed at least in triplicate.

3. Results and discussion

3.1. Cr(VI) solution characterization

The UV-vis spectra of an aqueous Cr(VI) solution at a concentration of 10 mg L^{-1} (Fig. 2) show two absorption bands corresponding to charge transfer transitions between oxygen and chromium. In water, Cr(VI) can be found as $Cr_2O_7^{2-}$, $HCrO_4^-$, and CrO_4^{2-}. In the three species, simple and double bonds between chromium and oxygen exist (Fig. 3). Increasing the pH causes a shift of the absorption bands towards higher wavelengths (batochrome effect) and an increase in the intensity of the bands (hyper chrome effect).

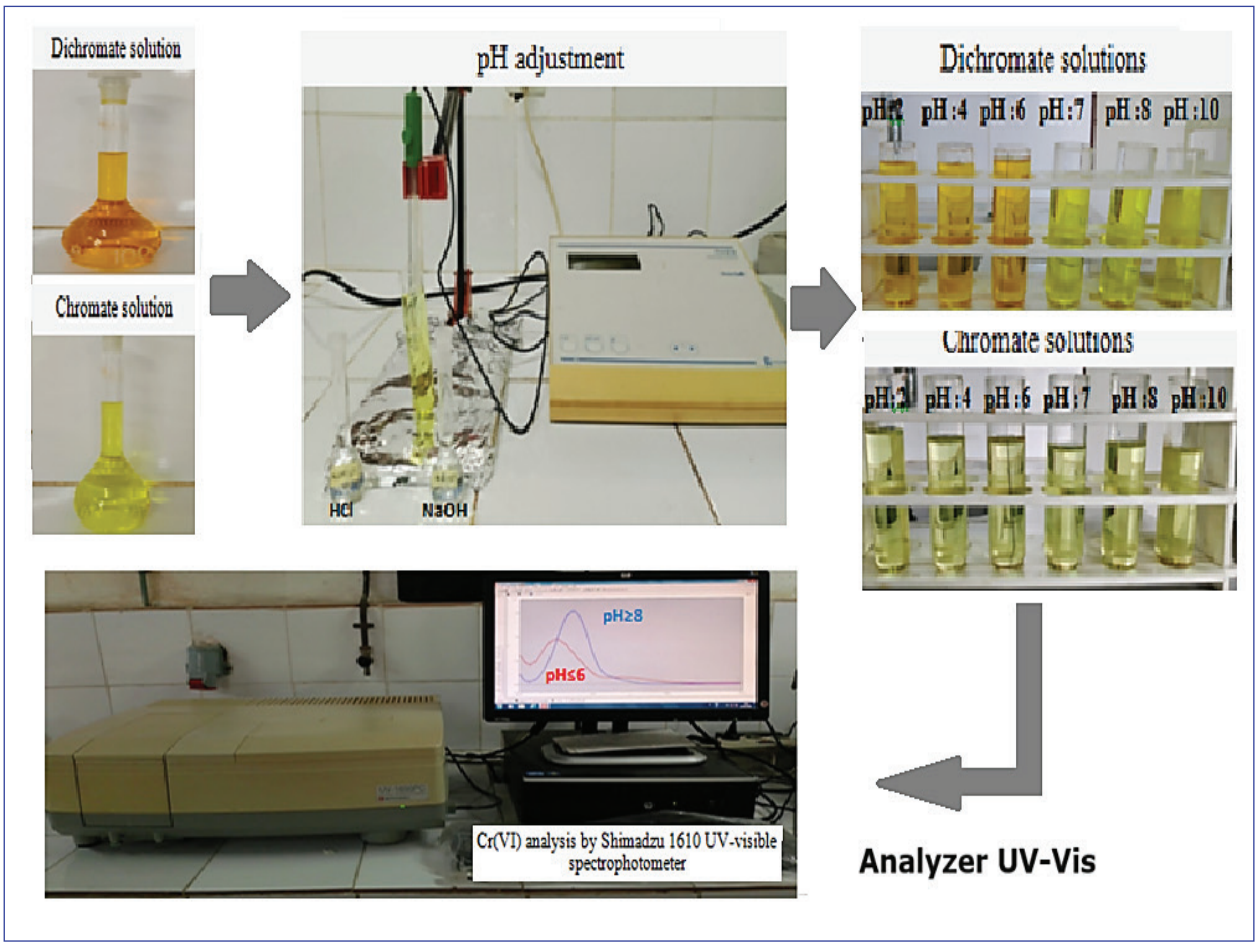

Fig. 1. Experimental procedure by UV-visible spectrophotometry

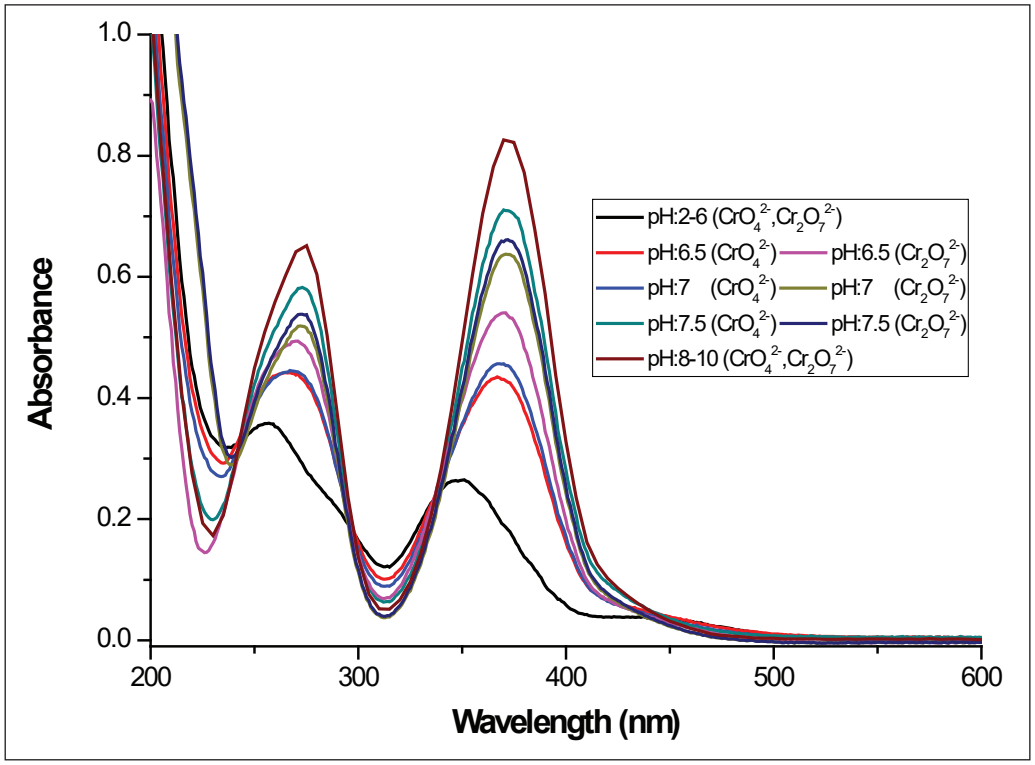

Fig. 2. Effect of pH on UV-Vis spectra of Cr(VI) solution (10 mg L^{-1})

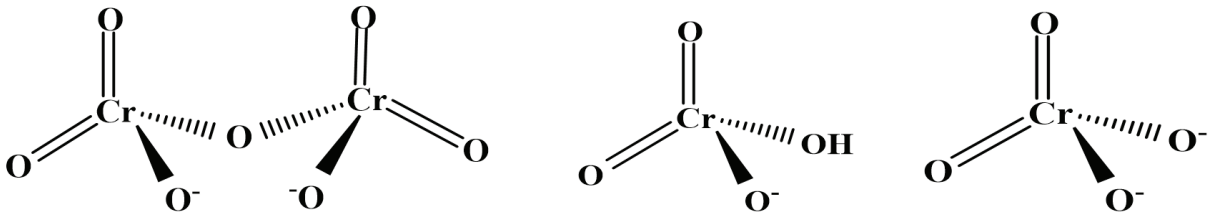

Fig. 3. Structures of Cr (VI) species

The intensity of the UV-Vis bands evolves according to three pH ranges (Fig. 4). Despite the possible presence of two Cr(VI) species ($HCrO_4^-$ and/or $Cr_2O_7^{2-}$), absorbance remains stable at pH ≤ 6. According to the results of Raman spectroscopic analysis [20], in the pH range 2-6, the dominant form of Cr(VI) at low concentration as is the case in our study is $HCrO_4^-$ rather than $Cr_2O_7^{2-}$. This can explain the observed stability of the optic density of the Cr(VI) solution in this pH range. At pH ≥ 8, where CrO_4^{2-} predominates, absorbance remains also stable. The wavelength of the maximum absorbance is 350 nm at pH≤6 and 372 nm at pH ≥ 8. In the pH range 6 < pH < 8, where Cr(VI) speciation evolves from $HCrO_4^-$ to CrO_4^{2-}, the measured absorbance increases with increasing pH and varies with the nature of chromium salt (Fig. 4). Consequently, Cr(VI) speciation has a significant effect in this pH range. In the pH range 6<pH <8, the same effect is also observed for Cr(VI) concentrations below or above 10 mg L^{-1} (Fig. 5); the measured absorbance increases with increasing pH.

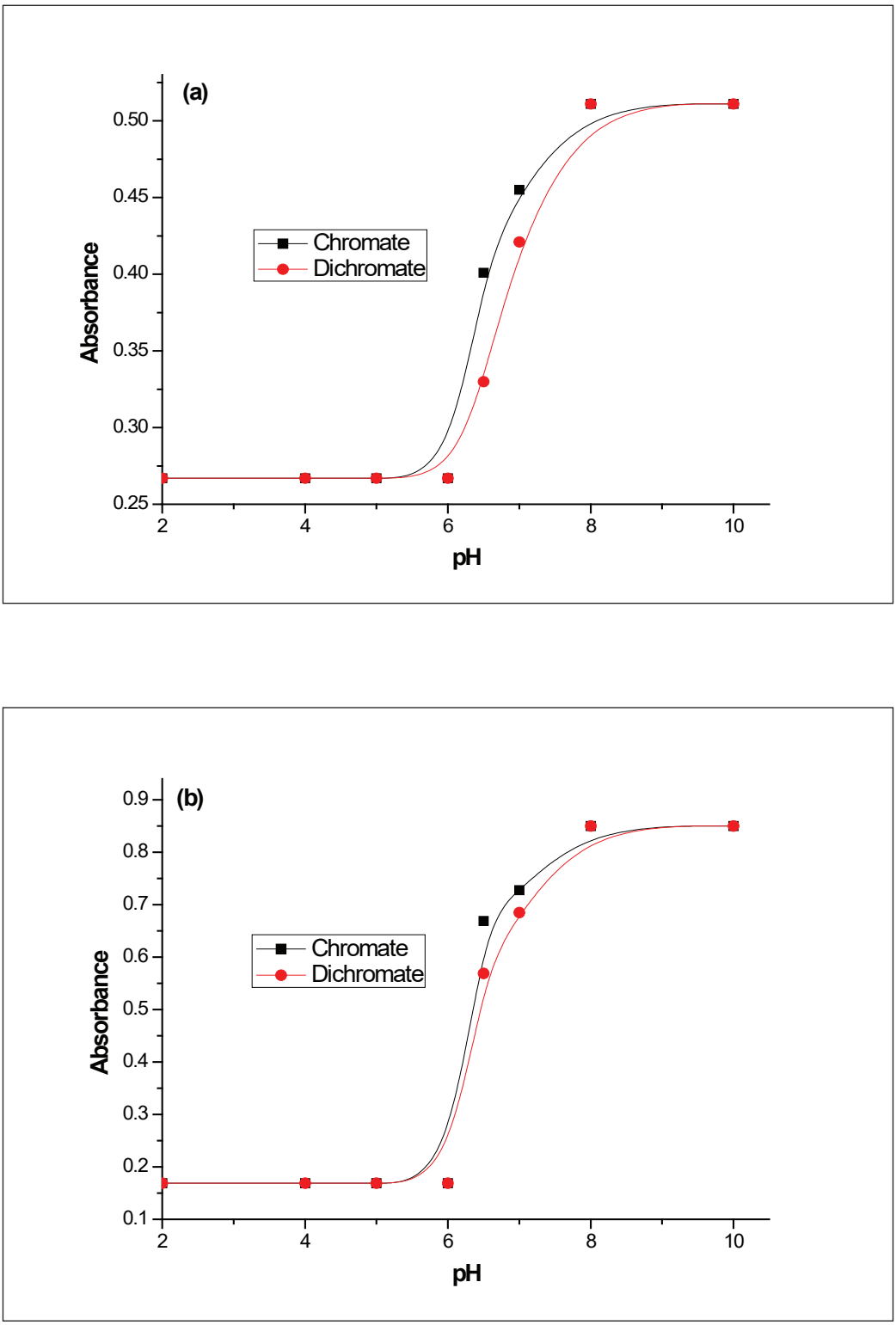

Fig. 4. Effect of pH on the absorbance of Cr(VI) solution (10 mg L^{-1}) at: a)350 nm and b)372nm

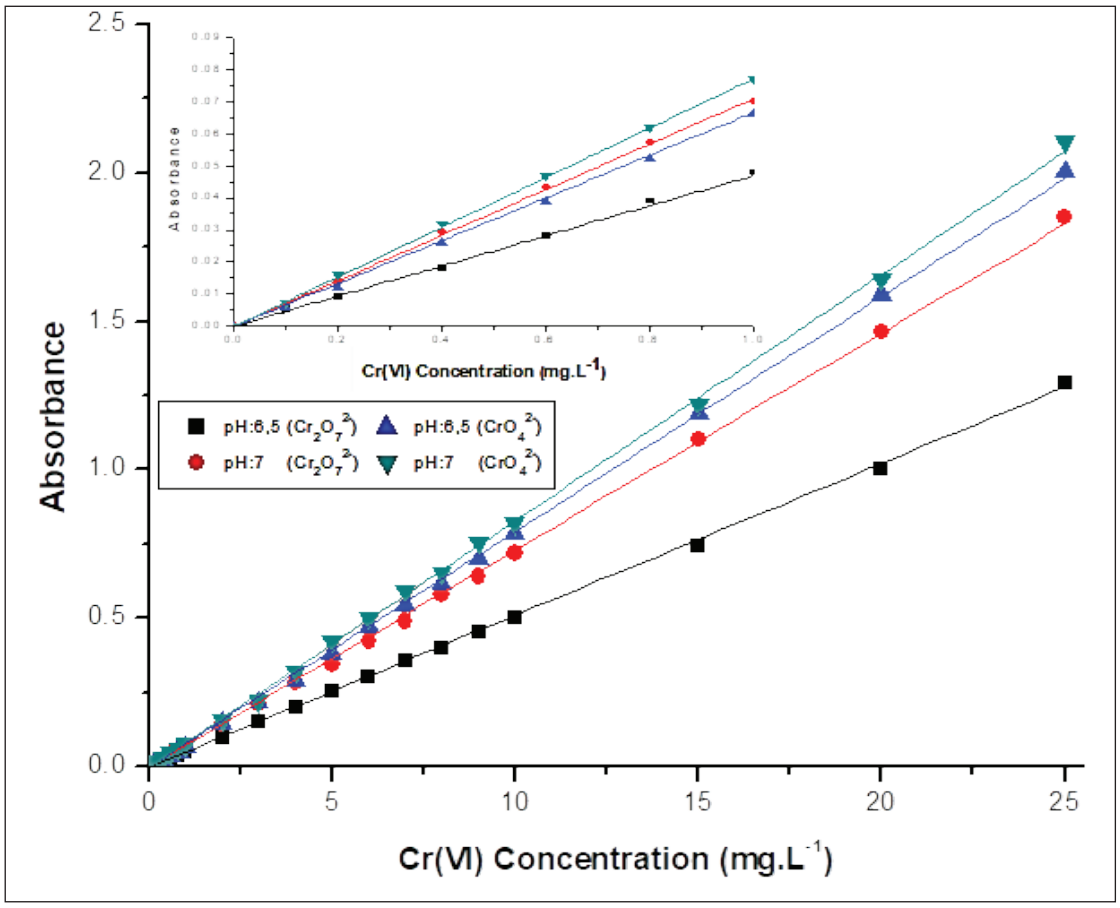

Fig. 5. Absorbance evolution of Cr(VI) solution for concentration below 10mg.L^{-1} in the pH range 6<pH<8 (372 nm)

3.2. Cr(VI) analysis

The above results imply that it is necessary to determine standard curves for acidic conditions (pH≤6) at 350 nm, and for alkaline conditions (pH≥ 8) at 372 nm. Contrary to what has been suggested in various studies, direct determination of Cr(VI) is not possible in the pH range (6 <pH<8). In these studies which were carried out at some pH values, it was suggested that Cr(VI) can be directly determined at pH< 6.4 [12] and at pH ≤7.4 [13]. The results obtained in the present study show that the Beer-Lambert law is valid for Cr(VI) concentrations up to 100 mg Cr(VI) L^{-1} at pH≤6 and up to 25 mg Cr(VI) L^{-1} at pH≥8. At higher concentrations, the absorbance does not respect the proportionality (Fig. 6). The absorbance measured at 372 nm at pH≥8, increases rapidly with the increase of Cr(VI) concentration. In these conditions, the absorbance measured for a solution with a concentration of 25 mg L^{-1} is reached for a concentration three times higher at 350nm at pH≤6.

In the two pH ranges, the proportionality is maintained up to a concentration of 0.1mg L^{-1} (Figures 7 and 8). The value of the mass absorption calculated from Beer Lambert's equation is 0.086 mg mol^{-1} cm^{-1} in acidic solutions and 0.028mg mol^{-1} cm^{-1} in alkaline solutions.

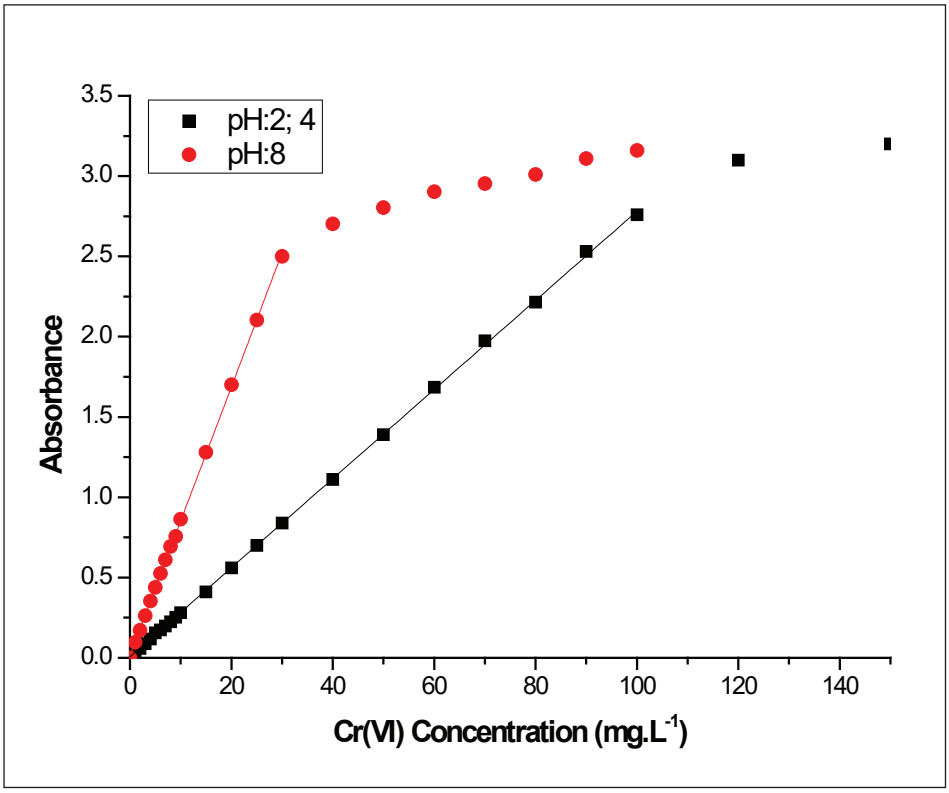

Fig. 6. Beer-Lambert law validity for Cr(VI) analysis

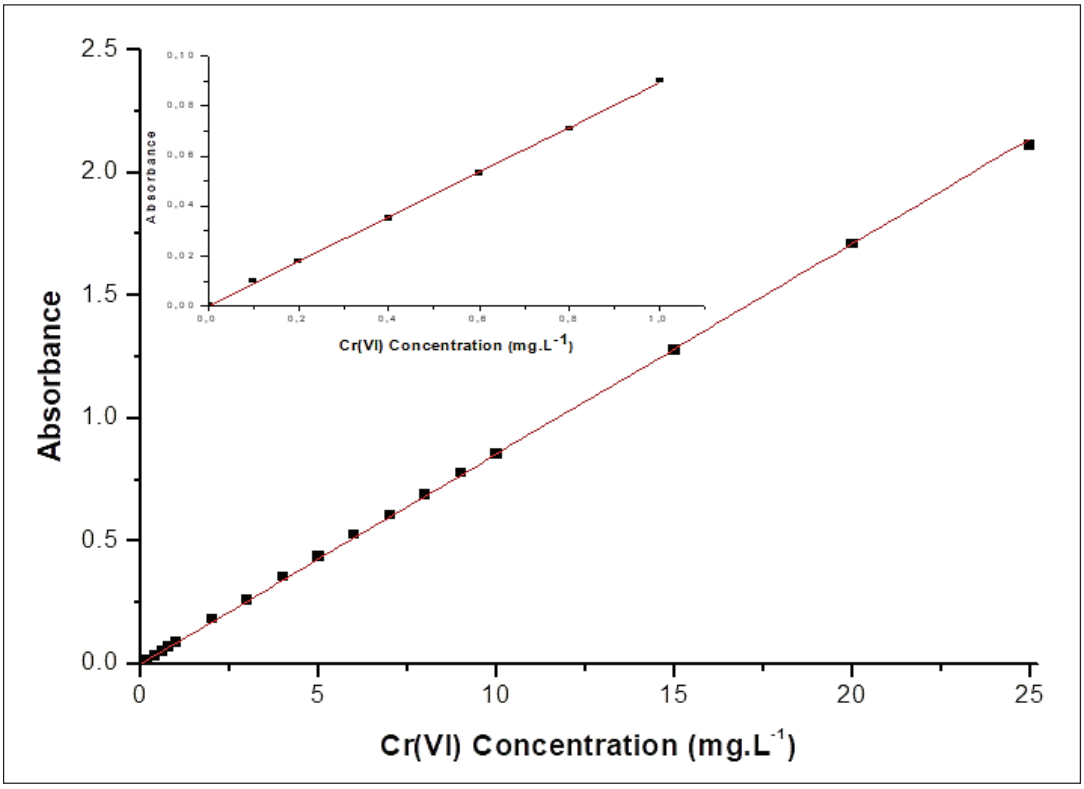

Fig. 7. Standard curve for Cr(VI) analysis at pH≤6.5 (350 nm)

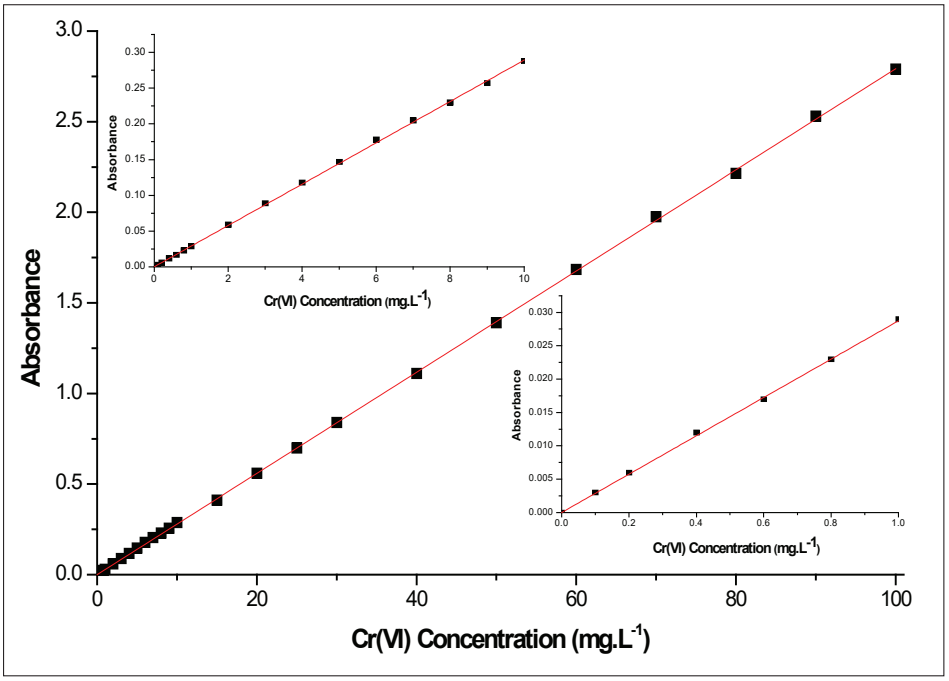

Fig. 8. Standard curve for Cr(VI) analysis at pH ≥ 8 (372nm)

At pH 2, the presence of Mn(II), Co(II), Ni(II), Cu(II), Zn(II), and Cd(II) with a concentration five times higher than that of chromium, does not affect the direct determination of Cr(VI) whatever the salt used. With increasing pH, the nature of the chromium species seems to have an effect. At pH 4, no effect is observed in the case of dichromate salt. However, in the case of chromate salt, the presence of these metallic cations has a significant effect. At pH 8, whatever the chromium salt is used, the presence of metallic ions interferes with the direct Cr(VI) determination (Fig. 9).

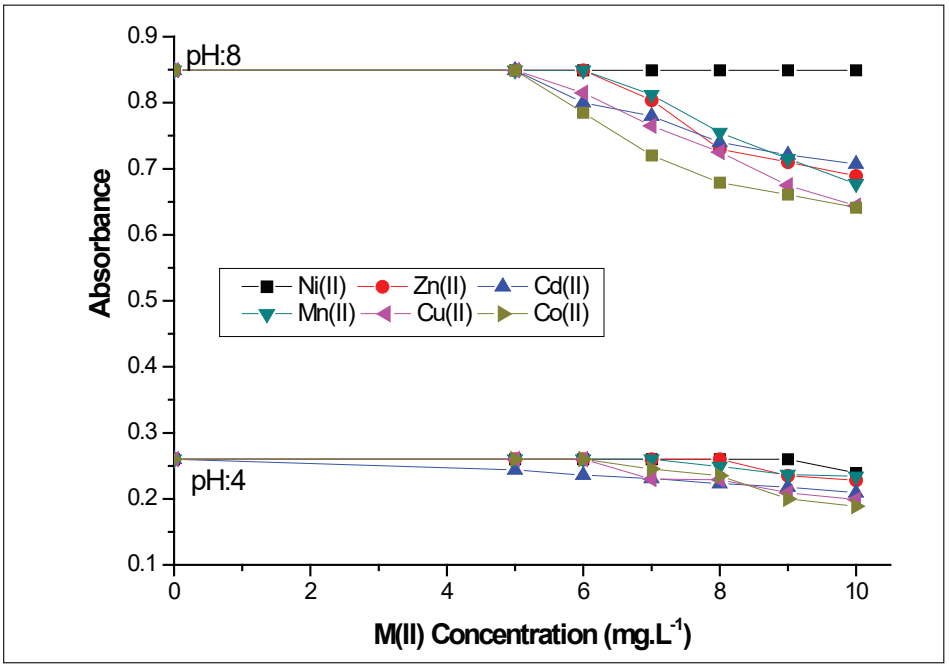

Fig.9. Effects of metallic cations (Cr(VI):10mg.L^{-1})

Whatever the pH of the solution and the Cr(VI) salt used, the presence of iron ions [Fe(III) or Fe(II)] interferes with the direct determination of Cr(VI). In their presence, the measured absorbance of the Cr(VI) solution increases significantly (Fig. 10). This is due to the interference of the absorption of the two iron chlorides which are characterized by an absorption band at about 334 nm in the case of Fe(III) and 367 nm in the case of Fe(II). Whatever the pH, the presence of oxalate, citrate, acetate, and tartrate anions with a concentration ten times higher than that of Cr(VI) does not affect its direct determination (Fig. 11).

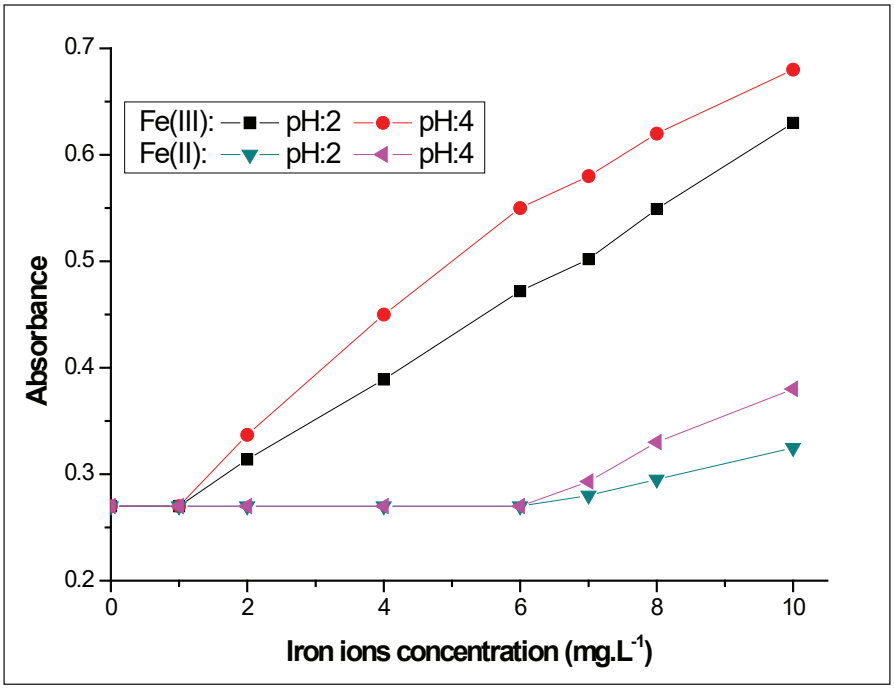

Fig. 10. Effects of iron ions (Cr(VI):10 mg L^{-1})

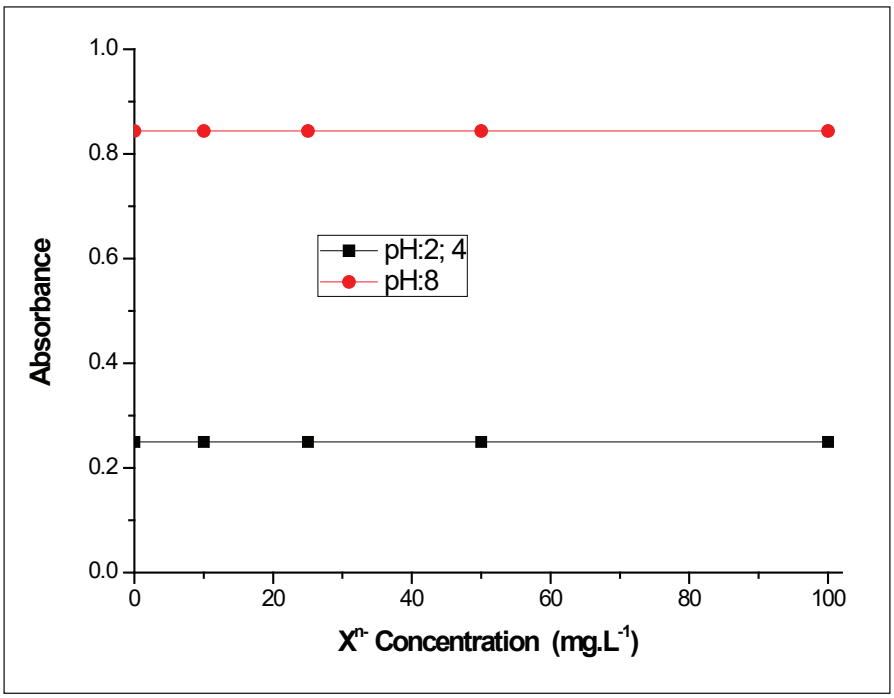

Fig. 11. Effects of anions (oxalate, citrate, tartrate, acetate) (Cr(VI):10mg.L^{-1})

4. Conclusion

The direct determination of Cr(VI) by UV-Vis spectrophotometry can be successfully applied in acidic solutions at pH≤6 and in alkaline solutions at pH ≥ 8. The presence of organic anions (oxalate, citrate, acetate, tartrate) has no effect. In the presence of metallic cations (Mn(II), Co(II), Ni(II), Cu(II), Zn(II), Cd(II)), the method must be carried out at very acid pH (pH: 2). The direct determination of Cr(VI) cannot be used in the pH range 6.5<pH<8 and in the presence of Fe(II) and Fe(III).

5. References

[1] N. Esmaeili, J. Rakhtshah, E. Kolvari, H. Shikhanoo, Ultrasound assisted-dispersive-modification solid-phase extraction using task-specific ionic liquid immobilized on multiwall carbon nanotubes for speciation and determination mercury in water samples, Microchem. J., 154 (2020) 104632. https://doi.org/10.1016/j.microc.2020.104632.

[2] H. Shikhanoo, M. Habibnia, A. Rashidi, A. Faghihi Zarandi, Simultaneously speciation of mercury in water, human blood and food samples based on pyrrolic and pyridinic nitrogen-doped porous, graphene nanostructure, Food Chem., 403 (2023) 134394. https://doi.org/10.1016/j.foodchem.2022.134394

[3] T. W. Clarkson, Molecular and ionic mimicry of toxic metals, Ann. Rev. Pharmacol., 33 (1993) 545-571. https://doi.org/10.1146/annurev.pa.33.040193.002553

[4] K. Shil, S. Pal, Metabolic adaptability in hexavalent chromium-treated renal tissue: an in vivo study, Clin. Kidney J., 10 (2017) 1-8. https://doi.org/10.1093/ckj/sfx069

[5] R. M. Park, J. F. Bena, L. T. Stayner, R. J. Smith, H. J. Gibb, P. S. Lees, Hexavalent chromium and lung cancer in the chromate industry: a quantitative risk assessment, Risk Anal., 24 (2004) 1099-1108. https://doi.org/10.1111/j.0272-4332.2004.00512.x

[6] P. Cazeneuve, Sur la diphénylcarbazide, réactif très sensible de quelques composés métalliques; cuivre, mercure, fer, acide chromique, Bull. Soc. Chim., 23 (1900) 701-706. http://www.societechemicaldefrance.fr

[7] A. Wiryawan, R. Retnowati, P. Burhan, S. Syekhfani, Method of analysis for determination of the chromium (cr) species in water samples by spectrophotometry with diphenylcarbazide, J. Environ. Eng. Sustain. Technol., 5 (2018) 37-46. http://jeest.ub.ac.id

[8] A. Lace, D. Ryan, M. Bowkett, J. Cleary, Chromium monitoring in water by colorimetry using optimized 1,5-Diphenylcarbazide method, Int. J. Environ. Res. Public Health, 16 (2019) 1803-1818. https://doi.org/10.3390/ijerph16101803

[9] A. Oumedjbeur, O. Thomas, Dosage rapide du chrome (VI) dans les eaux naturelles, Analusis, 17 (1989) 221-224. https://hal.univ-smb.fr/hal-02869678v1

[10] M. C. Fournier-Salaün., P. Salaün, Quantitative determination of hexavalent chromium in aqueous solutions by UV-Vis spectrophotometer, Cent. Eur. J. Chem., 5 (2007) 1084-1093. https://doi.org/10.2478/s11532-007-0038-4

[11] O. Thomas, S. Gallot, E. Naffrechoux, Ultraviolet multiwavelength absorptiometry (UVMA) for the examination of natural waters and wastewaters, Part III. Determination of Chromium(VI), Fresenius J. Anal. Chem., 338 (1990) 241-244. https://doi.org/10.1007/BF00323016

[12] A. Sanchez-Hachair, A. Hofmann, Hexavalent chromium quantification in solution: Comparing direct UV–visible spectrometry with 1,5-diphenylcarbazide colorimetry, C. R. Chim., 21 (2018) 890-896. https://doi.org/10.1016/j.crci.2018.05.002

[13] D. Kim, J. Om, Direct spectroscopic determination of aqueous phase hexavalent chromium, Univers. J. Eng. Sci., 1 (2013) 1-4. https://doi.org/10.13189/ujes.2013.010101

[14] M.M. Eskandari, Cloud point assisted dispersive ionic liquid-liquid microextraction for chromium speciation in human blood samples based on isopropyl 2-[(isopropoxy-

carbothiolyl) disulfanyl] ethane thioate, Anal. Chem. Res., 10 (2016) 18-27. https://doi.org/10.1016/j.ancr.2016.10.002

[15] A. Khaligh, F. Golbabaei, A Vahid, On-line micro column preconcentration system based on amino bimodal mesoporous silica nanoparticles as a novel adsorbent for removal and speciation of chromium (III, VI) in environmental samples, J. Environ. Health Sci. Eng., 13 (2015) 47. https://doi.org/10.1186/s40201-015-0205-z

[16] A.A.Miran Beigi, M.M. Eskandari, Dispersive liquid-liquid microextraction based on task-specific ionic liquids for determination and speciation of chromium in human blood, J. Anal. Chem., 70 (2015) 1448-1455. https://doi.org/10.1134/S1061934815120072

[17] H.Z. Mousavi, Chromium speciation in human blood samples based on acetyl cysteine by dispersive liquid–liquid biomicroextraction and in-vitro evaluation of acetyl cysteine/cysteine for decreasing of hexavalent chromium concentration, J. Pharm. Biomed. Anal., 118 (2016) 1-8. https://doi.org/10.1016/j.jpba.2015.10.018

[18] M. Arjomandi, A review: analytical methods for heavy metals determination in environment and human samples, Anal. Methods Environ. Chem. J., 2 (2019) 97-126. https://doi.org/10.24200/amecj.v2.i03.73

[19] A. Rouhollahi, Preconcentration and determination of heavy metals in water, sediment and biological samples, J. Serb. Chem. Soc., 76 (2011) 1583-1595. https://doi.org/10.2298/JSC101024139S

[20] JD. Ramsey, L. Xia, MW. Kendig, RM. McCreery, Raman spectroscopic analysis of the speciation of dilute chromate solutions, Corros. Sci., 43 (2001) 1557-1572. https://doi.org/10.1016/S0010-938X(00)00145-1

Anal. Methods Environ. Chem. J. 7 (2) (2024) 29-44

AMECJ

Research Article, Issue 2
Analytical Methods in Environmental Chemistry Journal
Journal home page: www.amecj.com/ir

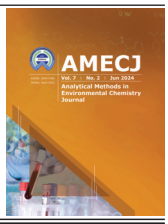

Analysis and preparation of phenolic and alkaloid compounds from Moroccan Berberis vulgaris organic extract: Molecular docking and optimization by UHPLC/DAD/ESI-MS

Zefzoufi Manal [a,b], El Mansouri Az-Eddine [c], Ait El Had Mustapha [d], Bouamama Hafida [b], Belaqziz Majdouline [e,f,*], Sammama Amal [f], Outaki Meriem[g], Elmasloumi Mohamed [h,I]

[a] *Laboratory of Bioorganic Chemistry, Department of Chemistry, Faculty of Sciences, University Chouaïb Doukkali, El Jadida*
[b] *Laboratory of Sustainable Research Development and Health, Faculty of Sciences and Techniques, University Cadi Ayyad, Marrakech*
[c] *Department of Chemistry, University of the Free State, P.O. Box 339, Bloemfontein 9300, South Africa*
[d] *Department of Fundamental Sciences, Faculty of Medicine and Pharmacy, and Dentistry of Fez, Sidi Mohamed Ben Abdellah University of Fez, Morocco*
[e] *Laboratory of Water, Biodiversity and Climate Change, Faculty of Sciences Semlalia, University Cadi Ayyad, Marrakech*
[f] *Platform chromatographic, Innovation City, University Cadi Ayyad, Marrakech*
[g] *Laboratory of Applied Chemistry and Environment, Faculty of Sciences and Technologies, University Hassan I, Settat*
[h] *Laboratory SCIMATOP Faculty of Sciences Semlalia, University Cadi Ayyad, Marrakech*
[I] *TCPAM, Polydisciplinary Faculty of Sciences University Sultan Moulay Slimane, Beni-mellal*

ARTICLE INFO:

Received 3 Feb 2024
Revised form 9 Apr 2024
Accepted 20 May 2024
Available online 29 Jun 2024

Keywords:
Analytical method
Alkaloids and phenolic compounds
Ultra-high-performance liquid chromatography
Tandem electrospray ionization mass spectrometry
Berberis vulgaris

ABSTRACT

Among the natural products, phenolic and alkaloid compounds have the most important constituents and common plant-derived secondary metabolites, and thus, analysis deserves particular attention for their therapeutic proprieties. In this study, the phenolic and alkaloid compounds were analyzed using ultra-high-performance liquid chromatography coupled with diode array detector-tandem electrospray ionization mass spectrometry (UHPLC/DAD/ESI-MS) for three extracts of Moroccan *Berberis vulgaris L*. Then we optimized and validated results for four phenolic compounds. To evaluate the biological activity of this species we chose the antimicrobial activity. For the antimicrobial activity of these extracts, we used molecular docking analysis of the compounds identified with DNA gyrase. The method validation results showed a good linear (R^2>0.99) with the coefficient correlation and the significance of regression tests confirmed a linear relationship between x and y. Two concentrations of phenolic and alkaloid compounds (31.25 mg L^{-1} and 500 mg L^{-1}) were determined by the UHPLC/DAD/ESI-MS and used in repeatability tests, the relative standard deviation of 10 repetitions varied to 0.35-2.33 with CV% 1.1-2%. In addition, the analytical method is sensitive, accurate, and precise (CV<5%). The analytical method successfully set for robust quality evaluation and standardization of phenolic and alkaloid compounds from *B. vulgaris* organic extract.

1. Introduction

Plants such as vegetables, fruit, and spices/medicinal herbs play an important role in degenerative diseases. However, it is not yet clear which constituent is responsible for this. Many medicinal plants contain chemical compounds such as flavonoids and alkaloids exhibiting antimicrobial properties. In Moroccan medicine, *Berberis vulgaris* belongs to the family of Berberidaceae locally named “Aghriss” and is used for her antipyretic,

*Corresponding Author: Belaqziz Majdouline
Email: m.belaqziz@uca.ac.ma
https://doi.org/10.24200/amecj.v7.i02.284

hepatoprotective, and anti-inflammatory properties [1]. In Iranian traditional medicine, it is used for an enlarged spleen, eye sores, asthma, and skin pigmentation (reference). A decoction of barberry and Emblic myrobalan combined with honey is prescribed to treat acrid urine or painful micturition from bilious [2]. *B. vulgaris* is mainly used as a food cooked with rice and *B. integerrima*, also referred to as black barberry and wild barberry, is used mainly for juice extraction in food industries and as medication [2]. The therapeutic properties of *B. Vulgaris* are probably due to the presence of secondary metabolites like phenolic compounds and alkaloids. To explore these natural sources, several phytochemical and pharmacological studies of Berberis species have been conducted. The presence of many families of natural compounds has been described in the different parts of these plants; alkaloids [3,4, 5], flavonoids [5, 6], fatty acid, and terpenoids [2]. Several studies have been conducted on the biological activities of Berberis species including; anticancer [7] and antioxidant activities [3]. The family of Berberidaceae is known for its strong biological activities. Recently work showed that Ethanol and ethyl acetate extracts of Berberis vulgaris have a higher cytotoxic effect against human breast adenocarcinoma cell line (MCF-7) using the MTT method which indicated their important anticancer capacity[3]. Some alkaloids, including oxyaconthine, berberine, berbamine, brolicin, and columbamine, are present in all of the organs of *B. vulgaris*. Compared to other *B. vulgaris* organs, the root bark contains more alkaloids. One of the plant's most significant alkaloids, berberine, may be useful in preventing coronary artery disease and perhaps lowering triglyceride and total cholesterol levels [2]. Various research showed that polyphenols and alkaloids are extensively used in the pharmaceutical, cosmetic, and food industries due to their various biological activities. Many chromatographical methods like UHPLC/DAD/ESI-MS have been used for the analysis of these compounds. Also, the phenolic and alkaloid compounds, organic compounds such as toluene, benzene, xylene, styrene, and dyes were determined based on nano adsorbents such as bismuth oxide-fullerene nanoparticles, nano-carbon structure, aminopropyl trimethoxysilane-phenanthrene carbaldehyde on graphene oxide, ionic liquids, heterogeneous graphene/graphene oxide, and hydroxyethyl methylimidazolium tetrafluoroborate immobilized on MWCNTs by gas chromatography-mass spectrometry (GC-MS) of gas chromatography flame ionization detection (GC-FID)[8-16].

The present study aims to characterize and validate the phenolic and alkaloid compounds from *B. vulgaris* native to Morocco extracts by the UHPLC/DAD/ESI-MS method. Therefore, this paper describes for the first time the molecular docking analysis and antibacterial activity of Morrocan *B. vulgaris* root extracts.

2. Material and Methods

2.1. Plant material and preparation of extracts

B. vulgaris root samples were collected from Ourika (30 km from Marrakech City, Morocco) in February 2022. The roots were dried at room temperature. Aqueous extracts were prepared by maceration of 10 g of dried roots in 300 mL sterile distilled water for 24 h and following filtration of particulate matter. 10 g of roots was extracted with acetonitrile 80% and methanol 80% separately for 48h.The extracts were evaporated to dryness in a vacuum by a rotary evaporator.

2.2. Chemicals and Reagents

Acetonitrile (HPLC grade ≥ 99.9 % from Honeywell Riedel-de Haen, Germany, CAS Number: 75-05-8) is used as solvent B and 0.1 % formic acid (98 % for LC-MS, Merck Germany, CAS Number: 64-18-6) aqueous solution (ultra-pure water from Pure Lab) is used as solvent A. The phenolic compounds (Gallic acid: CAS Number: 149-91-7, Caffeic acid: CAS Number: 331-39-5, P-coumaric acid: CAS Number: 501-98-4, and Rutin: CAS Number: 207671-50-9) were purchased from Merck (Germany).

2.3. UHPLC-DAD-ESI/MS Analysis

The examined extracts were analyzed using UHPLC-

DAD-ESI/MS. Chromatographic separation was carried out using a triple quadrupole mass spectrometer with heated-electrospray (H-ESI) (TSQ Endura, Thermo Fisher Scientific, CA, USA) and the Dionex Ultimate 3000 system (CA, USA). The suggested technique was carried out using a Kinetex C18 reversed-phase column (250 x 4.6 mm, 2.6 m particles, Thermo Fisher Scientific). The mobile phases have acetonitrile as solvent B and formic acid as solvent A in concentrations of 0.1% each. Following are the multiple-step gradients used: With a flow rate of 1 mL min^{-1} and an oven temperature of 25°C, the time intervals are as follows: 0–2 min, 2% B; 2–20 min, 2-25% B; 20–25 min, 25–35% B; 25–28 min, 35–95% B; 28–30 min, 95–95% with a final plateau of 2 min, 2% B. The range of the UV-Vis spectra that were recorded in the range 220–800 nm and chromatograms were also acquired to 350 nm. The capillary temperature was 295◦C. The MS/MS experiments were performed on some selected precursor ions with energy of fragmentation is 50V in negative ion mode with 2500V and the analyses were performed in full scan mode in the range of 100–1000 m/z[17].

2.4. Antibacterial test

In this study, two types of bacteria were tested: Escherichia coli (ATCC 25922), a Gram-negative bacteria, and Staphylococcus aureus (ATCC 25923), a Gram-positive bacteria. The Pasteur Institute (Casablanca, Morocco) provided the bacterial strains. They were kept alive by recurring subcultures and stored at +4 °C before usage.

2.4.1.Disc diffusion method

The agar disc diffusion method was carried out according to the directions provided by Smaili et al. [18]. In a nutshell, Mueller-Hinton agar was updated with 3.10^8 CFU mL^{-1} of bacteria before sterile cellulose discs of 6 mm diameter were placed on it. These discs were impregnated with 10µL of the extracts at a concentration of 500 $\mu g.mL^{-1}$ dissolved in DMSO. A disc containing the common antibiotic tetracycline served as the positive control, and a disc containing DMSO served as the negative control. 24 hours after being incubated at 37 °C. By measuring the inhibitory diameter around the discs in comparison to the common antibiotic, it was possible to quantify how susceptible the harmful bacteria were to the examined chemicals. All experiments were done in triplicate and the results were expressed in mean value ± standard deviation.

2.4.2.Determination of minimum inhibitory concentration (MIC)

The determination of the minimum inhibitory concentration assay was performed using 96-well microdilution plates as described by Anthony et al. [19]. Two-fold serial dilutions of extract products were made in Mueller-Hinton ((3.9-1000 μgmL^{-1}) at a volume of 100 µL /well in 96-well microtiter plates. Each well was then inoculated with 10 µL of the bacterial culture (adjusting the turbidity to reach an optical density of 0.5 McFarland standards). Optical density readings were taken at 24-hour intervals. Experiments were conducted in triplicates each. Positive controls (samples in nutrient broth with no bacterial inoculation) and negative controls (nutrient broth inoculated with inoculum but no samples were included). Turbidity was monitored by measuring absorbance/ optical density at 600 nm (OD600) of the UV-Vis spectrophotometer and corrected by subtracting the background absorbance of the positive control.

2.5. Molecular docking analysis

In silico computational docking studies were performed using AutoDock. The X-ray crystallographic structure of DNA Gyrase B was downloaded from the RCSB Protein Data Bank (RCSB PDB) ID: 4URO. The protein was prepared separately by removing water and co-crystalized ligand bounds with the protein to make receptors free of any ligands before docking. Then, Polar hydrogen and Gastieger charges were added using the MGL Tools (Molecular Graphics Laboratory), and proteins saved in PDBQT format (Protein Data Bank, Partial Charge (Q), and Atom Type (T)). Ligands' structures were created separately using

ChemDraw Ultra 12.0, energy was minimized in Chem3D, and torsional bonds of ligands were set flexibly and saved in PDBQT format. Next, the receptor was kept rigid, and the grid covering all the amino acid residues present inside the active site of proteins was built (grid box size of 30Å x 40Å x 32Å with a spacing of 0.375 Å between the grid points and centered at -0.97 (x), 0.152 (y) and -12.373 (z)). The best conformers were searched by the Lamarckian genetic algorithm (LGA), the population size was set to 150 and the maximum number of energy evaluations was set to 25000000. Finally, the results were analyzed and visualized by Discovery Studio. In molecular docking results, the tetrahydroberberine, berberines, and reticuline as major identified compounds in *B. vulgaris* roots show comparable residual interactions (GLU58, ARG84, PRO87, and ARG144) and docking score of novobiocin.

2.6. Statistical analysis

Statistical analysis was carried out of one-way analysis of variance (ANOVA) test using a statistical package program (SPSS version 23.0) and the significance of the difference between means was followed by the Tukey test, using $p < 0.05$ as the level of significance. Data were expressed with Mean ± Standard error of three parallel measurements.

3. Results and Discussion

Several research reported the UHPLC methods for the characterization of phenolic compounds and alkaloids, in medicinal plants, use organic solvents for their extraction like methanol and acetonitrile[20, 21]. However, most people use the infusion method (water) for the extraction of many secondary metabolites [21]. For this reason, in the present study, we proposed a UHPLC/DAD/ESI-MS method which can be used for aqueous extracts and methanolic, acetonitrile extracts and applied for the analysis of *B. vulgaris* growing in Morocco, to identify and quantify the alkaloids and phenolic compounds in the same method analysis.

3.1. UHPLC-DAD-ESI/MS Analysis

Methanol 80%, acetonitrile 80%, and aqueous extracts of *B. vulgaris* roots were analyzed by UHPLC/DAD/ESI-MS. The chromatographic profiles obtained are given in Figure 1. Under the same chromatographic conditions carried out, 6 peaks were detected in the various extracts of *B. vulgaris* roots (Table 1). The identification of these peaks was based on their UV characteristics and by comparing their mass spectra $(M-H)^-$ with those reported in the literature (Table 1 and Fig. 1) For the convenience of explanation, the 6 identified compounds have been classified into two classes of secondary metabolite namely: alkaloids, and phenolic compounds (Table 1). The profile chromatographic of the aqueous extract showed the predominance of protoberberine alkaloids (m/z 335.2087) with fragment ion m/z 320 (M-H- 15Da) and 305 (M-H- 30Da) loss of two methyl (CH3), followed by glycoside flavones Rutin (m/z 609.1085), the typical ions fragments (m/z 301) corresponding to quercetin was observed in MS^2 mode. We identified tentatively tetrahydroberberine (m/z 339.1064) with an ion fragment (m/z 335.108) corresponding to berberine. The UHPLC-DAD-ESI/MS chromatogram of the acetonitrile 80% showed the presence of two subgroups of phenolic compounds notably, phenolic acid (gallic acid; m/z 169.1052) and flavonol glycosylated (rutin; m/z 609.1085), In addition the acetonitrile 80% extract rich on benzylisoquinoline compounds notably reticuline (m/z 328.4039) with ion fragment m/z 192.021. Likewise, berberine and tetrahydro berberine were identified in acetonitrile and methanol 80% extracts. As can be seen in Figure 1, the reticuline was found only in methanol and acetonitrile extracts. Also, we identified tentatively the Guaijaverin and arabinose quercetin (m/z 433.1059) in three *B. vulgaris* extract.

Based on the literature the most important compound in Berberis species is Berberine, many research revealed that this compound can be effective in preventing coronary artery disease and possibly reducing the levels of total cholesterol

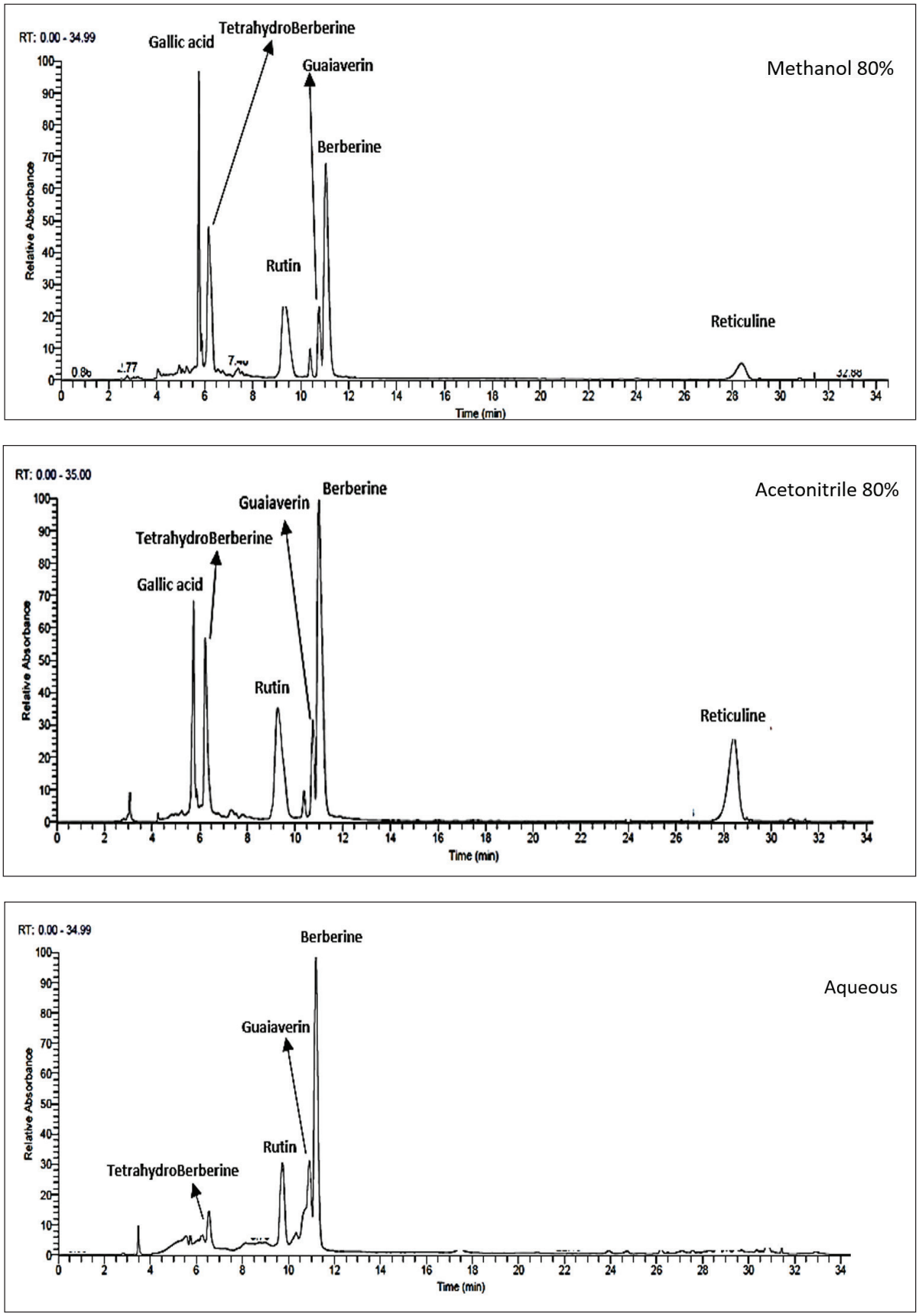

Fig. 1. Profil chromatographic Berberis vulgaris extracts at 350 nm

Table 1. Tentatively identification of phenolic compounds and alkaloids from *B. vulgaris* extracts

RT	Λ_{max} (nm)	m/z experimental	m/z calculated	Mass error (mDA)	MS/MS fragments	Proposed compound	Molecular formula	Reference
5.74	210/272	169.1052	169.0169	-0.088	125/ 107/ 97/ 79/ 69	Gallic acid	$C_7H_6O_5$	This work
6.55	225/258/360	3391064	339.1228	-0.016	335/308/110	Tetrahydroberberine	$C_{20}H_{21}NO_4$	[22]
9.45	255/355	609.1085	609.2959	-0.187	300 /169	Rutin	$C_{27}H_{30}O_{16}$	[5]
10.9	227/274/355	433.1059	433.0776	-0.028	300	Guaijaverin	$C_{20}H_{18}O_{11}$	[5]
11.2	225/257/350	335.2087	335.1230	-0.085	308/231/110	Berberine	$C_{20}H_{18}NO_4$+	[22]
28.88	235/286/350	328.4039	328.3125	-0.091	207/192	Reticuline	$C_{19}H_{23}NO_4$	[22]

and triglyceride. In addition, berberine has been reported protective effects on the central nervous system and helps to treat diseases of this system [2]. Reticuline is one of the alkaloids that possesses potent central nervous system depressing effects and a higher anti-inflammatory effect. When we compared our results with the literature, we found it similar. A few studies reported the presence of reticuline in berberis species, but only the authors [22] have been identified benzylisoquinoline alkaloids (reticuline) in berberis microphylla. Another work, [5] reported the presence of Rutin, berberine, Guaijaverin, citric acid, and palmatine in *Berberis iliensis* extract. Concerning alkaloids, in the first report we detected the presence of reticuline in *B. vulgaris*. As can be seen in our results, rutin and guaijaverin are the derivative of quercetin while, rutin is quercetin-3-O-rutinoside and guaijaverin is quercetin 3-O-arabinose. Besides alkaloids, three phenolic compounds (Guaijaverin, gallic acid, and rutin) were identified for the first time in Moroccan *B. vulgaris* roots.

Based on the characterization results of three extracts of B.vulgaris we optimized and validated a UHPLC/DAD/ESI-MS method for four phenolic compounds: gallic acid, p-coumaric acid, caffeic acid, and Rutin

3.2. Statistical methods

3.2.1.Specificity, Linearity, Repeatability and Reproducibility

For specificity, multistandard solutions such as gallic acid, caffeic acid, rutin, and p-coumaric acid were characterized by UHPLC/DAD/ESI-MS [23]. For linearity**,** three series of standard stock solutions at 5 concentration levels were used (31.75, 61.5, 125, 250, and 500 mgL^{-1}). Three repetitions for each level of each series were performed by UHPLC/DAD/ESI-MS. To evaluate the linearity test we used six assays as the test of intercept, the nullity of the slope, the significance of slope, the Cochran test, the significance of the regression, and the coefficient correlation [24]. For repeatability, two concentration levels (31.75 and 500 mg L^{-1}) were measured by the same operator and characterized by UHPLC/DAD/ESI-MS. Ten repetitions were performed for each level on the same day. We calculated the average, standard deviation, and coefficient of variation (CV%) of ten measurement [25]. As reproducibility**,** for 3 days, a series of multi-standard solutions with five concentration levels (31.75, 61.5, 125, 250, and 500 mg L^{-1}) was prepared by the same operator. Three repetitions for each level of each series were performed by UHPLC/DAD/ESI-MS[24].

3.2.2.Statistica Tests

In the intercept test, The following inequality will make it possible to establish the correlation from our right with zero (Equation 1). For the nullity of the slope test, we used Equation 2. For the test of the significance of the slope, we used Equation 3. For the Cochran test, we used Equation 4. The purpose of this test is to verify the homogeneity of the variances constituting

the experimental error and thus detect the presence of suspicious values. For the test of the significance of the regression, F was calculated using the LINEST function in Microsoft Excel, and the acceptance criteria were calculated when the slope was not different from zero if $F_{calculated} \leq F_{(1-\alpha,\ 1,\ k-2)}$. Also, the coefficient correlation is calculated by Equation 5.

$$tc = \left|\frac{b}{Sb}\right| \qquad \text{(Eq. 1)}$$

b: intercept; Sb: Standards deviation of intercept; tc: T calculated

Acceptance criteria:_The line passes through the origin if $t_{calculated} \leq t_{(1-\alpha/2,\ k-2)}$

$$tc = \left|\frac{a}{Sa}\right| \qquad \text{(Eq. 2)}$$

a: slope; Sb: Standards error of slope; tc: T calculated

Acceptance criteria:_The slope is null if $t_{calculated} \leq t_{(1-\alpha/2,\ k-2)}$

** One-tail student test: Equation of regression curve: (y: area; x: concentration mg L^{-1}) / α: risk = 0.05 / k: number of concentration levels

$$F = \frac{Si^2}{Sr^2} \qquad \text{(Eq. 3)}$$

Si^2: variance due to linear regression; Sr^2: residual variance which represents the difference between the theoretical value and the actual value

Acceptance criteria: The slope is not significant if $F_{calculated} \leq F_{(1-\alpha,\ 1,\ Nk-2)}$;

One-tail Fischer test: Equation of regression curve: (y: area; x: concentration mg L^{-1})

$$C = \frac{S^2max}{\sum S^2j} \qquad \text{(Eq. 4)}$$

$S^2_{max:}$ highest variance of j groups; S^2j: Variance of j groups

Acceptance criteria:_There is a homogeneity of variances if $C_{calculated} \leq C_{(1-\alpha,\ s,\ nk-1)}$

$$Sr = \sqrt{\left(\frac{1-Coefficient\ of\ determination}{n-2}\right)}$$

$$to = \sqrt{\left(\frac{R}{Sr}\right)}$$

(Eq. 5)

With: n: number of repetitions; R: coefficient of determination

Acceptance criteria:_if $t_{calculated} > t_{(1-\alpha/2,\ k-2)}$ there is a linear relationship between x and y

α: risk = 0.05 / s: Number of series / n: number of repetitions per level in the series/ k: number of concentration levels / N: number of repetitions per level all series combined

3.2.3.Detection and quantification limit

Ten repetitions for the control (acetonitrile) were performed by UHPLC/DAD/ESI-MS and detection and quantification limits (DL/LOD and QL/LOQ) were calculated using Equations 6 and 7 [25].

$$DL = 3 \times h_{max} \times R \qquad \text{(Eq. 6)}$$

$$QL = 10 \times h_{max} \times R \qquad \text{(Eq. 7)}$$

h_{max}: Average of h_{max} of each repetition of the control sample (10 repetitions in total)

Factor R: quantity/signal of peak

3.3. Validation method

Validation of four phenolic compounds, gallic acid, p-coumaric acid, caffeic acid, and rutin was conducted on UHPLC/DAD/ESI-MS analysis. We estimated various tests like specificity, linearity, repeatability, intermediate precision and detection, and quantification limits.

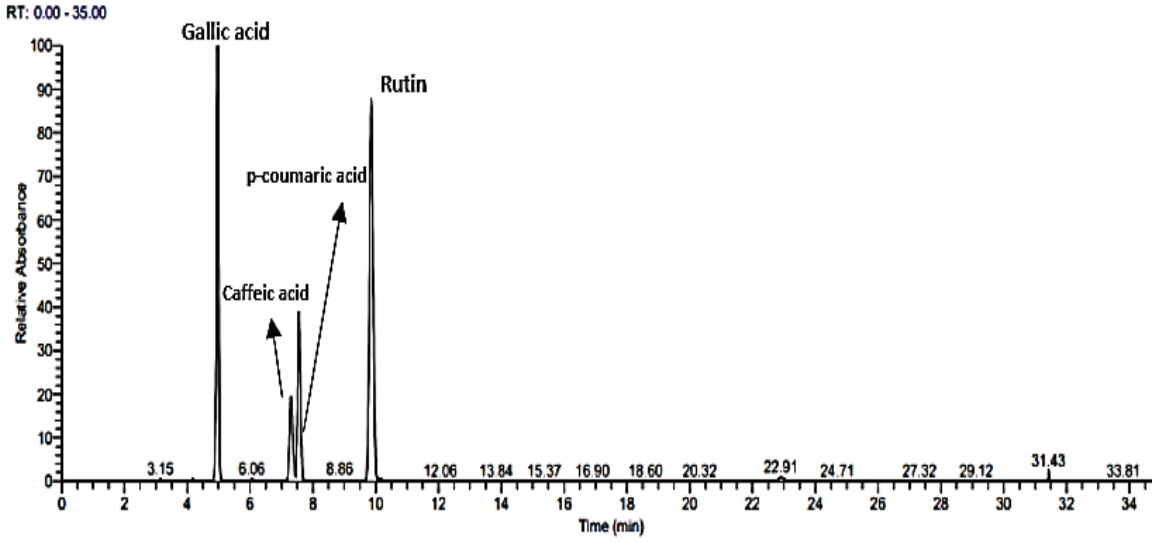

Fig. 2. Profil chromatographic of multi-standards solution at 350nm

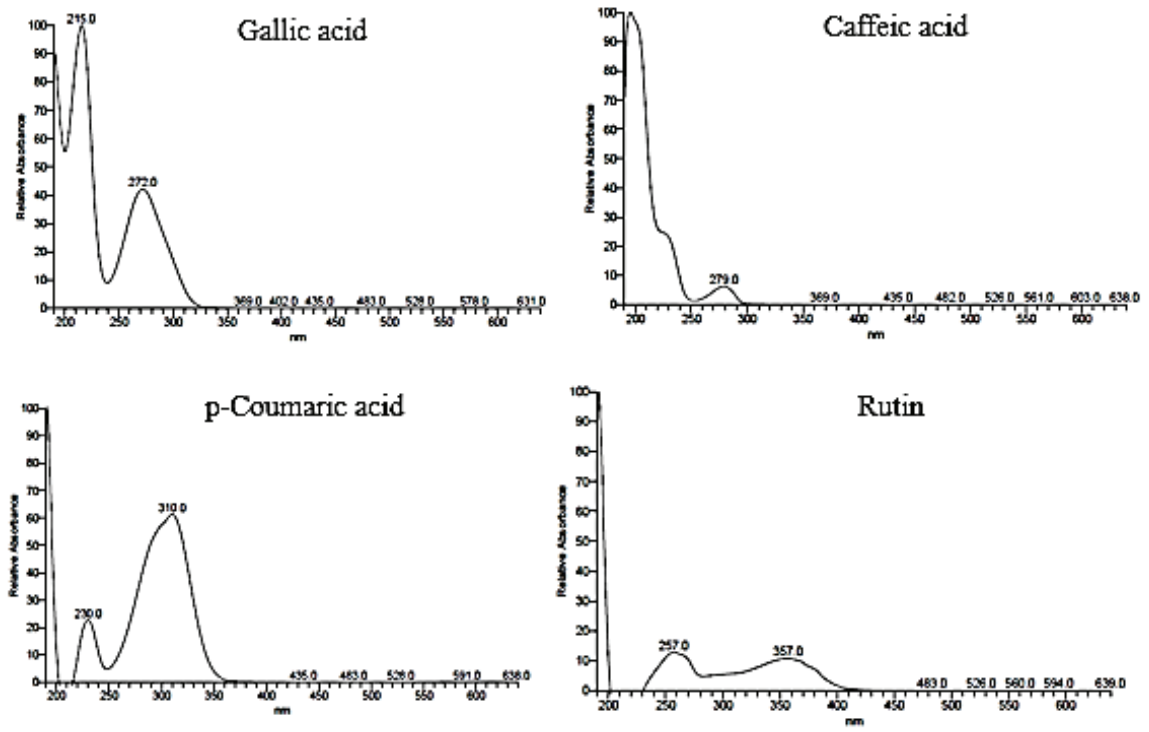

Fig. 3. UV spectrum of four phenolic compounds at 350nm

3.3.1. The specificity

The chromatograms show that the separation of all four phenolic compounds was successfully achieved with good resolution. Additionally, no interfering peaks were observed in Figures 2 and 3.

3.3.2. Linearity tests

Linear regression was plotted between standard concentration and peak area. These plots were found to be linear with a correlation coefficient (R^2) in the range of 0.993 to 0.997. In this study, we

calculated various parameters like the coefficient of determination (R^2), slope, intercept, and standard deviation and we deduced six approaches such us: a test of intercept, the test of the nullity of the slope, a Test of the significance of slope, Test of the significance of regression, Test of Coefficient correlation and Cochran test (Table2).

The regression was found in Equations 8-11.

(gallic acid): y=14708746,13x+155441,9785 (Eq. 8)

(caffeic acid): y=4399929,254x+28863,56444 (Eq. 9)

(p-coumaric acid): y=8097205,429x+55936,00681 (Eq. 10)

(rutin): y=22760604,74x+227220,6614 (Eq. 11)

the linearity method was evaluated by considering retention time precision, R^2 values which are superior to 0.96 for all the compounds tested and can confirm the linearity of the method.

The coefficient correlation and significance of regression tests confirmed that there is a linear relationship between x and y with calculated values

Table 2 .Linearity parameters for selected phenolic compounds using UHPLC/DAD/ESI-MS

Standards		**Gallic acid**	**Caffeic acid**	**p-Coumaric acid**	**Rutin**
Slope a		14708746,13	4399929,254	8097205,429	22760604,74
The standard deviation of the slope a		669530,3449	139784,4542	258921,3805	629993,4294
Intercept b		155441,9785	28863,56444	55936,00681	227220,6614
The standard deviation of intercept b		172787,5609	36074,56344	66820,56183	162584,159
Coefficient of determination R^2		0,993822407	0,996981198	0,996941865	0,99770687
number of degrees of freedom		3	3	3	3
square sum residual (residual variation)		1,95418E+11	8518085198	29225372620	1,7302E+11
Test of intercept	T	0,899613246	0,800108489	0,8371077	1,397557196
	t(0,975, 3)	3,1824			
	Conclusion	The line passes through the origin			
Test of nullity of the slope	T	21,97	31,48	31,27	36,13
	t(0,975, 3)	3,1824			
	Conclusion	The slope is different from zero, there is a linear relationship between x and y			
Test of the significance of slope	F	26011,31	23034,82	23098,18	33126,60298
	F(0,95, 1, 43)	4,08			
	Conclusion	The slope is different from zero, there is a linear relationship between x and y			
Test of the significance of regression	F	482,1	990,77	977,9	1305,26
	F(0,95, 1, 3)	10,13			
	Conclusion	there is a linear relationship between x and y			
Cochran test	C	0,76	0,78	0,83	0,84
	C(0,95;5;2)	0,877			
	Conclusion	The homogeneity of variances is confirmed			
Test of Coefficient correlation	T	21,97	31,48	31,27	36,13
	t(0,975, 3)	3,1824			
	Conclusion	there is a linear relationship between x and y			

of each compound ≤ t critical (3.1824) and > F critic (10.13) respectively. The Cochran test confirmed the homogeneity of variances with C values of gallic acid (0.76), p-coumaric acid (0.78), caffeic acid (0.83), and Rutin (0.84) inferior to C critical (0.877). As can be seen in Table 2**,** the nullity of the slope and significance of the slope test revealed that the slope is different from zero with t values of each standard superior to t critical (3.1824) and F calculated superior to F critical (4.08) according to student and Fischer test respectively. In our study, the six approaches confirm the linearity of the method. Comparatively with the literature[26], mentioned that the method validation of phenolic compounds using UHPLD/DAD/ESI-MS presented a good linearity with a correlation coefficient higher than 0.98 to all phenolic compounds.

3.3.3.Repeatability and Intermediate precision

Repeatability was calculated by intra-day variation from the same sample at two levels (level 1 and 5) *B. vulgaris* extracts and analyzing them ten times, for reproducibility by inter-day variation, analyzing the same sample at five levels in triplicate on three different days. Repeatability and intermediate precision methods were evaluated by calculating the standard of deviation (RSD) and coefficient of variation (CV%). The coefficient variation values ranged from 1% to 2.8% in the case of the samples analyzed on the same day and on different days (Tables 3 and 4).

The CV% during intra-dayis less than 5% for gallic acid (1.39-2.8%), caffeic acid (1.17-1.48%), p-coumaric acid (1.06-1.15%), and rutin(1.19-1.32%) which is acceptable. The intermediate precision of the analysis method was also measured by calculating %CV of inter-day precision of four standards, which were found in the range of 1.15 to 2.8% (Table 4)

Table 3. Repeatability parameters for phenolic compounds using UHPLC/DAD/ESI-MS

Standards	**Gallic acid**		**Caffeic acid**		**p-Coumaric acid**		**Rutin**	
Concentration (mg L^{-1})	31.25	500.00	31.25	500	31.25	500	31.25	500.00
*Average (mg L^{-1})	31.46	507.27	29.54	502.70	33.07	502.80	31.32	502.54
*SD (mgL^{-1})	0.82	0.70	0.42	2.33	0.35	2.49	0.41	0.63
(CV)	2.80	1.39	1.48	1.17	1.06	1.15	1.32	1.19
Repeatability (r)	2.28	1.96	1.18	5.21	0.98	6.92	1.15	1.96

*10 repetitions

Table 4. Intermediate precision parameters for selected phenolic compounds using UHPLC/DAD/ESI-MS

Concentration (mgL^{-1})		**0.03125**	**0.0625**	**0.125**	**0.25**	**0.5**
Gallic acid	CV (%)	2.8	1.61	0.38	1.47	1.36
	Reproducibility	1.98	2.38	1.25	5.95	2.96
Caffeic acid	CV (%)	1.48	1.53	0.28	1.38	1.17
	Reproducibility	1.28	1.54	0.54	5.11	5.21
p-Coumaric acid	CV (%)	1.06	1.39	0.04	1.18	1.15
	Reproducibility	0.98	2.5	0.15	6.99	6.94
Rutin	CV (%)	1.32	1.31	0.21	1.21	1.19
	Reproducibility	1.15	4.45	1.15	2.94	1.96

3.3.4.LOQ and LOD Analysis

LOD and LOQ were determined to define the sensitivity of the developed method. Detection and quantification limits were calculated using signal-to-noise ratios (S/N) of ten replicates. LOD and LOQ with their respective for gallic acid (0.35 and 4.38 mg L^{-1}), caffeic acid (0.32 and 3.57 mg L^{-1}), p-coumaric acid (0.1 and 3.62 mg.L^{-1}), and rutin (0.06 and 2.22 mg L^{-1}) (Table 5). When we compared our results with the literature we found similar results with other method validation, for example[27], reported a lower detection and quantification limit in the method validation of phenolic compounds analysis.

3.4. Antibacterial activity

The antibacterial effect of *Berberis vulgaris* extracts against *E coli and staphylococcus aureus*, are shown in Table 6. The formation of inhibition zones around the wells shows bacterial sensitivity to antibacterial and antibiotics (which are used as positive controls). The positive control used in the well was a tetracycline. These results revealed that the antibacterial activity against *E coli* and *staphylococcus aureus* was increased in acetonitrile 80% extract. However, lower antibacterial activity against E coli and *staphylococcus aureus* was indicated in the inhibition zone diameter equal to 7mm and 9 mm respectively, in methanol 80% extract.

Based on the literature, previous studies have also reported the antibacterial activity of *Berberis vulgaris*, Kazemipoor, et al [28] revealed that the ethanol extract of leaves and fruits showed moderate antibacterial activity against *streptococcus sp* with the diameter zone inhibition increase from 7mm to 13mm. Another work[29], reported that ethanolic extracts from Berberis vulgaris have a higher antibacterial capacity against *E coli and Staphylococcus aureus.* The Minimum inhibitory

Table 5. Data used for the calculation of the detection and quantification limits[27]

Standard	Gallic acid	Caffeic acid	p-Coumaric acid	Rutin
Retention time (min)	5.76	7.14	7.68	9.47
Detection limit (mg L^{-1})	0.35	0.32	0.10	0.06
Quantification limit (mg L^{-1})	4.38	3.57	3.62	2.22

Table 6. Inhibition zone (mm) of three *B. vulgaris* extracts and antibiotic against two pathogenic bacteria

Compound	Inhibition zones (mm)	
	***E. coli* (ATCC 25922)**	***S. aureus* (ATCC 25923)**
Methanol 80%	9±0.1	8±0.57
Acetonitrile 80%	15±0.15	13±0.14
Aqueous	11±0.11	10±0.2
Tetracycline	20±0.028	19±0.05
DMSO	------	------

Table 7. Minimum inhibitory concentration (MIC) ppm of samples

Bacteria	Methanol 80%	Acetonitrile 80%	Aqueous	Tetracycline
E coli	250 ± 0.05	62.5± 0.11	250±0.50	50±0.3
SA	500± 0.02	125± 0.07	250±0.06	25±0.08

concentration test of aqueous, methanol 80%, and acetonitrile 80% extracts was determined by E. *coli* and *Staphylococcus aureus*. These results have been reported in Table 7. The acetonitrile 80% extract exhibited a higher activity with MIC values ranging from 62.5 and 125 µg mL^{-1} against *E coli and Staphylococcus aureus(SA),* respectively.

3.5. Molecular docking analysis

The molecular docking of the identified compounds was performed to understand the mechanism of antimicrobial activity and explain the obtained results. Thus, gallic acid, caffeic acid, p-coumaric acid, tetrahydroberberine, berberine, rutin, and reticuline were docked to the active site of DNA gyrase protein (4RUO) and compared to the potential inhibitor novobiocin. Indeed, DNA gyrase plays a crucial role in bacterial survival and is considered a target of antibacterial agents [30]. First, our docking protocol was validated by redocking the cognate ligand (novobiocin) on the crystal structure 4URO. The RMSD (root-mean-square deviation) between expected and actual poses is 0.86 Å (<2 Å). Thus, the selected protocol is suitable for reproducing the native poses. All molecular docking results are summarized in Table 8 and Figures 4-6. The eight products displayed minimum binding energies ranging from −3.63 to −7.36 kcal/mol. For instance, tetrahydroberberine, berberines, and reticuline have comparable estimated free energy of binding compared to novobiocin. As a result, they are the most potent inhibitors of DNA

Table 8. Binding affinities and potential molecular interactions of identified compounds with DNA Gyrase

Product	E (Kcal mol^{-1})	Ki (µM)	Hydrogen Bonds Interactions	Electrostatic Interactions	Hydrophobic Interactions
Gallic acid	-3.63	2190	ARG144, GLY85, GLU58, ASP81	GLU58	ILE86 (×2), GLY85
Caffeic acid	-5.1	183.75	ARG144, GLY85, ASP81 (×2)	GLU58	ILE86
p-coumaric acid	-6.11	248.08	,ARG144, GLY85 ASP81	GLU58	ILE86, ASN54
Tetrahydro-berberine	-7.36	4	ARG144, GLY125	GLU58, ARG84	ILE86 (×3), PRO87 (×2), ARG84 (×2)
Berberine	-7.37	3.9	ARG144, ASP81	GLU58, ARG84	ILE86 (×4), PRO87 (× 3), ARG84 ,(×2), ASN54, SER55, GLY85 ILE175 (×2)
Rutin	-3.97	1230	ARG84, GLY85, GLY125, ASP81 GLU58 (×2), ASP57, ASN54(×3), PRO87	GLU58	ILE86 (×5), PRO87, ASN54, SER55, GLY85 (×2), ILE102
Reticuline	-7.14	5.8	,ARG144 (×2), ASP81 GLU58, ASN54 (×2), ASP57	ARG84	ILE86,PRO87 (×2), ARG84
Guaijaverin	-5.66	70.84	ARG144 (×3), GLU58, ASP81 (×2)	GLU58	ILE86 (×2), PRO87
Novobiocin	-8.57	0.52	ARG144 (×3), GLN91, ASN54, ASP89, SER55	GLU58, ARG84 ,(×2) ARG144, ,ARG200	PRO87 (×4), ARG84 (×2),ILE102 ,(×2) ALA98

E = Estimated Free Energy of Binding Ki = Estimated Inhibition Constant

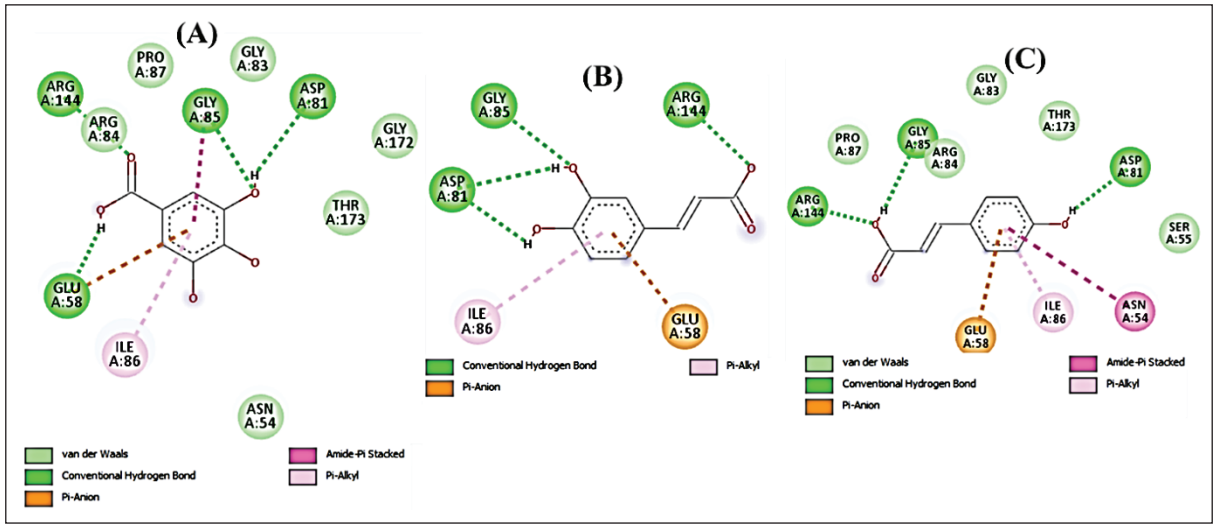

Fig. 4. 2-D interactions of Gallic acid (A), Caffeic acid (B), and p-coumaric acid (C) with DNA Gyrase

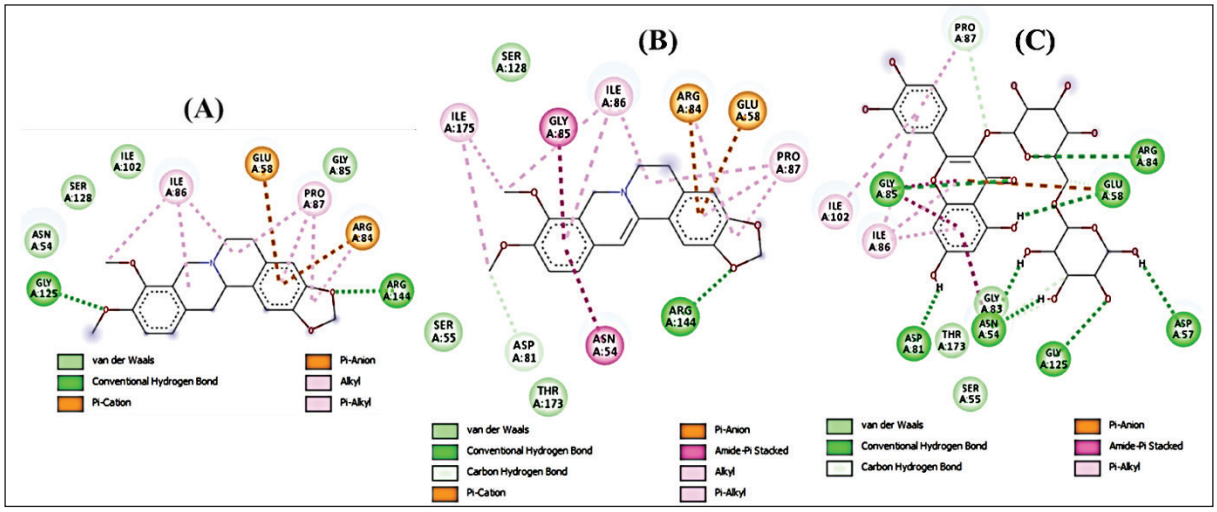

Fig. 5. 2-D interactions of Tetrahydro-berberine (A), Berberine (B), and Rutin (C) with DNA Gyrase

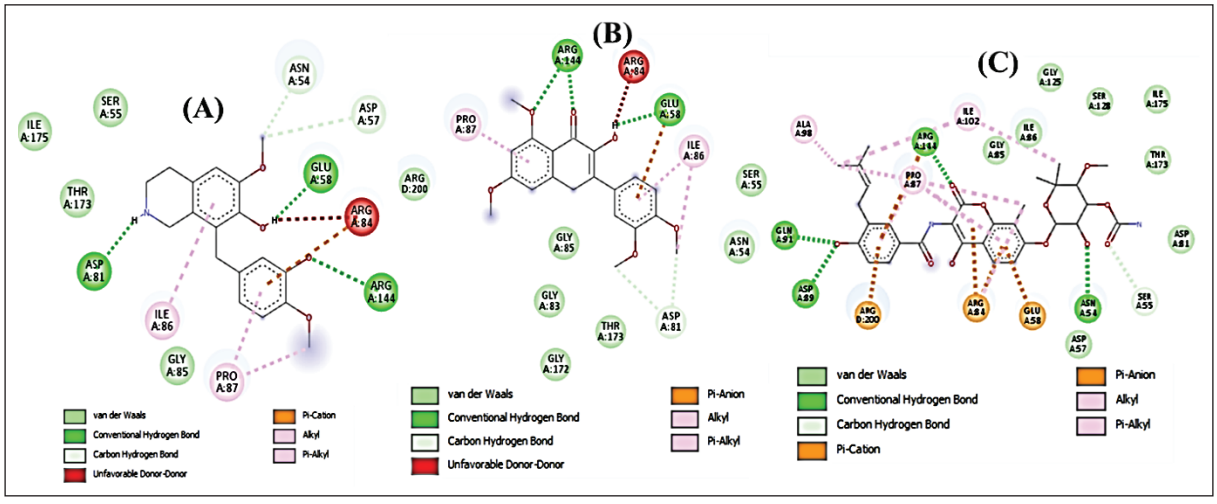

Fig. 6. 2-D interactions of Reticuline (A), Guaijaverin (B), and Novobiocin (C) with DNA Gyrase

gyrase, with estimated inhibition constants of 3.9 - 5.8 µM. From antimicrobial results, we notice that the acetonitrile extract is the most active compared to aqueous and methanolic solutions. This result may be explained by the fact that the potent compounds (tetrahydroberberine, berberines, and reticuline) were abundant in acetonitrile compared to the other extracts.

For the interaction studies, all compounds (except rutin) make hydrogen bonds with the crucial amino acid ARG144 as the reference inhibitor (novobiocin). Also, most products form electrostatic interactions with the amino acid GLU58 (rutin interacts with ARG84). The tetrahydroberberine and berberines make additional residual interaction with ARG84. In comparison to novobiocin, the most active ligands (tetrahydroberberine, berberines, and reticuline) have shown similar residual amino acids binding hydrophobic interactions with PRO87 and ARG84. Overall, in silico molecular docking analysis of the identified compounds matches with antibacterial results. Among analyzed compounds, tetrahydroberberine, berberines, and reticuline show comparable residual interactions and docking scores of novobiocin.

4. Conclusion

In the present study, The UHPLC/DAD/ESI-MS method was also successfully applied to *B. vulgaris* extracts and analysis which identified the phenolic compounds and alkaloid content in the same method for the first time (recovery more than 95%). The antimicrobial activity of the extracts was demonstrated by molecular docking studies of identified compounds to DNA-gyrase, and the mechanism was explained. A validation method showed good linearity, intermediate precision, repeatability and quantification, and detection limits. Our results revealed the successfully applied determination of phenolic and alkaloid compounds in medicinal plants.

5. Acknowledgments

The authors thank the Innovation City of Cadi Ayyad University (Marrakech-Morocco) for their support

6. References

[1] J. Belakhdar, La Pharmacopee Marocaine Traditionnelle, Ibis Press, MA, USA, 1998. https://redwheelweiser.com/imprints/ibis-press/

[2] M. Rahimi-Madiseh, Z. Lorigoini, H. Zamani-gharaghoshi, M. Rafieian-kopaei, Berberis vulgaris: specifications and traditional uses, Iran. J. Basic. Med. Sci., 20 (2017) 569-587. https://doi:10.22038/IJBMS.2017.8690

[3] L. El Khalki, M. Tilaoui, A. Jaafari, H. Ait Mouse, A. Zyad, Studies on the dual cytotoxicity and antioxidant properties of Berberis vulgaris extracts and its main constituent Berberine, Adv. Pharmacol. Sci., 2018 (2018) 3018498. https://doi.org/10.1155/2018/3018498

[4] I. Naaz, S.A. Ali, Identification and characterization of bioactive compound berberine in the Berberis vulgaris root extract using HR-LC-MS analysis, J. Anal. Pharm. Res., 7 (2018) 467–470. https://doi.org/10.15406/japlr.2018.07.00268

[5] S. Abdykerimova, Z. Sakipova, S. Nakonieczna, W. Koch, A. Biernasiuk, A. Grabarska, Superior antioxidant capacity of berberis iliensis—HPLC-Q-TOF-MS based phytochemical studies and spectrophotometric determinations, Antioxidants, 9 (2020) 504. https://doi:10.3390/antiox9060504

[6] L. Nuralın, M. Gürü, *Berberis Vulgaris* Fruit: Determination of phenolic compounds in extracts obtained by supercritical CO_2 and soxhlet methods using HPLC, Food. Anal., 15 (2022) 877–889. https://doi.org/10.1007/s12161-021-02136-8

[7] G. Motalleb, P. Hanachi, O. Fauziah, R. Asmah, Effect of Berberis vulgaris fruit extract on alpha-fetoprotein gene expression and chemical carcinogen metabolizing enzymes activities in hepatocarcinogenesis rats, Iran. J. Cancer. Prev., 1 (2012) 33-42. https://brieflands.com/articles/ijcm-80395.pdf

[8] C. Jamshidzadeh, A new analytical method

based on bismuth oxide-fullerene nanoparticles and photocatalytic oxidation technique for toluene removal from workplace air, Anal. Methods Environ. Chem. J., 2 (01) (2019) 73-86. https://doi.org/10.24200/amecj.v2.i01.55

[9] S. Teimoori, New extraction of toluene from water samples based on nano-carbon structure before determination by gas chromatography, Int. J. Environ. Sci. Technol., 20 (2023) 6589-6608. https://doi.org/10.1007/s13762-023-04906-9

[10] S. Teimoori, A.H. Hassani, M. Panahi, N. Mansouri, An immobilization of aminopropyl trimethoxysilane-phenanthrene carbaldehyde on graphene oxide for toluene extraction and separation in water samples, Chemosphere, 316 (2023) 3137800. https://doi.org/10.1016/j.chemosphere.2023.137800

[11] C. Jamshidzadeh, A new method for removal of hazardous toluene vapor from air based on ionic liquid-phase adsorbent, Int. J. Environ. Sci. Technol., 16 (2019) 2797-2808. https://doi.org/10.1007/s13762-018-1975-5

[12] A. Faghihi-Zarandi, J. Rakhtshah, BB. Yarahmadi, A rapid removal of xylene vapor from environmental air based on bismuth oxide coupled to heterogeneous graphene/graphene oxide by UV photo-catalectic degradation-adsorption procedure, J. Environ. Chem. Eng., 8 (2020) 104193. https://doi.org/10.1016/j.jece.2020.104193

[13] R. Ashouri, S.A. Hajiseyed Mirzahosseini, Synthesis of carbon quantum dots from olive stones for efficient adsorption of benzene from the ambient air, J. Nanostructures, 11 (2021) 480-497. https://doi.org/10.22052/JNS.2021.03.007

[14] M Arjomandi, A review: analytical methods for heavy metals determination in environment and human samples, Anal. Methods Environ. Chem. J., 2 (2019) 97-126. https://doi.org/10.24200/amecj.v2.i03.73

[15] R. Ashouri, Dynamic and static removal of benzene from air based on task-specific ionic liquid coated on MWCNTs by sorbent tube-headspace solid-phase extraction procedure, Int. J. Environ. Sci. Technol., 18 (2021) 2377-2390. https://doi.org/10.1007/s13762-020-02995-4

[16] J. Rakhtshah, A rapid extraction of toxic styrene from water and wastewater samples based on hydroxyethyl methylimidazolium tetrafluoroborate immobilized on MWCNTs by ultra-assisted dispersive cyclic conjugation-micro-solid phase extraction, Microchem. J., 170 (2021) 106759. https://doi.org/10.1016/j.microc.2021.106759

[17] M. Khatib, G. Pieraccini, M. Innocenti, F. Melani, N. Mulinacci, An insight on the alkaloid content of *Capparis spinosa L*. root by HPLC-DAD-MS, MS/MS and 1H qNMR, J. Pharm. Biomed., 123 (2016) 53–62. https://dx.doi.org/10.1016/j.jpba.2016.01.063

[18] A. Smaili, N. Mazoir, L.A. Rifai, T. Koussa, K. Makroum, A. Benharref, L. Faize, N. Alburquerque, L. Burgos, M. Belfaiza, M. Faize, Antimicrobial activity of two semisynthetic triterpene derivatives from *Euphorbia Officinarum* Latex against fungal and bacterial Phytopathogens, Nat. Prod. Commun., 12 (2017) 331-336. https://doi.org/10.1177/1934578X1701200305

[19] K.B. Anthony, N.O. Fishman, D.R. Linkin, L.B. Gasink, P.H. Edelstein, E. Lautenbach, Clinical and microbiological outcomes of serious infections with multidrug-resistant gram-negative organisms treated with tigecycline, Clin. Infect. Dis., 46 (2008) 567–570. https://doi.org/10.1086/526775

[20] H.K Ozer, Phenolic compositions and antioxidant activities of Maya nut (Brosimumalicastrum): comparison with commercial nuts, Int. J. Food Prop., 20 (2017) 2772–2781. https://doi.org/10.1080/10942912.2016.1252389

[21] F.B Pires, C.B. Dolwitsch, V. Dal-Prá, H. Faccin, D.L. Monego, L.M. Carvalho, C. Viana, O. Lameira, , F.O Lima, L. Bressan,, M.B da-Rosa, Qualitative and quantitative analysis of the phenolic content of Connarus

var. angustifolius, Cecropiaobtusa, Cecropia palmata and Mansoaalliacea based on HPLC-DAD and UHPLC-ESI-MS/MS, Rev. Bras. Farmacogn., 27 (2017) 426–433. https://doi.org/10.1016/j.bjp.2017.03.004

[22] L. Manosalva, A. Mutis, J. Díaz, A. urzúa, V. Fajardo, A. Quiroz. Identification of isoquinoline alkaloids from Berberis microphylla by HPLC ESI-MS/MS, Bol. Latinoam Caribe. Plant. Med. Aromat., 13 (2014) 323-334. https://www.blacpma.usach.cl/

[23] J. Abraham, International conference on harmonization of technical requirements for registration of pharmaceuticals for human use, in Brouder, A., Tietje, C. (Eds.), Handbook of Transnational Economic Governance Regimes. Brill, pp. 1041–1054, 2009. https://sro.sussex.ac.uk/id/eprint/24306

[24] M. Monique, B. Guilhem, Validation d'une méthode de chimie analytique : Application au dosage des anions fluorure, chlorure, nitrite, bromure, nitrate, phosphate et sulfate par chromatographie ionique, Validation des méthodes d'analyse quantitative par le profil d'exactitude, Le Cahier des Techniques de l'Inra, 2010. https://docplayer.fr/6047339-Validation-d-une-methode-de-chimie-analytique.html

[25] OIV-MA, Practical guide for the validation, quality control, and estimation of the uncertainty of an alternative oenological method of analysis, a compendium of international methods of analysis, 2005. https://www.oiv.int/public/medias/2754/oiv-ma-as1-12fr.pdf

[26] A.P. Lopes, M.E. Petenuci, M.B. Galuch, V.V. Almeida Schneider, E.A. Canesin. Visentainer Evaluation of effect of different solvent mixtures on the phenolic compound extraction and antioxidant capacity of bitter melon (Momordica charantia), Chem. Pap., 72 (2018) 2945–2953 . https://doi.org/10.1007/s11696-018-0461-3

[27] J. CarrascoSandoval, P. Rebolledo, D. PeterssenFonseca, W. Fischer Susana, A.M. Rosemarie, K. HenríquezAedo, A fast and selective method to determine phenolic compounds in quinoa (Chenopodium quinoa Will) seeds applying ultrasoundassisted extraction and highperformance liquid chromatography, Chem. Pap., 75 (2021) 431–438. https://doi.org/10.1007/s11696-020-01313-z

[28] M. Kazemipoor, P.F. Tehrani, H.Zandi, R. G.Yazdi. Chemical composition and antibacterial activity of Berberis vulgaris (barberry) against bacteria associated with caries, Clin. Exp. Dental Res., 7 (2020) 601–608. https://doi: 10.1002/cre2.379

[29] V. Jacquelyn, D. Elizabeth, C. Hee-Byung, P. John, R. Angerhofer, Antibacterial activity and alkaloid content of Berberis thunbergia, Berberis vulgaris and Hydrastis canaensis, Pharm. Biol., 41 (2003) 551-557. https://doi.org/10.1080/13880200390500768

[30] R. Ziraldo, A. Hanke, S.D. Levene, Kinetic pathways of topology simplification by Type-II topoisomerases in knotted supercoiled DNA, Nucleic Acids Res., 47 (2019) 69–84. https://doi:10.1093/nar/gky1174

Anal. Methods Environ. Chem. J. 7 (2) (2024) 45-58

AMECJ

Research Article, Issue 2
Analytical Methods in Environmental Chemistry Journal
Journal home page: www.amecj.com/ir

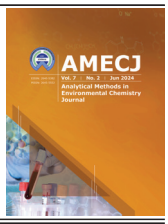

Removal of nitrate from contaminated water of river Rushikulya using natural adsorbent

Sasmita Hota[a], Manoranjan Mishra[b] and Upendra Prasad Tripathy [c,*]
[a,b] *Gandhi Institute for Technology, Bhubaneswar, India, PIN-752054*
[c] *Pulp and Paper Research Institute, Jaykaypur, Rayagada, Odisha (India), PIN-765017*

ARTICLE INFO:
Received 2 March 2024
Revised form 25 Apr 2024
Accepted 22 May 2024
Available online 29 Jun 2024

Keywords:
Composite Adsorbent
Nitrate
Spectrophotometric method
Contaminated water
Rice Husk
Bagasse Waste,

ABSTRACT
Nitrate contamination of surface water through different human activities is an alarming issue for human sound health survivorship. So, we have attempted to estimate and remove nitrate contamination levels in water samples, collected from the Rushikulya River in Odisha, India. A detailed study is done on the impact of nitrate contamination in various aspects and their removal is absorbed through an experimental composite adsorbent that is prepared taking rice husk dust and Bagasse waste from corn (Argo-based waste product) with different proportions of each. The nitrate absorbance was analyzed with the spectrophotometric method. The efficiency of adsorbents is identified through SEM and found that with an increase in the alkaline state of water sample up to 13 and composite proportion ratio with 20% rice husk and 80% bagasse waste from corn, removes nitrate up to 95% from contaminated water sample. A maximum of 98.0% of nitrate was removed from the water at a pH of 11. Also, by maintaining the COD range of 250 mgL^{-1}, the nitrate could be removed up to 94%. Out of all the combinations, the matrix composite of Type- 9 (CM - 9), made with the combination of RH and BW in Ratio 1:9, is found to have with good compressive strength of 0.44 MPa, tensile strength of 1.003 MPa and highest density of 279.88 kg m^{-3}. These matrices are applied for the treatment of contaminated river water samples to remove nitrate.

1. Introduction

Deterioration of surface water is not a new phenomenon however, quality of surface water changes from time to time worldwide, due to both natural processes and anthropogenic activities. Due to increasing population, urbanization, and extensive agricultural practices, the surface and groundwater are contaminated. Over the last 20 years, several small and large-scale industries have been developed in the basin of the Rushikulya River. This river feeds the maximum agricultural and consumptive needs of two major districts of the state of Odisha, India. This River is also known to be the second largest olive ridley turtle nesting site at its river mouth in India. Hence, the water quality of this river influences human and animal life living nearby directly or indirectly. This research paper attempts to determine the anionic parameter nitrate, in the river water sample, which is mostly responsible for damaging the water quality and making the water unhealthy for domestic as well as consumptive purposes. So, towards remedial measures of treatment of Nitrate, an efficient adsorbent matrix made up of agro-based waste products is prepared and subsequent treatment is experimented. The observations are estimated, and recordings are analyzed. In this research, the organic contamination of the river water is also analyzed.

*Corresponding Author: Upendra Prasad Tripathy
Email: uptripathy@gmail.com
https://doi.org/10.24200/amecj.v7.i02.317

Nitrate remediation is mostly attempted by engineered processes and experimented with for the efficient removal of Nitrate. A few of them are discussed here. Nitrate contamination in the groundwater is a global issue which took so much research interest. Many natural and engineered processes have already been experimented for removing it. The reviews show that microbial autotrophic and heterotrophic mechanisms are efficient enough for nitrate removal from groundwater by the in-situ and ex-situ processes. It is found, that engineered processes can remove a much better percentage of nitrate than natural methodologies [1]. The hazardous impact of nitrate contamination in drinking water on human health is critically analyzed [2]. The effectiveness of biological denitrification against reverse Osmosis and ion exchange methodology for nitrate removal from groundwater are studied for full-scale application [3]. A detailed photocatalytic removal of nitrate from water using activated carbon loaded with bimetallic Pd-Ag nanoparticles under solar radiation is given by Soliman A. M. *et. al*. [4]. A quantities assessment of factors influencing nitrate accumulation in groundwater is studied and biological denitrification using cyanobacterial is found an effective method for removal on a large scale [5]. Nitrate removal from water using amine-grafted agricultural waste adsorbents is given by Kalaruban M. *et. al.* (2016) [6]. The removal of nitrate and fluoride using membrane and adsorption technique is given by Munoth P *et. al.* (2015) [7]. Efficient and continuous removal of nitrate from water with cationic cellulose nano paper membranes is given by Mautner A et. Al. (2017). The performance of these cationic nanopapers exceeds 100 L m^{-2} h^{-1} M Pa^{-1}[8]. Electrodialysis and electro-deionization technology are applied and attempted for the removal of nitrate from groundwater. It was a fundamental in-situ remediation method and provided the foundation for further research on the removal of nitrate using ED and Ion exchange methods [9]. A pilot-scale biochar-amended woodchip bioreactor was developed by Ashoori et al in 2019. They remove nitrate, metals, and trace organic contaminants from urban stormwater. [10]. Critical analysis of the hazardous impact of nitrate contamination in groundwater and their sources of contamination is conducted [11]. Some research concluded that anthropogenic pollution is the main source of groundwater pollution and towards remedial measures Ion exchange, biological denitrification, and reverse osmosis are used on full scale for their removal. Biological denitrification from drinking water found that autotrophic denitrification is relatively more complex than heterotrophic denitrification [12]. The removal of nitrate was attempted with a Sulfur-siderite autotrophic denitrification system (SSAD) to remove phosphorous and conducted with batch, column, and pilot mode. This method was found to be one of the most effective and promising ways for both phosphate and nitrate removal. Nitrate is attempted to be removed along with arsenic and fluoride from drinkable water using integrated combined techniques taking Ion exchange resin and activated alumina. Studies on the stratification of reactivity for nitrate in groundwater are attempted and discussed. Many detailed reviews are carried out to select the best methodologies among chemical precipitation, Distillation, RO, ED, IE, and bio-denitrification along with natural zeolite attempted for groundwater with suitable surface modification [13-16]. The phytoremediation process is attempted to remove nitrate from water [17]. Nitrate removal from agricultural runoff water, by the chitosan-graphite composite adsorption method is studied using bio-composite of synthesized benign, from naturally abundant chitosan by doped with graphite and siO_2. From kinetic analysis, this method was found to be non-expensive, and benignly prepared chitosan composites are very effective adsorbents for the separation of specific nutrients like nitrates/phosphates from water [18-24]. Mosavi et al. in 2009 developed a highly selective and sensitive catalytic spectrophotometric method to determine nitrite amounts in water samples. It is based on its catalytic effect on the nuclear fast red–potassium bromates redox reaction in an acidic medium [25]. Arjomandi et al. in 2019 discussed on quantification of heavy metals in human bodies, soil, and water. They assessed the effect of toxicity of each heavy metal on human health [26]. Moussavi et al. in 2015 investigated the heavy metal pollution in waters, soils, and vegetables from farms, near an oil refinery in the south of Tehran city, Iran. They used the Geographic information systems (GIS) to estimate the levels of heavy metal concentration at unmeasured locations [27]. Also, some adsorbents such as carbon nanotubes, Nitrogen-doped porous graphene nanostructured, and bimodal mesoporous silica nanoparticles were used for removal of anion and cation in water samples

[28-30]. In the present research, an attempt has been made to establish the role of composite material made up of raw rice husk and bagasse waste, to provide a medium for nitrate removal from sample water of river Rushikulya.

2. Materials and Method

2.1. Area Study

All the samples are being collected during the April-Pre-monsoon seasons, July-Monsoon, and October-post monsoon seasons. The samples are being collected in triplicate and the mean is considered as the database for further treatment. The samples were collected in 5 L plastic containers, and thoroughly washed with water for analysis. The COD was used by the APHA method. To carry out the study, Sample water was collected from ten different areas (Table 1) near and far from industrial sites in the river basin. The location of all ten sampling sites is presented in Figure 1.

Table 1. Study Sites for Sample Collection

Name of the Site	Code
Nandika	S-1
Baradaballi	S-2
Jagamohan	S-3
Pataliguda	S-4
Pittal	S-5
Pratappur	S-6
Karapada	S-7
Kainchapur	S-8
Patagada	S-9
Pallibandha	S-10

Fig.1. Study Sites for Sample Collection in relation to Google Map

The bio-based waste raw materials are being collected from various agricultural units present nearby. The corn tree is shown in Figure 2 and the rice husk in Figure 2. After removing the corn from the plant all parts in the form of powder form can be taken as adsorbent similarly powder from corn cobs and rice husk is used to act as adsorbent shown in Figures 3 and 4.

They are mixed in different desired proportions to prepare 10 different types of composite matrix. Contaminated water is allowed to be treated through the adsorbent matrix and the efficiency of removal of Nitrate is studied under different conditions, COD, pH, and doses of composite matrix. For that 500 mL of contaminated water is taken for each reaction. SEM analysis is conducted with scanning electron microscope model no. JSM-651OLV. Nitrate is determined by the Chromotropic acid method as per IS:3025(Part 34)-1988, spectrophotometrically using UV-Vis. A spectrophotometer (Model number: SL 218, Elico, Double beam UV-VIS Spectrophotometer) was used at 410 nm [31].

2.2. Determining Procedure

Nitrate was determined by the Chromotropic acid method using a UV-Vis Spectrophotometer. Nitrate is determined spectrophotometrically by the Chromotropic acid method as per IS:3025(Part 34)-1988, spectrophotometrically at 410nm [32]. Filter photometer with violet filter was used with maximum absorbance at 400-425 nm. Dissolve 3.8 g of ammonium chloride (CAS No.: 12125-02-9) in water and dilute to 1000 mL. Dilute 1 mL of stock solution to 100 ml of DW. The method is nitrate reacts with chromotropic acid to form a new product. First, the sample is added to a Test 'N Tube™ vial containing sulfuric acid (Hach Company Nitrogen-Ammonia Reagent Set, Thermo Fisher Scientific, USA). This sample and sulfuric acid mixture was used for calibrating by the spectrophotometer (blank, zero-point calibration). Then, the chromotropic acid was added as a nitrate reagent. Two moles of nitrate react (2.0 M) with one mole of chromotropic acid (CA: 1.0 M) to create a yellow color reaction product with maximum absorbance at 410 nm. The absorbance of CA with nitrate was caused to determine the nitrate concentration in water samples by spectrophotometer (Fig.5).

3. Result and Discussion

Due to different urbanized acts, from time to time, the water contamination level is increasing day by day. This is a high call for more advanced and innovative products designed for Pre-treatment of the wastewater from small water bodies before being discharged to a nearby river or Ocean. The data obtained for different water samples are represented in Figure 6. The data revealed that nitrate concentration in water sources is effluent addition dependent. It's all because water samples collected from sites no. 1, 2, 3, 4, and 5 are very low in nitrate content as compared to sites no. 6, 7, 8, 9, 10, site no. 7 and 9 i.e., Karapada and Patagada show maximum nitrate content ranging between

Fig. 2. Corn tree

Fig. 3. Corn cobs

Fig. 4. Rice husk

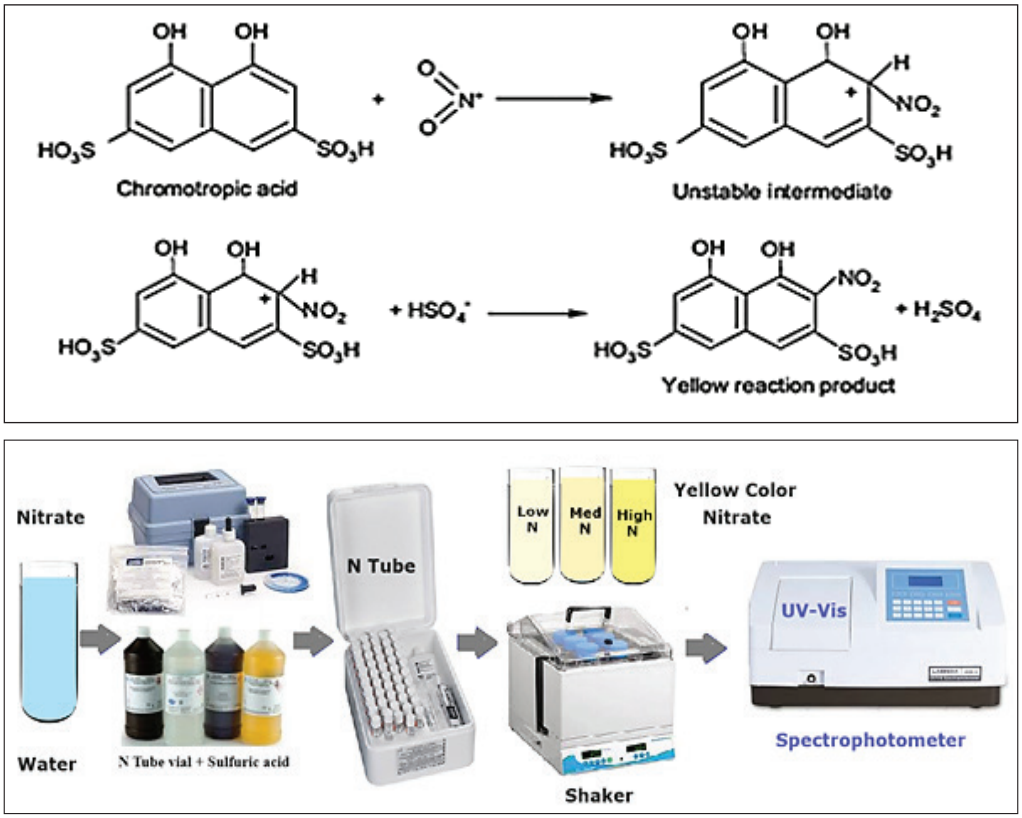

Fig. 5. Nitrate determination procedure by N Tube and UV-Vis spectrophotometer

150 mgL^{-1} to 190 mgL^{-1} which may be attributed to the fact that the addition of industrial waste from chemical industries and fertilizer industries nearby are the major sources of nitrate pollution. Also, nearby public using this water, have complaints of blue baby syndrome in children. Here, a suitable adsorbent matrix is prepared for treatment of contaminated water samples. For the preparation of CM, rice husk and bagasse waste are chosen and are being collected from the nearby local areas. Each of these two waste materials is set for Physiochemical analysis before being added together for preparation of an efficient adsorbent matrix. The data are represented in Table 2 and Table 3.

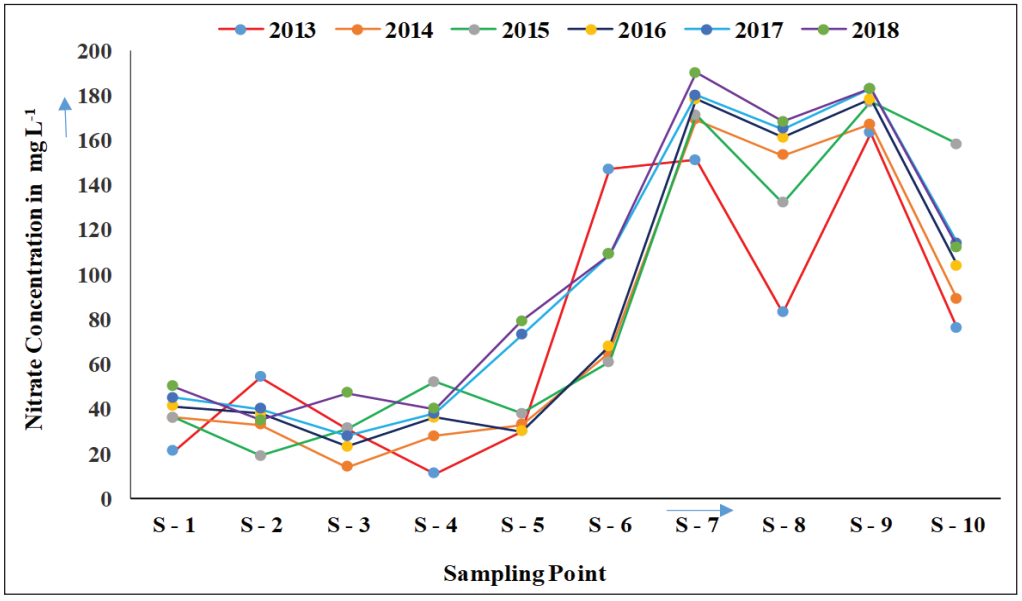

Fig. 6. Nitrate concentration profile of the sampling Sites for 2013 ($mg\ L^{-1}$)

Table 2. Physical parameters of the raw material

Physical Properties	Rice Husk	Bagasse waste from Corn
Carbon: Nitrogen Ratio	65.8	92.4
pH Value	8.3	9.7
Bulk Density	118 Kg m^{-3}	310 Kg m^{-3}
Maximum water holding capacity	512 mL kg^{-1}	588 mL kg^{-1}

Table 3. Chemical composition of raw material (%)

Chemical Composition	Rice Husk	Bagasse waste from Corn
SiO_2	81.08	88.2
K_2O	3.11	1.3
CaO	1.98	0.6
P_2O_5	4.78	0.4
MgO	2.83	0.4
Al_2O_3	2.01	2.3
Fe_2O_3	1.59	5.1
Na_2O	0.53	0.1
SO_3	0.66	< 0.1
TiO_2	0.07	0.05
ZnO	0.02	0.08

These two bio-based waste materials are mixed in different proportion ratios, to prepare ten different adsorbent matrixes, as represented in Table 4. For the preparation of an efficient absorbent towards nitrate removal, both the raw materials are dried and activated to attain the best absorbance efficiency, as represented in the flow sheet in Figure 7.

The activated biowaste is subsequently mixed with the addition of an organic binder and the matrix is prepared using a mechanical mold and followed by a determination of their physical properties, to identify the most efficient matrix out of all (Table 5). It is revealed that out of all the combinations, the matrix composite of Type- 9 (CM - 9), made with the combination of RH and BW in Ratio 1:9, is found to have with good compressive strength of 0.44 MPa, tensile strength of 1.003 MPa and with highest density of 279.88 kg m^{-3}. These matrices are used for nitrate removal in the contaminated river water sample. The nitrate removal is processed against a composite matrix and different conditions for efficient removal of Nitrate are studied.

Table 4. Represents the ratio for the addition of Rice Husk to Bagasse waste

Sl. No.	Rice Husk (g)	Bagasse waste (g)	Ratio (RH:BW)
S - 1	90	10	9:1
S - 2	80	20	8:2
S - 3	70	30	7:3
S - 4	60	40	6:4
S - 5	50	50	5:5
S - 6	40	60	4:6
S - 7	30	70	3:7
S - 8	20	80	2:8
S - 9	10	90	1:9
S-10	00	100	0:10

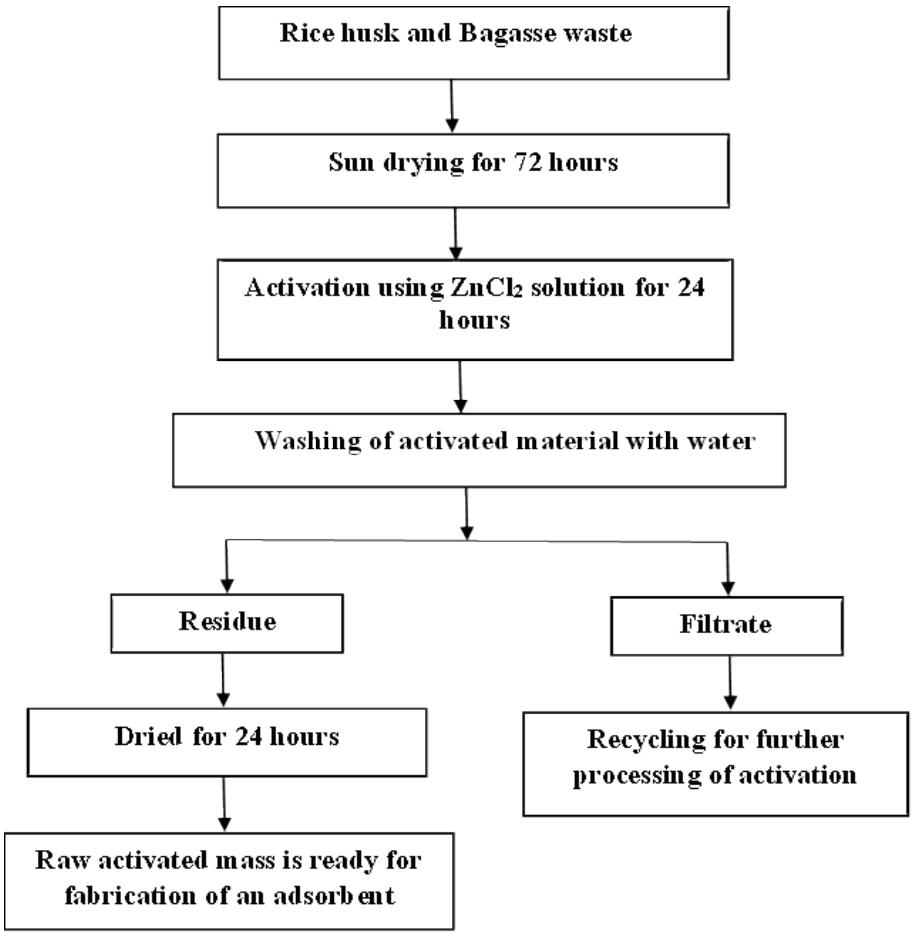

Fig. 7. Process flow sheet for nitrate absorptio

Table 5. Composite Matrix: Physical Properties

Sl. No.	Density (Kg m^{-3})	Compressive Strength (MPa)	Tensile Strength (MPa)
CM - 1	307.22	0.29	0.884
CM - 2	259.14	0.21	0.901
CM - 3	291.45	0.37	0.893
CM - 4	314.08	0.34	1.207
CM - 5	284.31	0.39	1.021
CM - 6	333.17	0.37	1.078
CM - 7	320.11	0.34	0.889
CM - 8	301.43	0.41	0.997
CM - 9	279.88	0.44	1.003
CM-10	342.12	0.38	1.102

3.1. Role of pH on Nitrate Removal

It is observed that the removal of nitrate under alkaline conditions is more favorable and is increasing to 11-12 pH and after that removal is slowed down, as presented in Table 6 and Figure 8. An acidic medium was found very weak for efficient nitrate removal from the water sample.

In acidic conditions, with increase in pH, there is a gradual increase in nitrate removal from contaminated water bodies. Similarly, when the pH is maintained in an acidic range, the recovery slowly increases from 65% to 80% with a pH variation of 4 to 6.5. This data revealed that acidic pH does not impact much on nitrate removal shown in Figure 9a. Nitrate removal is partially pH-dependent. When the composite matrix is added to the water sources, due to the alkalinity of the material there is a gradual increase in pH of the medium.

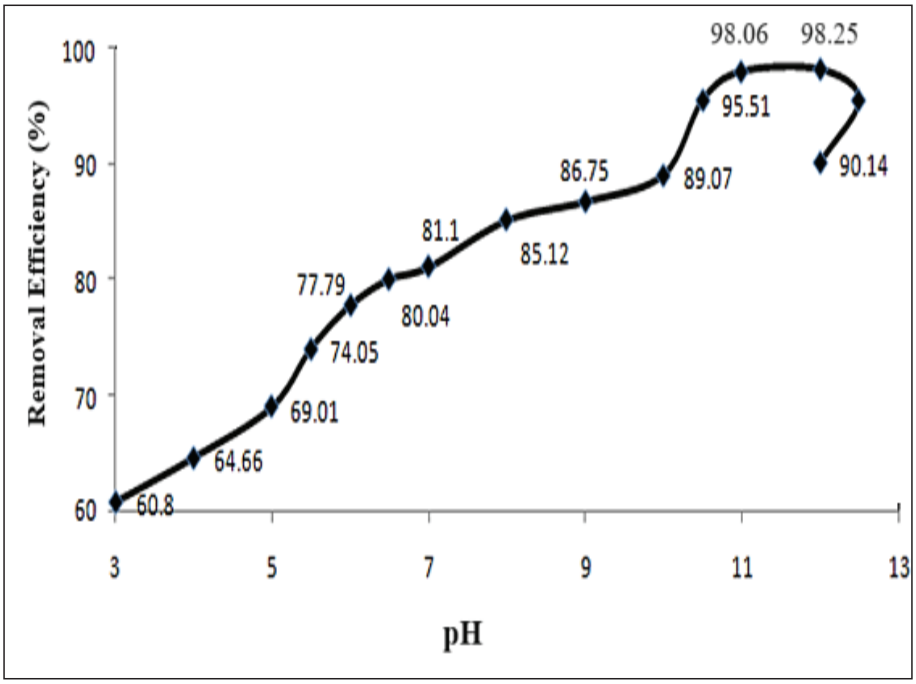

Fig. 8. Impact of acidic and alkaline pH on nitrate removal

The result obtained showed that at a pH range of 8 - 12, there is a removal of 85% (or) above the amount of nitrate. The optimum pH is found to be 11, where a maximum of 98.0% of nitrate could be removed from the water source. Again, with the further attempt of increase in pH, there is gradual decrease in removal of nitrate. The decrease in removal of nitrate with the increase in pH may be attributed to the fact that, the presence of Iron in the form of ferric Fe^{3+} state in the Baggase waste at a suitable pH ≈ of 12.5 may lead to formations of ferric nitrate, which might get coagulated in the water medium leading decrease in nitrate removal. For maximum removal of nitrate in the contaminated water was obtained at pH 11.

3.2. Role of Composite Matrix doses on nitrate Removal

The impact of Nitrate removal from contaminated water samples with variable doses of composite matrix is studied. Due to Figure 9b, It has been revealed that the removal efficiency of nitrate is directly affected by the dose of the composite matrix. Out of all experimented doses, 70 mgL^{-1} addition of composite matrix dose provided the best efficiency for nitrate removal. The gradual rise in the removal of nitrate concerning the rise in the concentration of doses of the composite matrix can be attributed to the fact that with the addition of more quantity of activated composite matrix, there may be the availability of a more porous surface on the composite matrix, which would have helped the colloidal suspension to penetrate.

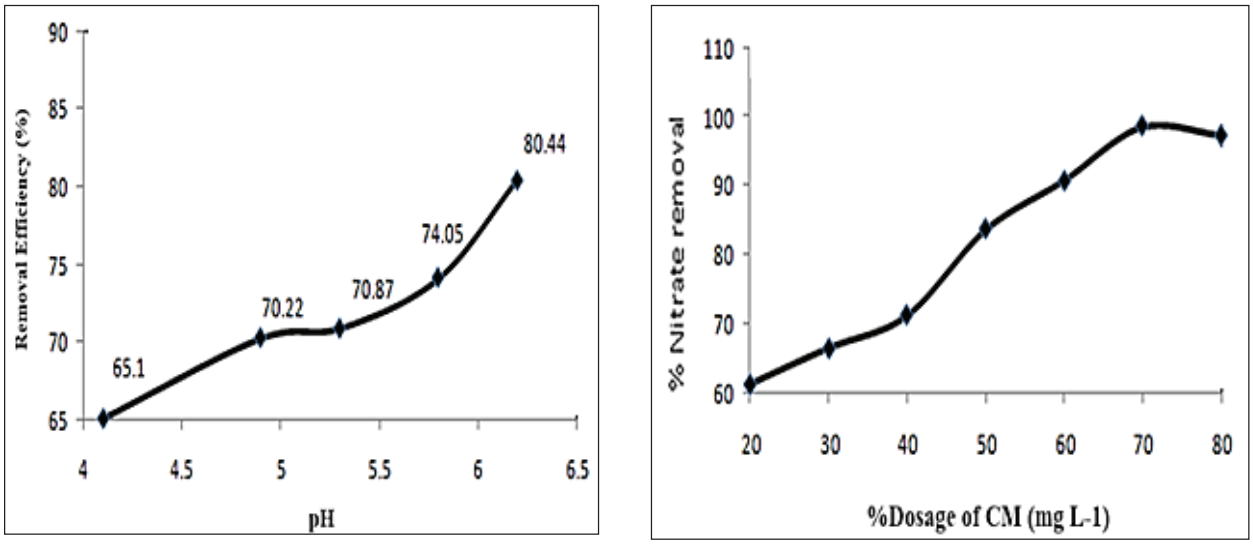

Fig. 9. a) Impact of acidic pH on nitrate removal (left)
b) Role of Composite Matrix doses on nitrate adsorption (right)

Table 6. Nitrate removal depends on doses of composite matrix

Sl. No.	Residual nitrate (mgL^{-1})	Dosages of CM-9, (mgL^{-1})	Nitrate Absorbed
1	38.8	20	61.2
2	12.6	30	66.4
3	8.4	40	71.1
4	2.1	50	83.5
5	4.8	60	90.7
6	8.9	70	98.4
7	10.6	80	91.4

Conditions: pH = 11.2, Nitrate Content = 100 mg L^{-1}, Room Temperature (30°C)

The percentage of removal of Nitrate is attempted with a most suitable adsorbent matrix and at standard pH 11.2, is studied, as shown in Table 6. It shows that with a sufficient dose concentration of composite matrix, up to 98% Nitrate removal is possible from the contaminated water sample.

3.3. Impact of COD of water sample on nitrate removal

The COD level in water samples usually restricts the determination of the organic matter present in any water medium. The impact of different COD levels of the contaminated water sample is studied for removal efficiency of nitrate which is shown in Table 7.

Due to Figure 10, nitrate could be removed from a range of 250 mgL^{-1}, up to 94%. Beyond 250 mgL^{-1}, the efficiency of removal is decreased. As in the sample water the dissolved oxygen level is much lower than the prescribed limit by WHO, the optimum COD should be limited to 250 mgL^{-1} for effective removal of Nitrate. The rise in COD influences directly more removal of nitrate from sample water. It may be because of the influence of COD on the pH level of water and the positive influence of the rise in nitrate removal percentage. But beyond the range, the adsorption decreases up to 18% at 550 mgL^{-1}. So, the research suggests adequate measures to be adopted to maintain the COD level for efficient nitrate removal.

Table 7. Nitrate Removal efficiency against variation of COD level

Sl. No.	COD (mgL^{-1})	% Residue (N)	% Removal
1	500	81	19
2	460	65	35
3	380	43	57
4	320	20	80
5	250	06	94
6	180	14	86
7	110	28	72
8	80	39	61
9	50	57	43
10	30	82	18

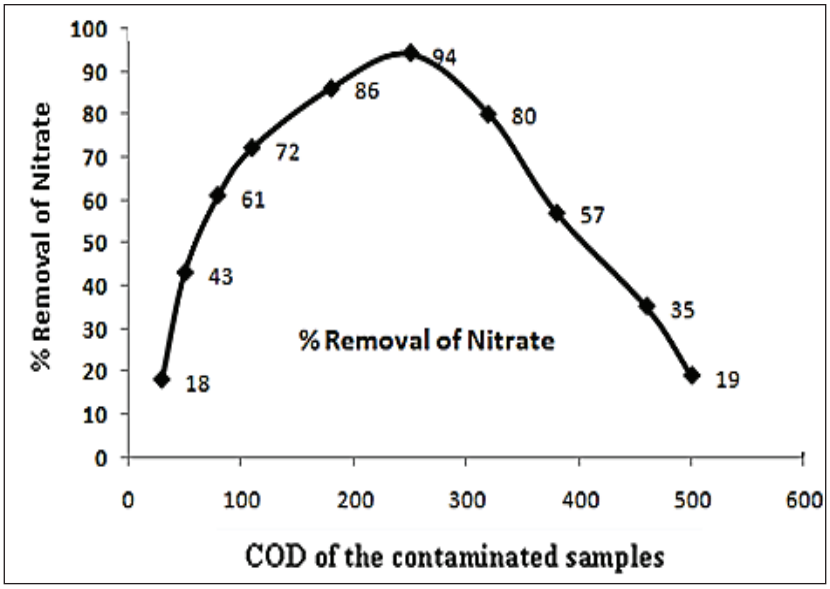

Fig. 10. Impact of COD of the sample on Nitrate adsorption

3.4. Scanning Electron Microscopic Studies on the Composite Matrix:

Scanning electronic microscopic studies are conducted to investigate the effect of pH conditions on nitrate removal. In this context, the SEM of a composite matrix was considered and the texture is found to be quite uniform throughout. The composite matrix exhibits a consistent blend of bagasse waste and rice husk dust particles, creating a porous structure for nitrate absorption, as depicted in Figure 11a. To study the effect of various pH-containing wastewater on the textural changes of the matrix, acidic, neutral, and alkaline mediums of wastewater are added to the composite medium to study the absorption rate and textural variations. When an alkaline medium passes through the composite material, it is observed that there is maximum textural variation attributed to alkaline water sources. After passing the alkaline water, there is a complete variation in the material texture. Figure 11b represents the SEM for the treated material, which is approximately 75% distorted. When an acidic medium passes through the composite material, there is minimal textural variation caused by acidic water sources. After passing the acidic water, there is minimal variation in the material texture.

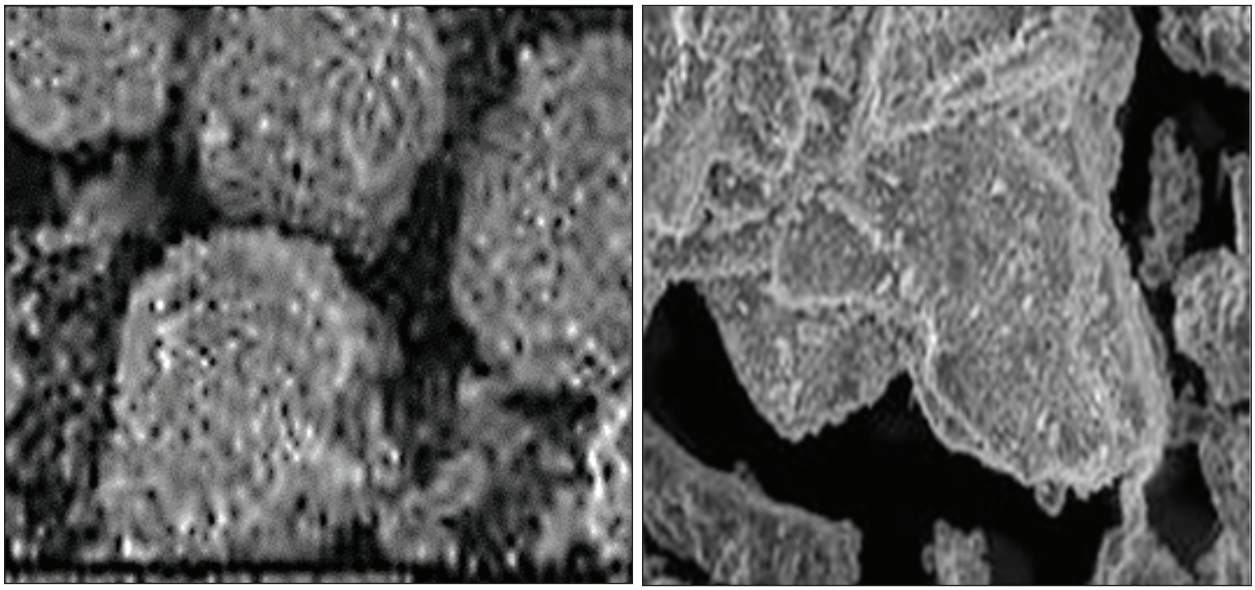

Fig. 11. a) SEM of the composite before treatment **b)** treatment of an alkaline wastewater

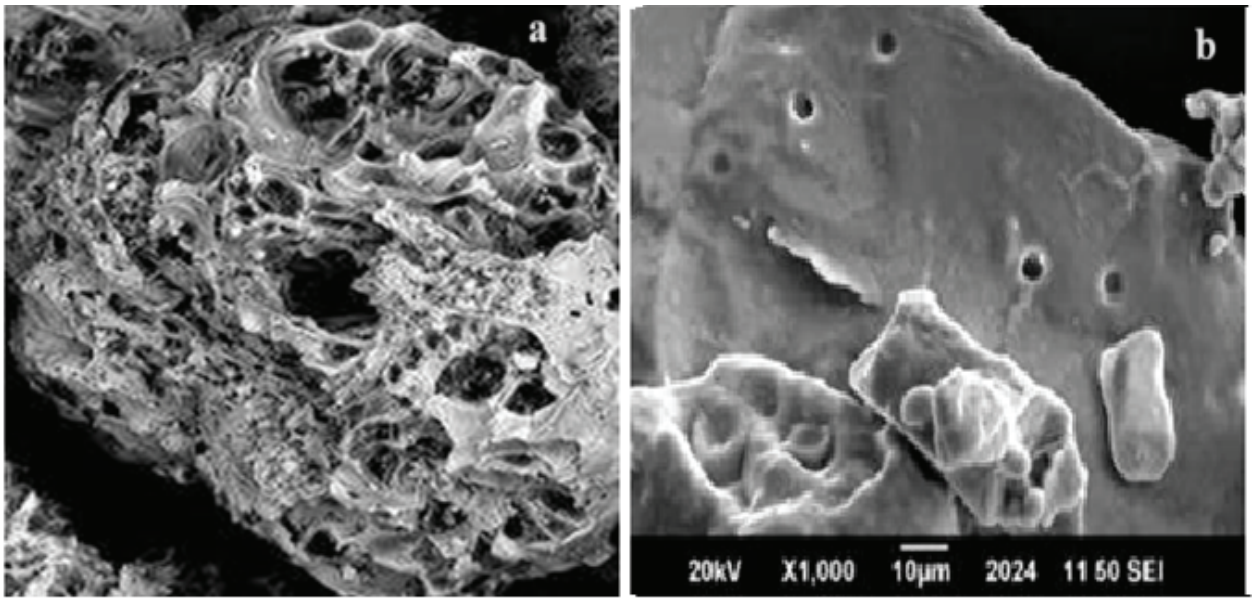

Fig. 12. a) SEM of the composite matrix after treatment with acidic wastewater **b)** after treatment of neutral

Figure 12a represents the SEM for the treated material, which is ~ 15% disturbed. When a neutral medium is passed through the composite material, it has been observed that there is variation in texture attributed to natural water sources. After passing the neutral water, there is a significant variation in the texture of the material. Figure 12b represents the SEM for the treated material, which is approximately 80% distorted. Thus, it is concluded that a neutral medium with an alkaline pH of 11 is the best for maintaining 96% nitrate removal from contaminated water sources.

4. Conclusion

The study on de-nitrification conditions for efficient removal of nitrate concluded that the removal is majorly dependent on the pH of the contaminated water, COD of the wastewater, and doses of composite matrices. Keeping a pH of 11, COD maintained with 250 mgL^{-1}, and a fixed dose of the composite matrix, about 96% of nitrate could be removed. The bio-based composite matrix is highly efficient for removing nitrates from contaminated water.

5. References

[1] K.M, Moloantoa, Z.P. Khetsha, E.V. Heerden, J.C. Castillo, E. D. Cason. Nitrate water contamination from industrial activities and complete denitrification as a remediation option, Water, 14 (2022) 799. https://doi.org/10.3390/w14050799

[2] M. Shrimali, K.P Singh, New Methods of nitrate removal from water, Environ. Pollut., 112 (2001) 351–359. https://doi.org/10.1016/S0269-7491(00)00147-0

[3] F. Rossi, O. Motta, S. Matrella, A. Proto, G. Vigliotta, Nitrate removal from wastewater through biological denitrification with OGA 24 in a batch reactor, Water, 7 (2014) 51–62. https://doi.org/10.3390/w7010051

[4] A.M. Soliman, D. Alshamsi, A. A. Murad, A. Aldahan, I. M. Ali, A. I. Ayesh, I.A. Elhaty, Photocatalytic removal of nitrate from water using activated carbon-loaded with bimetallic Pd-Ag nanoparticles under natural solar radiation, J. Photochem. Photobiol. A: Chem., 433 (2022) 114175. https://doi.org/10.1016/j.jphotochem.2022.114175

[5] R.M. Awadallah, M.E. Soltan, M.S.A. Shabeb, S.M.N. Moalla, Bacterial removal of nitrate, nitrite and sulphate in wastewater, Water Res., 32 (1998) 3080–3084. https://doi.org/10.1016/S0043-1354(98)00069-4

[6] M. Kalaruban, P. Loganathan, W.G. Shim, J. Kandasamy, H.H. Ngo, S. Vigneswaran, Enhanced removal of nitrate from water using amine-grafted agricultural wastes, Sci. Total Environ., 565 (2016) 503–510. https://doi.org/10.1016/j.scitotenv.2016.04.194

[7] P. Munoth, K. Tiwari, R. Goyal, Fluoride and nitrate groundwater contamination in Rajasthan, India: A review, 20th International Conference on Hydraulics, 2015. https://doi.org/10.13140/RG.2.1.2859.6241

[8] A. Mautner, T. Kobkeatthawin, A. Bismarck. Efficient continuous removal of nitrates from water with cationic cellulose nanopaper membranes, Resource-Efficient Technol., 3 (2017) 22–28. https://doi.org/10.1016/j.reffit.2017.01.005

[9] M. AL-Housni, A. Hashim Hussein, D. Yeboah, R. Al Khaddar, B. Abdulhadi, A. Abdulhussein Shubbar, K. S. Hashim, Electrochemical removal of nitrate from wastewater, IOP Conference Series: Mater. Sci. Eng., 888 (2020) 012037. https://doi.org/10.1088/1757-899X/888/1/012037

[10] N. Ashoori, M. Teixido, S. Spahr, G. H. LeFevre, D. L. Sedlak, R. G. Luthy, Evaluation of pilot-scale biochar-amended woodchip bioreactors to remove nitrate, metals, and trace organic contaminants from urban stormwater runoff, Water Res., 154 (2019) 1–11. https://doi.org/10.1016/j.watres.2019.01.040

[11] D.L. Correll, T. E. Jordan, D. E. Weller, Failure of agricultural riparian buffers to protect surface waters from groundwater nitrate Contamination, In groundwater/

surface water Ecotones, edited by Janine Gibert, Jacques Mathieu, and Fred Fournier, 1st ed., Cambridge University Press, p.p.162–65, 1997. https://doi.org/10.1017/CBO9780511753381.021

[12] A. Boubakri, S. Al-Tahar Bouguecha, A. Hafiane, FO–MD integrated process for nitrate removal from contaminated groundwater using seawater as draw solution to supply clean water for rural communities, Sep. Purif. Technol., 298 (2022) 121621. https://doi.org/10.1016/j.seppur.2022.121621

[13] A. Gupta, M. Ronghang, P. Kumar, I. Mehrotra, S. Kumar, T. Grischek, C. Sandhu, and K. Knoeller, Nitrate contamination of riverbank filtrate at Srinagar, Uttarakhand, India: A case of geogenic mineralization, J. Hydrol., 531 (2015) 626–37. https://doi.org/10.1016/j.jhydrol.2015.10.065

[14] N. Ozturk T. Ennil Bektaş, Nitrate removal from aqueous solution by adsorption onto various materials, J. Hazardous Mater., 112 (2004) 155–62. https://doi.org/10.1016/j.jhazmat.2004.05.001

[15] G. Pinay, T. C. O'Keefe, R. T. Edwards, R. J. Naiman, Nitrate removal in the hyporheic zone of a Salmon River in Alaska, River Res. Appl., 25 (2009) 367–75. https://doi.org/10.1002/rra.1164

[16] V. Yakovlev, Y. Vystavna, D. Diadin, Y. Vergeles, Nitrates in springs and rivers of east Ukraine: distribution, contamination and fluxes, Appl. Geochem., 53 (2015) 71–78. https://doi.org/10.1016/j.apgeochem.2014.12.009

[17] L. Regni, M. Luce Bartucca, E. Pannacci, F. Tei, D. Del Buono, P. Proietti, Phytodepuration of nitrate contaminated water using four different tree species, Plants, 10 (2021) 515. https://doi.org/10.3390/plants10030515

[18] K. Li, L. Liu, H. Yang, C. Zhang, H. Xie, C. Li, Phytoremediation potential of three species of macrophytes for nitrate in contaminated water, Am. J. Plant Sci., 07 (2016) 1259–67. https://doi.org/10.4236/ajps.2016.78121

[19] S. Mishra, S. Suresh, M. S. Chauhan, V. Subbaramaiah, V. Gosu, Recent progress in carbonaceous materials for the nitrate adsorption, J. Hazard. Toxic Radioact. Waste, 26 (2022) 04022013. https://doi.org/10.1061/(ASCE)HZ.2153-5515.0000699

[20] J.J. Lado, R. E. Pérez-Roa, J. J. Wouters, M. I. Tejedor-Tejedor, C. Federspill, J. M. Ortiz, M. A. Anderson, Removal of nitrate by asymmetric capacitive deionization, Sep. Purif. Technol., 183 (2017) 145–52. https://doi.org/10.1016/j.seppur.2017.03.071

[21] O. Gibert, M. Abenza, M. Reig, X. Vecino, D. Sánchez, M. Arnaldos, J. Luis Cortina, Removal of nitrate from groundwater by nano-scale zero-valent iron injection pulses in continuous-flow packed soil columns, Sci. Total Environ., 810 (2022) 152300. https://doi.org/10.1016/j.scitotenv.2021.152300

[22] A. Rajta, R. Bhatia, H. Setia, P. Pathania, Role of heterotrophic aerobic denitrifying bacteria in nitrate removal from wastewater, J. Appl. Microbiol., 128 (2020) 1261–78. https://doi.org/10.1111/jam.14476

[23] W.K. Biftu, M. Suneetha, K. Ravindhranath, Sequential adsorptive removal of phosphate, nitrate and chromate from polluted water using active carbon derived from stems of Carissa Carandas plant, Water Practice Technol., 16 (2021) 117–34. https://doi.org/10.2166/wpt.2020.102

[24] P. Nagaraja, M. S. Hemantha Kumar, Spectrophotometric determination of nitrate in polluted water using a new coupling reagent, Anal. Sci., 18 (2002) 355–57. https://doi.org/10.2116/analsci.18.355

[25] H. Z. Mousavi, H. Shirkhanloo, Spectrophotometric determination of nitrite based on its catalytic effect on the reaction of nuclear fast red and potassium bromate, J. Serb. Chem. Soc., 74 (2009) 985-992. https://doi.org/10.2298/JSC0909985M

[26] M. Arjomandi, H. Shirkhanloo, A review: analytical methods for heavy metals determination in environment and human

samples, Anal. Methods Environ. Chem. J., 2 (2019) 97-126. https://doi.org/10.24200/amecj.v2.i03.73

[27] S. A. Moussavi, H. Farahani, S. A. H. Mirzahosseini, N. Shirkhanloo, The evaluation and determination of heavy metals pollution in edible vegetables, water and soilin the south of Tehean province by GIS, Arch. Environ. Prot., 41 (2015) 63-72. https://doi.org/10.1515/aep-2015-0020

[28] M. Habibnia, A. Rashidi, A. Faghihi Zarandi, Simultaneously speciation of mercury in water, human blood and food samples based on pyrrolic and pyridinic nitrogen-doped porous, graphene nanostructure, Food Chem., 403 (2023) 134394. https://doi.org/10.1016/j.foodchem.2022.134394

[29] N. Esmaeili, J. Rakhtshah, Ultrasound assisted-dispersive-modification solid-phase extraction using task-specific ionic liquid immobilized on multiwall carbon nanotubes for speciation and determination mercury in water samples, Microchem. J., 154 (2020) 104632. https://doi.org/10.1016/j.microc.2020.104632.

[30] A. Khaligh, F. Golbabaei, A Vahid, On-line micro column preconcentration system based on amino bimodal mesoporous silica nanoparticles as a novel adsorbent for removal and speciation of chromium (III, VI) in environmental samples, J. Environ. Health Sci. Eng., 13 (2015) 47. https://doi.org/10.1186/s40201-015-0205-z

[31] D. Jenkins, L. L. Medsker, Brucine method for the determination of nitrate in ocean, estuarine, and fresh waters, Anal. Chem., 36 (1964) 610-612. https://doi.org/10.1021/ac60209a016

[32] M. Kisan Shakti Sangathan, Methods of sampling and test (Physical and chemical) for water and wastewater, Part 34 Nitrogen, Environ. Prot. Waste Manage., IS 3025 (1988) 7-10. https://law.resource.org/pub/in/bis/S02/is.3025.34.1988.pdf

Anal. Methods Environ. Chem. J. 7 (2) (2024) 59-73

AMECJ

Research Article, Issue 2
Analytical Methods in Environmental Chemistry Journal
Journal home page: www.amecj.com/ir

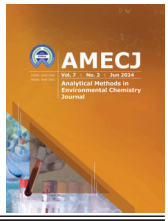

Synthesis-activated carbon based on various agri-food wastes for highly efficient removal of an anionic dye before analysis by UV-Vis spectrometry

Mohamed Ennabely [a,*], Abdessamad Ouedrhiri[a], Youssef Lghazi[a], Boubaker Youbi[a], Abderrafie Kettani Halabi [a], Mostafa Khoukhi [a], and Itto Bimaghra[a]

[a]*Bio-Geosciences and Materials Engineering Laboratory, Ecole Normale Superieure, Hassan II University of Casablanca, Morocco*

ARTICLE INFO:

Received 16 Feb 2024
Revised form 20 Apr 2024
Accepted 18 May 2024
Available online 29 Jun 2024

Keywords:
Analytical method
Activated carbons
Adsorption
MB-Dye
Agricultural-food wastes
UV-Vis spectrometry

ABSTRACT

This study aims to valorize three agricultural-food (agri-food) wastes: Argan husks, dates seeds, and olive stones collected from various regions of Morocco to produce three types of activated carbons (ACah),(ACds) and (ACos) respectively. These activated carbons were used to compare their effectiveness in removing methyl orange, an organic pollutant in aqueous solutions. The precursor materials were carbonized at a temperature of T=900°C for 2 hours and subsequently chemically activated using phosphoric acid (H_3PO_4) in a weight ratio of 1:2. The obtained samples were characterized by Fourier-transform infrared spectroscopy (FTIR), scanning electron microscopy (SEM), and BET-analysis to determine the specific surface area. The analysis revealed that (ACah) displayed a rough surface with more pores and O-H chemical bonds, indicating its superior adsorption properties. This finding corresponds to the BET-specific surface areas obtained, which were 476 m^2g^{-1} for ACah, 441 m^2g^{-1} for ACds, and 362 m^2g^{-1} for ACos. In all methyl orange adsorption experiments (10 mg L^{-1}), 60 mg of each activated carbon was used for 30 minutes, resulting in removal efficiencies of 93.87% for ACah, 91.83% for ACds, and 89.79% for ACos. The examination of adsorption kinetics and isotherm analysis demonstrated a strong alignment of the adsorption data with both the pseudo-second-order and Langmuir models across various materials.

1. Introduction

Undoubtedly, discharging untreated wastewater or aqueous solutions containing chemical pollutants into the environment poses significant risks, potentially harming human health[1] and causing adverse environmental effects[2]. The presence of organic pollutants in the environment can lead to a reduction in dissolved oxygen levels in water[3]. Thus, removing these organic pollutants from aqueous solutions becomes crucial before their release. Our focus in water treatment is to tackle this issue using cost-effective and straightforward methods, such as activated carbon adsorption. This method is highly effective in eliminating organic substances from aqueous solutions[4], the methyl orange (MO, anionic dye, offering the additional benefit of reusing agricultural waste and safeguarding the environment from pollutants. Notably, Morocco generates a substantial volume of agricultural residues annually, including olive stones[5], date seeds[6], and Argan husks[7], which can pose challenges related to aesthetics

*Corresponding Author: Mohamed Ennabely
Email: ennabely.mohamed@gmail.com
https://doi.org/10.24200/amecj.v7.i02.310

and environmental impact. Dyes, particularly MO (methyl orange), are commonly utilized materials in the food, pharmaceutical, printing, and textile industries[8]. Although not extremely toxic, this dye can still have adverse effects on the environment and human health, causing symptoms like an increased heart rate, diarrhea, and imparting an unpleasant color and odor to water bodies[9]. Additionally, it obstructs sunlight, crucial for photosynthesis[10]. Therefore, before releasing solutions containing MO molecules into the environment, treatment is necessary. We aim to achieve this by producing three distinct types of activated carbons: ACah, ACds, and ACos; from Argan husks, date seeds, and olive stones, respectively. Subsequently, we will assess their efficacy in removing the methyl orange molecule from an aqueous solution. This study serves a dual purpose: firstly, it involves the valorization of Argan shells, and secondly, it evaluates the capacity to eliminate the MO dye.

2. Materials and Methods

2.1. Materials

The biomass derived from agricultural waste illustrated in Figure 1 originates from different regions across Morocco. Olive pits were specifically sourced from the olive mill situated in the Settat region, whereas date seeds and argan shells were collected in the Sidi Ifni province. Methyl orange (C.I. No: 13025)[11] was employed as the adsorbate in all experiments. Phosphoric acid (H_3PO_4, molar mass:97.9952 g mol^{-1})[12] was utilized at a concentration of 1 mol L^{-1}, and all procedures were conducted using distilled water.

2.2. Synthesis of activated carbons

A batch of collected waste was cleansed using distilled water to eliminate impurities and then dried at 120°C for 12 hours in an oven. This resultant material underwent a drying, grinding, and sieving process through a sieve with five micrometer pores to yield the untreated raw materials in a powdered state. Subsequently, the carbonization step took place in an oven (PROTERM-PLF 120/6) at 900°C for two hours. The chemical activation process was carried out by mixing the powder with phosphoric acid, maintaining a weight ratio of 1:2. Following this, distilled water was added to the mixture, reaching a volume of 50 ml while being stirred for 10 minutes. The samples were then left for overnight drying at 120°C and subjected to washing, using demineralized water along with sodium hydroxide until neutralization was achieved to delete any remaining residual amounts of acid H_3PO_4. Finally, the activated carbons underwent filtration and further drying at 120°C for 12 hours.

Fig. 1. The three precursors and their activated carbons

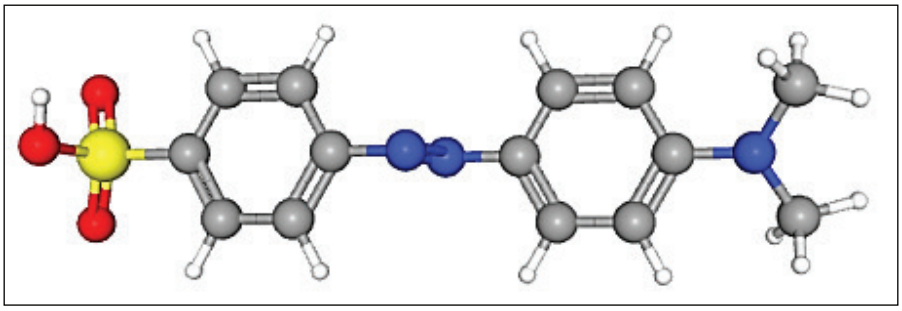

Fig. 2. Three-dimensional molecular model of methyl orange.

2.3. Characterizations of Activated carbons

The physical and chemical properties of the materials utilized are crucial in understanding adsorption behaviors. Fourier transform infrared spectroscopy is one of the most important tools for this purpose because it allows for a qualitative examination of the surface functional groups of ACah, ACds, and ACos. The FTIR analysis was carried out using a TENSOR 27 type spectrometer (Bruker Company, Germany) for three samples obtained by mixing 100 mg of potassium bromide with 1 mg of each activated carbon, the data was recorded in the 4000-500 cm^{-1} range plot IR spectra. Scanning Electron Microscopy (SEM) of three activated carbons has been performed with an Energy Dispersive Spectrometer using a Philips XL 30FEG with a secondary electron detector (SE) and an electron acceleration voltage of 20 kV. Also, our activated carbons' BET surface area was ascertained by N_2 adsorption-desorption measurements using an automated Micromeritics system running at 77 K.

2.4. Adsorption Procedure

MO-dye, also recognized as Sodium-4-(4-dimethylamino phenyl diazenyl), represents an anionic dye[13] ($C_{14}H_{14}N_3SO_3Na$) dissolved in distilled water for its preparation. The reason behind its absorption of light within the visible spectrum lies in the dye molecule's extensive conjugated system. Its absorption spectrum demonstrates a peak at λmax = 465 nm, as determined by a UV-Vis spectrophotometer (UV-1800, Bejing Rayleigh Co. Ltd). This particular wavelength corresponds to the color that complements yellow-orange, thus justifying the name "methyl orange." The optimized three-dimensional structure depicted in Figure 2 was obtained via the Gaussian program. Equation (1) is utilized to compute the adsorption percentage (R%) of methyl orange, using the initial absorbance value A0 and the final absorbance value A1 [14] The quantity qe (mg/g) of methyl orange adsorbed onto the treated material can be determined using Equation (2)[15]. The methyl orange concentration was determined by the UV-Vis spectrophotometer and the relationship between absorbance for the methyl orange is illustrated in Figure 3.

$$\mathbf{R\%} = \frac{\mathbf{A0-A1}}{\mathbf{A0}} * 100 \qquad \text{(Eq.1)}$$

$$\mathbf{q_e} = \frac{\mathbf{V(C_0 - C_e)}}{\mathbf{M}} \qquad \text{(Eq. 2)}$$

The variables included in this equation are as follows:
C_0 denotes the initial concentration of MO-dye (mg L^{-1})
C_e stands for the equilibrium concentration of the MO-dye (mg L^{-1})
V represents the volume of the solution (L)
M denotes the mass of the adsorbent (g)

The instrument employed for UV-Vis spectrometry utilizes a UV-Vis spectrophotometer, measuring absorbance across specific wavelengths [16]. This high-sensitivity equipment enables precise quantification of sample concentrations. Calibration curves were generated to correlate absorbance with concentration, ensuring accurate analyses. The instrument's capabilities enhance the study's capacity for investigating molecular absorption characteristics with increased precision.

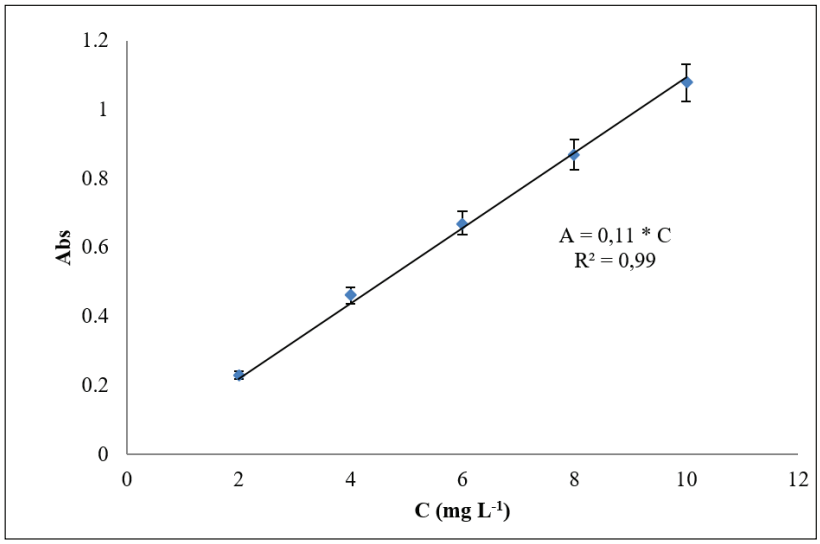

Fig. 3. Concentration versus absorbance (abs) for methyl orange by the UV-Vis spectrophotometer

3. Results and discussions

3.1. FTIR-analysis

Figure 4 displays the FTIR spectra of the three adsorbents. These spectra reveal unique properties for each material. Due to the stretching vibration of the hydroxyl groups produced by the O-H bond, ACah exhibits a distinct and broadband at about 3405 cm^{-1}[17]. The ACds exhibit a peak around 1101 cm^{-1}, which corresponds to the presence of C-O groups in secondary alcohol groups[18]. The ACos, shows a distinct peak at approximately 1475 cm^{-1}, indicating C-H vibrations within the methylene linkage. Additionally, there are peaks at 1051 cm^{-1}, signifying C-O vibrations related to oxygen-containing groups[19].

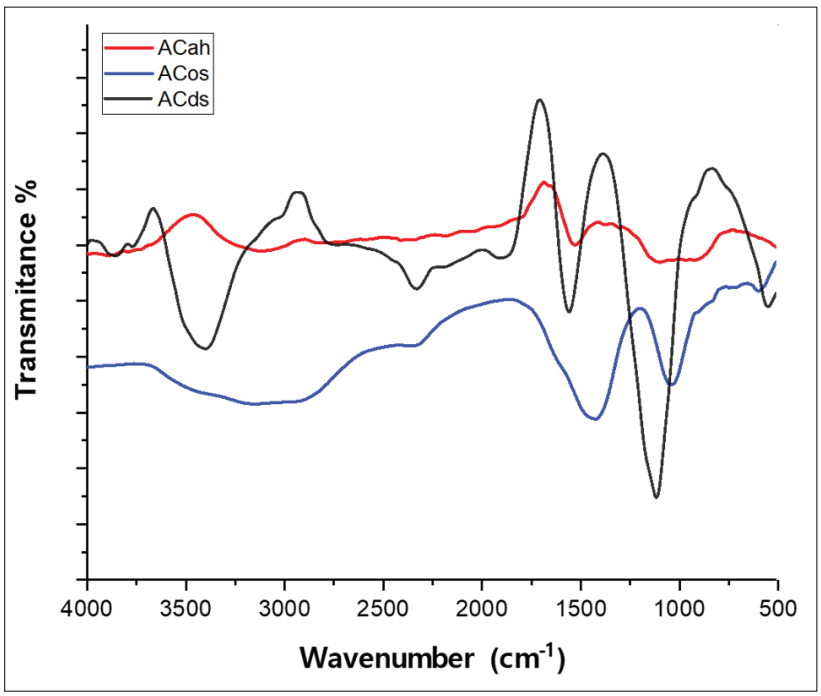

Fig. 4. FTIR-spectra of ACah, ACds, and ACos adsorbents

Figure 4 illustrates numerous peaks, indicating several functional groups existing on the surface of our adsorbents. These groups actively participate in the adsorption of MO, primarily due to the distinct O-H stretching vibration observed specifically on the ACah surface. This phenomenon could be the key reason behind the strong attraction of MO molecules through electrostatic forces[20]. Nevertheless, the presence of the C-O group on the surfaces of ACds and ACos can slow down the adsorption process. This disparity might provide an explanation as to why ACah functions as a more effective adsorbent compared to the others.

3.2. SEM analysis

The SEM images presented in Figure 5 reveal the structural and morphological characteristics of ACah, ACds, and ACos. It is clear that the rough texture of the ACah surface, which has many small-diameter pores, makes it unique. This porous structure provides an abundance of adsorption sites for the dye, making it well-suited to the size of the MO molecule. This promotes the dye's penetration into the material and raises the possibility of adsorption. Whereas ACos has a rough surface with thin layers and granules that may improve the physical adsorption of MO[21], ACds have an uneven surface structure with micropores. As shown in Table 1, the specific surface areas (SSA) of our adsorbents are also calculated using the BET analysis method. Compared to the other two adsorbents under study, ACah has a noticeably larger specific surface area, per the data in Table 1. The reason for the higher adsorption efficiency of ACah compared to the other two adsorbents can be better understood with the aid of all these observations.

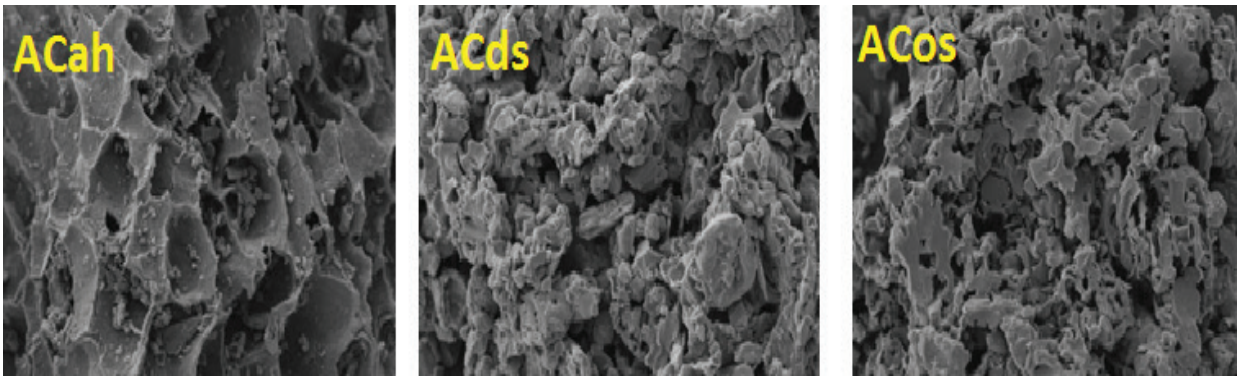

Fig. 5. SEM-images of ACah, ACds, and ACos adsorbents

Table 1. BET values for ACah, ACds, and ACos.

SSA	ACah	ACds	ACos
BET (m^2 g^{-1})	476	441	362

3.3. Adsorption Studies

3.3.1. Contact time effect

Figure 5 displays the results obtained from experiments investigating the impact of varying contact time duration on the adsorption process aiming to determine the quantities of methyl orange (MO) removed from a 25 mL solution with a concentration of 10 mg L^{-1}. The adsorption process utilized 0.06 grams of three distinct adsorbents: ACah, ACds, and ACos. The experiments encompassed contact times ranging from 5 to 30 minutes while ensuring a constant stirring speed of 500 rpm.

Two separate stages are shown in Figure 6. At the beginning of the experiment, the adsorption process moves rather quickly. The high accessibility of active empty sites on the surface of ACah, ACds, and ACos, could be the reason for this. But once 20 minutes pass, there is a slower phase that is noticed. Because there is a tendency for these active empty sites to become less available for MO molecule binding[22] this slower phase is thought to be the most optimal one. We also measured the removal efficiency, which can reach 93.87% for ACah, 91.83% for ACds and 89.79% for ACos. This high efficiency is due to the microporous structure of the materials. Based on these results, we can conclude that the activated carbon of Argan husks stands out as the superior adsorbent for methyl orange dye in comparison to the other two precursors. These findings align with the BET values acquired and listed in Table 2.

3.3.2. MO-concentration effect

Five specimens were created, each holding 25 milliliters of MB solution at concentrations of 2, 4, 6, 8, and 10 mg L^{-1}, they were mixed at 500 rpm for 20 minutes, and 0.06 g of each adsorbent ACah, ACds, and ACos. were added to each sample. This experiment was designed to evaluate the effects of adsorbate concentration on the adsorption process. Figure 7 illustrates the results obtained.

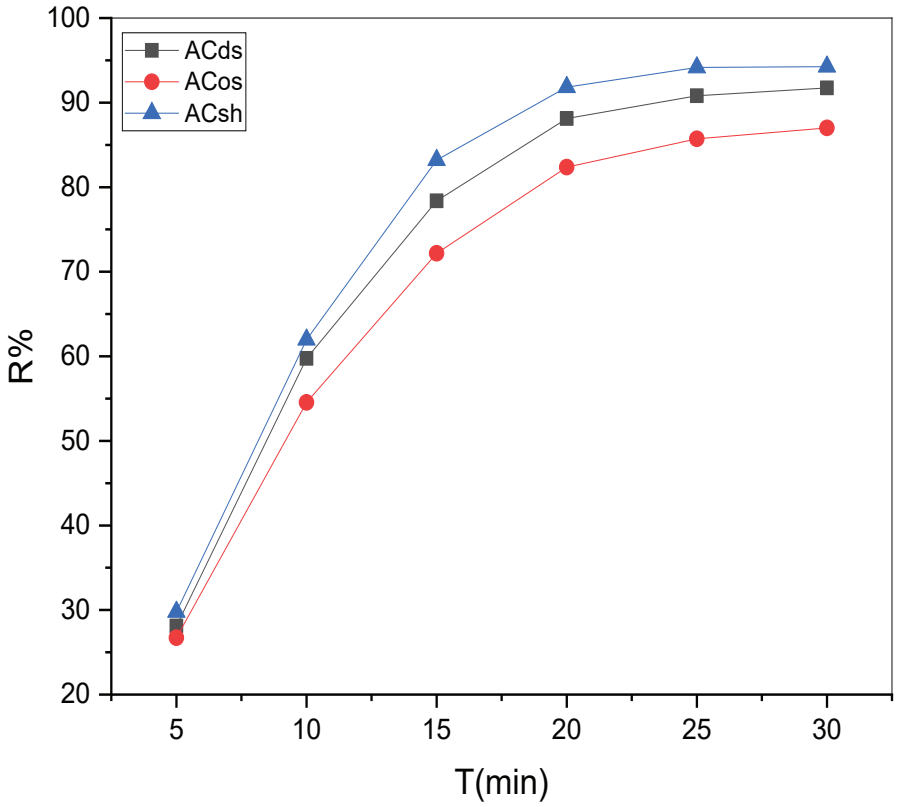

Fig. 6. The recovery of MO removal as a function of t (min) for ACah, ACds, and ACos adsorbents

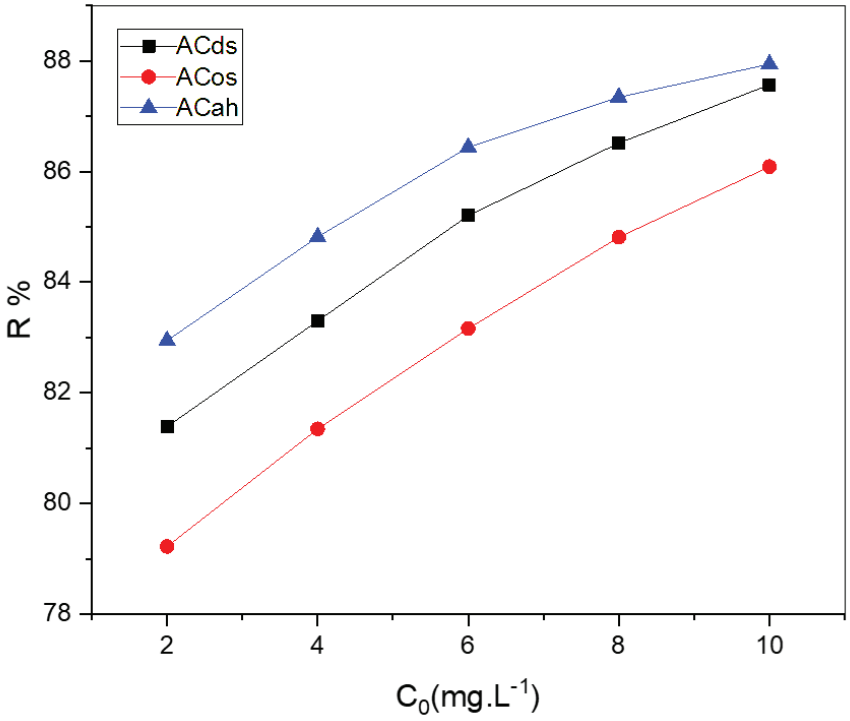

Fig. 7. The effect of MO concentration on removal efficiency(%R)

As the concentration rises, the rate of MO removal also increases, as indicated by the data presented in Figure 7. This implies that a significant proportion, if not nearly all, of the pores are nearly completely occupied. Among the adsorbents tested, ACah continues to stand out as the most effective adsorbent for MO dye, with a percentage difference of approximately 8%.

3.3.3.Effect of temperature

The study examined how altering temperatures between 20°C and 60°C affected the adsorption processes. The experimental conditions included consistent parameters: a fixed volume (V) of 25 mL, an initial concentration (C) of 10 mg L^{-1}, a pH maintained at 7.3, a reaction time of 20 minutes, agitation at 500 rpm, and an adsorbent mass of 0.06 g, Figure 8 displays the findings obtained from these tests.

We observe that when the temperature rises, MO's adsorption capacity on ACah, ACds, and ACos decreases. The adsorption process exhibits an exothermic nature as confirmed by these observations, this gives negative values for standard enthalpy ($\Delta H<0$)[23]. The reverse adsorption process, which begins at a temperature of about 30°C, is what causes this decrease in the adsorbed amount. It is essential to comprehend this phenomenon to restore activated carbons. The experimental data presented in the figure suggest that the highest adsorption occurs between 20 and 30°C, which corresponds to room temperature. We were also able to achieve a similar removal percentage of 80% for all three activated carbons at a temperature of around 50°C.

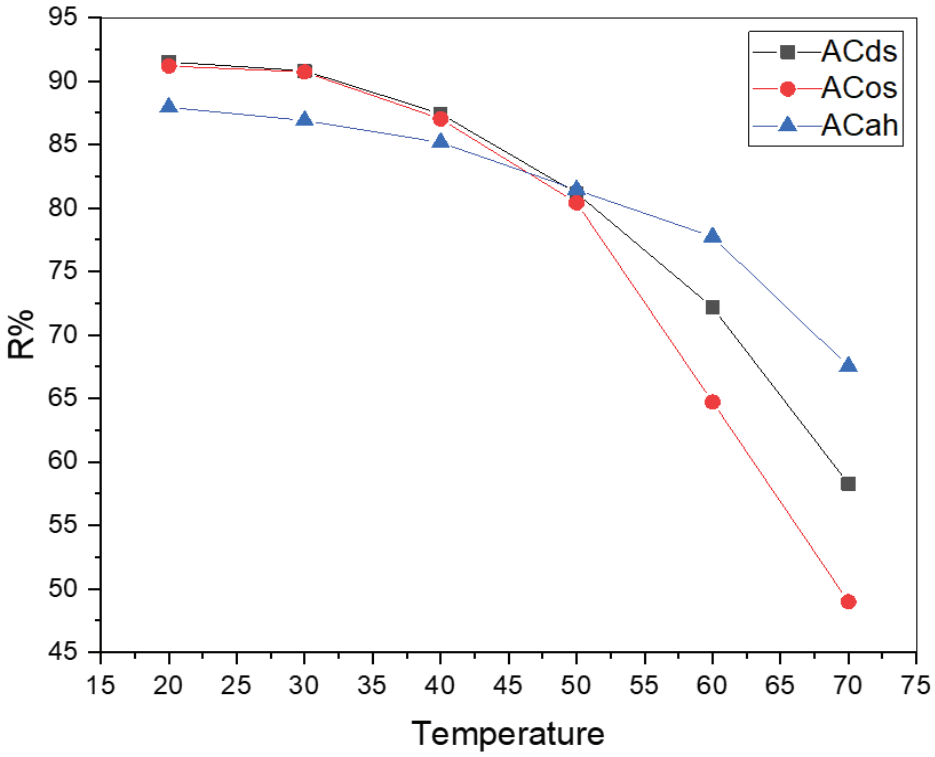

Fig. 8. The impact of temperature on the extent of removal

3.4. Adsorption isotherms

An adsorption isotherm, which generally depicts the adsorption capacity at equilibrium as a function of concentration under particular experimental conditions, can be used to further characterize the adsorption process. The obtained experimental data is used for this. Two of the most commonly used models for fitting experimental adsorption data are the Langmuir and Freundlich models. These models provide parameters that shed light on the mechanisms underlying the adsorption process.

3.4.1.Langmuir Isotherm

To determine the Langmuir isotherm, a graph is constructed by plotting 1/qe as a function of 1/Ce, as depicted in Figure 9. The linear representation of this relationship is expressed by Equation 3. In this Equation, qe signifies the quantity of adsorbed dye, Ce represents the equilibrium concentration of the adsorbate, Qm indicates the maximum adsorption capacity observed during the reaction, and K denotes the Langmuir constant[24]. The plot Figure 9 shows a straight line with $q_{(max)}$ and *kL* determined from the y-intercept and slope, respectively, with a correlation factor of 0.99 for all three materials confirming the validity of the Langmuir model.

$$\frac{1}{qe} = \frac{1}{Qmax} + \frac{1}{K.qmax}.\frac{1}{Ce} \quad \text{(Eq. 3)}$$

3.4.2.Freundlich isotherm

The Freundlich adsorption isotherm is an empirical relationship describing the connection between the adsorbed amount (qe) and the concentration (Ce) of a solute adsorbed on the surface. The experimental findings demonstrate a direct relationship between the concentration and the adsorption of the adsorbate as illustrated in Figure 10. This relationship can be established by graphing the natural logarithm of qe against the natural logarithm of Ce and is represented by the linear form of the Freundlich Equation (4), with the constants KF indicating the capacity of adsorption and (n^{-1}) representing the intensity of adsorption [25].

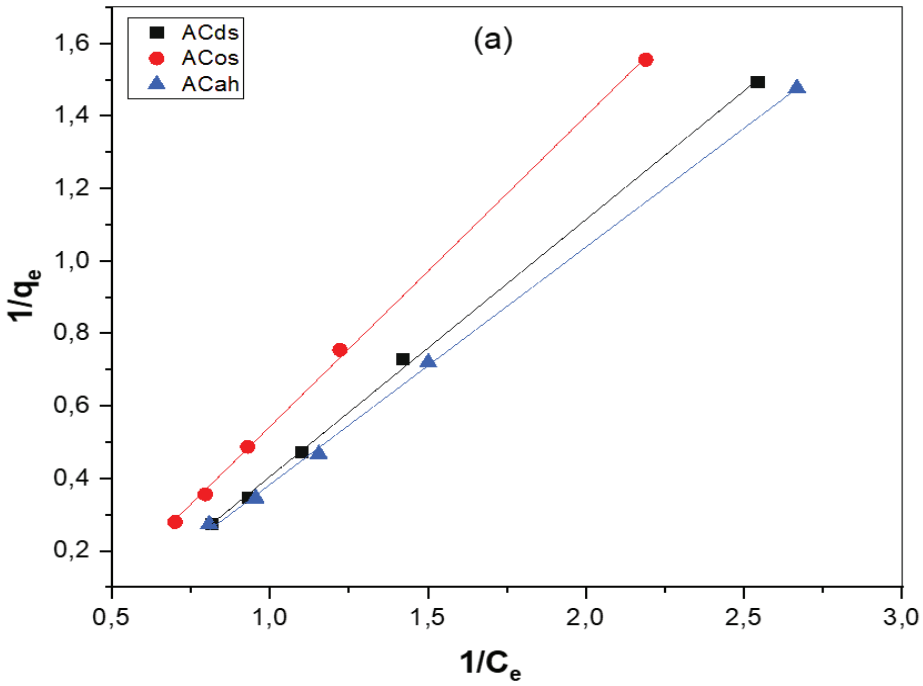

Fig. 9. Isotherm of Langmuir (a) for MO-adsorption on ACah, ACds, and ACos

$$\mathbf{Ln(qe)} = \mathbf{Ln(KF)} + \frac{\mathbf{1}}{\boldsymbol{n}}.\mathbf{Ln(Ce)}$$

(Eq. 4)

k_F and n are the Freundlich constants for adsorption capacity and adsorption intensity, derived from the linear plot in Figure 10 and listed in Table 2. The Freundlich's parameters, n, and KF, as well as the Langmuir parameters, KL and Qm, were determined after the previous adsorption isotherm analysis. These results are listed in Table 2.

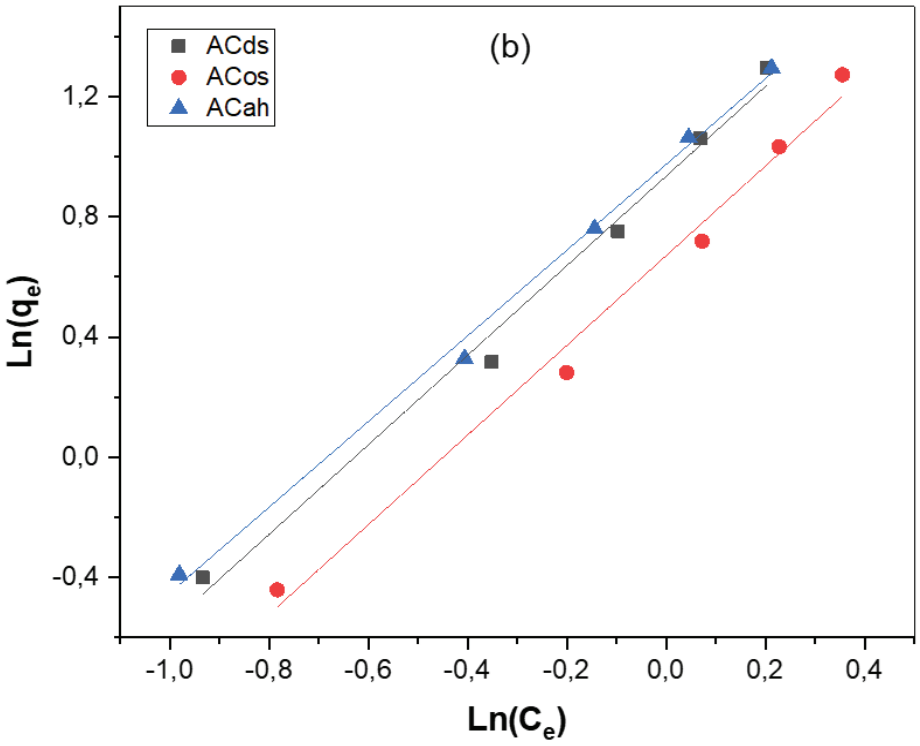

Fig. 10. Isotherm of Freundlich(b) for MO-adsorption on ACah, ACds, and ACos

The Langmuir equation yielded higher correlation coefficients (R^2> 0.99) compared to other models. This indicates that the Langmuir equation is a favorable choice for fitting the experimental adsorption data, enabling the evaluation of the maximum adsorption capacities of the adsorbate on the three adsorbents. Figure 11 offers a comparative examination of the maximum adsorption capacities of MO dye on the three activated carbons used ACah, ACds, and ACos, and Langmuir's Qmax, K_L were determined and listed in Table 3. Within a half-hour of contact time, the maximum adsorption capacities for ACah, ACds, and ACos are recorded as 3.67 mg g^{-1}, 3.27 mg g^{-1}, and 3.19 mg g^{-1}, respectively, as depicted in Figure 11. This indicates that, in comparison to the other two adsorbents, ACah demonstrates the most efficient removal of MO dye. To assess the performance of the material obtained, the adsorption capacity found in this study was compared with other results available in the literature dealing with the adsorption of methyl orange (Table 3**).** Also, many nano adsorbents such as activated carbon, carbon nanotubes, carbon quantum dots, fullerene nanoparticles, and graphene were used for the removal of organic material in different matrixes [26-29]. This comparison more or less confirms that agricultural waste can be considered a precursor to activated carbon, which is used effectively as an adsorbent for toxic dyes at low concentrations.

Table 2. Freundlich and Langmuir adsorption isotherm parameters of MO adsorbed by ACah, ACds, and ACos

Adsorbent	Langmuir parameters			Freundlich parameters		
	Qmax (mgg^{-1})	*K_L (L.mg^{-1})*	*R^2*	*n*	*K_F*	*R^2*
AC ah	3.67	0.43	0,993	0.70	2.65	0,991
AC ds	3.27	0.44	0,991	0.67	2.54	0,981
AC os	3.19	0.37	0,991	0.67	1.95	0,980

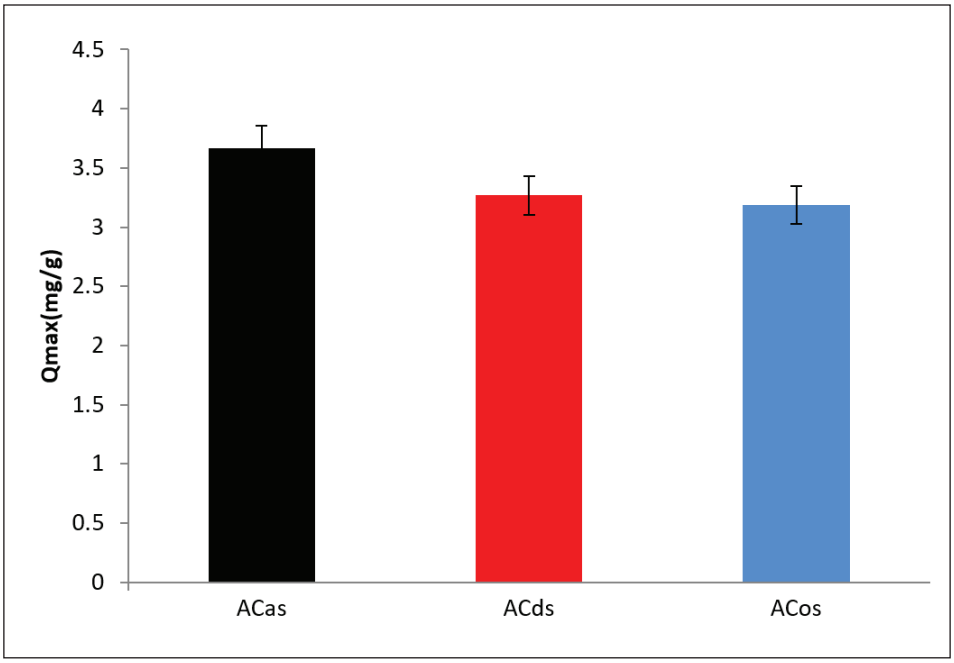

Fig. 11. Adsorption capacities comparison of ACah, ACds, and ACos by Langmuir model

Table 3. Comparison of adsorption capacity (mg g^{-1}) for methyl orange onto ACah, ACds, and ACos with other adsorbents

Adsorbents	qmax (mg g^{-1})	Concentration (mg L^{-1})	pH	T (C°)	Time (min)	Ref.
AHM	15.56	50	6	30	30	[30]
MGGP	16.94	50	3.7	25	60	[31]
N–TiO_2	14.1	21	-	20	300	[32]
ACah	3.67	10	7	25	30	This study
ACds	3.27	10	7	25	30	This study
ACos	3.19	10	7	25	30	This study

AHM: Amino-crosslinked hypromellose
N–TiO_2: Nitrogen-doped–titanium oxide
MGGP: Multigene genetic programming

3.5. Adsorption kinetics

The adsorption rate of the adsorbate is described by kinetic studies. This aspect is crucial in understanding the adsorption process as it directly influences the duration of the adsorption process. This study employed the pseudo-first-order model, pseudo-second-order model, and intraparticle diffusion model to explore the kinetics of adsorption processes and determine the reaction order of MO on three activated carbons: ACah, ACds, and ACos.

3.5.1. The pseudo-first-order model

Equation (5) delineates the pseudo-first-order model, and after a straightforward mathematical integration, it assumes the linear form denoted by Equation (6). In this context, qe and qt represent the quantity of MO adsorbed at equilibrium and at a specific time, respectively, while Kf denotes the pseudo-first-order rate constant[33]. Kinetic is depicted in Figure 12 as a pseudo-first-order for the adsorption of MO onto activated ACah, ACds, and ACos.

$$\frac{dq_t}{dt} = K_1(q_e - q_t) \qquad \text{(Eq. 5)}$$

$$\ln(q_e - q_t) = \ln(q_e) - K1 \times t \qquad \text{(Eq. 6)}$$

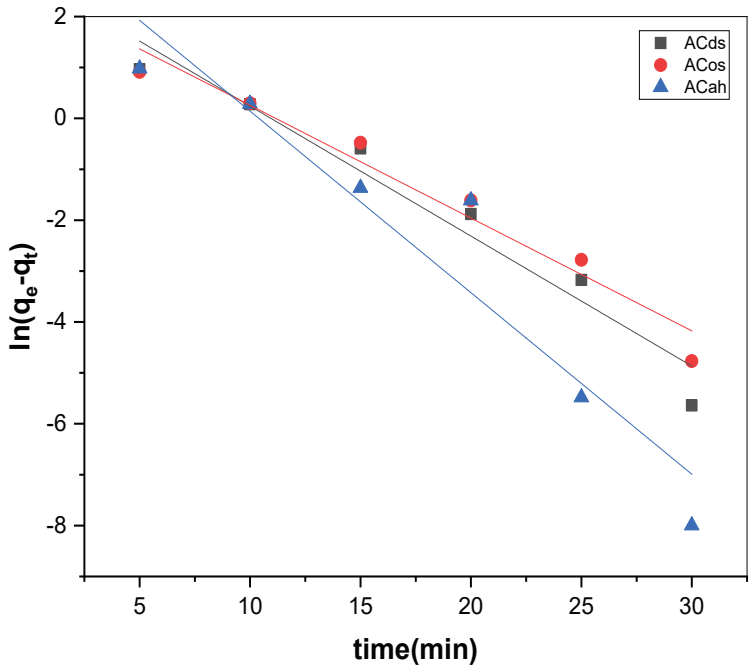

Fig. 12. Pseudo-first order kinetic of MO-adsorption on ACah, ACds, and ACos adsorbents

3.5.2. The pseudo-second-order kinetic model

The pseudo-second-order model is expressed by the differential Equation (7). Upon mathematical integration, Equation (8) is obtained, with K_2 representing the rate constant associated with the pseudo-second-order[34]. Kinetic is depicted in Figure 13, as the second-order for the adsorption of MO onto activated ACah, ACds, and ACos.

$$\frac{dq_t}{dt} = k_2(q_e - q_t)^2 \qquad \text{(Eq.7)}$$

$$\frac{t}{q_t} = \frac{1}{(k_2 q_e^2)} + \frac{1}{q_e}t \qquad \text{(Eq. 8)}$$

Kinetic comparison is depicted in Figure 12 and Figure 13, and the pseudo-first-order and second-order parameters for the adsorption of MO onto activated ACah, ACds, and ACos are detailed in Table 4. The results suggest that the pseudo-second-order model is more suitable than the pseudo-first-order model for studying the adsorption kinetics of MO on the three activated carbons. This preference arises from the pseudo-second-order model's dependence on a longer period, facilitating close or complete adsorption of the adsorbing element. Experimentally, the correlation between the amount of adsorbent and the periods is evident from the curve, with a high coefficient of determination ($R^2 > 0.99$).

4. Conclusions

Three carbonaceous materials such as ACah, ACds, and ACos adsorbents were prepared by activating different precursors with phosphoric acid. They were tested for removal of methyl orange dye in aqueous media. Adsorption rates reached 93.87%, 91.83%, and 89.79% respectively. AC ah can be said to be the most powerful adsorbent, with a slightly higher rate. This is in line with the results of SEM, FTIR, and BET. However, the adsorption of methyl orange onto the three activated carbons is not solely attributed to the pores. It is also influenced by the diverse specific surface areas and the variety of functional groups present on the material surfaces, leading to electrostatic attraction forces.

The isotherm study showed that the Langmuir model proved to be the most appropriate, and the experimental results of the kinetic study corresponded well with the pseudo-second-order kinetic model. As a result, significant efficiencies were achieved

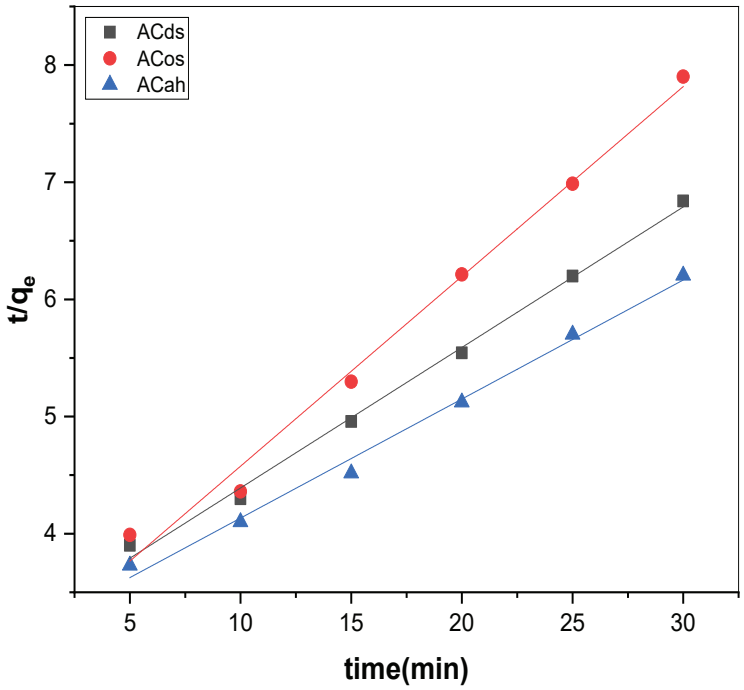

Fig. 13. Pseudo-second-order of MO adsorption on ACah, ACds, and ACos adsorbents

Table 4. Parameters of pseudo-first-order and second-order adsorption of MO on ACah, ACds, and ACos

Adsorbent	Pseudo-first order parameters			Pseudo-second order parameters		
	K_1(1/min)	q_e(mg.g^{-1})	R^2	K_2 (g.mg min^{-1})	qe (m.g^{-1})	R^2
ACah	0.356	8.850	0.911	0.0033	9.840	0.999
ACds	0.255	7.361	0.955	0.0045	8.341	0.991
ACos	0.221	6.121	0.950	0.0001	6.172	0.992

in the removal of a toxic and polluting dye by three activated carbons, with the possibility of regenerating them, this holds significant ecological importance.

5. List of abbreviations

AC	Activated carbon
MO	Methyl orange
ACOP	Activated carbon of olive pomace
ACDP	Activated carbon of date pits
ACAS	Activated carbon of argan shells
FTIR	Fourier-transform infrared
SEM	Scanning electron microscopy
BET	Brunauer-Emmett-Teller
R (%)	The adsorption rate

6. Acknowledgment

This research was carried out at the Laboratory of Research in Bio-Geosciences and Materials Engineering, ENS Casablanca, Morocco. The authors would like to express their gratitude to all those who contributed to the characterization analyses.

7. References

[1] R.R. Karri, G. Ravindran, M.H. Dehghani, Chapter 1 - Wastewater—Sources, Toxicity, and their consequences to human health, Soft Computing Techniques in Solid Waste and Wastewater Management, Elsevier, pp. 3–33, 2021. https://doi.org/10.1016/B978-0-12-824463-0.00001-X

[2] S. Garg, Z.Z. Chowdhury, A.N.M. Faisal, N.P. Rumjit, P. Thomas, Impact of Industrial Wastewater on Environment and Human Health, in: S. Roy, A. Garg, S. Garg, T.A. Tran (Eds.), Advanced Industrial Wastewater Treatment and Reclamation of Water: Comparative Study of Water Pollution Index during Pre-Industrial, Industrial Period and Prospect of Wastewater Treatment for Water Resource Conservation, Springer International Publishing, Cham, pp. 197–209, 2022. https://doi.org/10.1007/978-3-030-83811-9_10

[3] C. Zhao, L. Meng, H. Chu, J.-F. Wang, T. Wang, Y. Ma, C.-C. Wang, Ultrafast degradation of emerging organic pollutants via activation of peroxymonosulfate over Fe3C/Fe@N-C-x: Singlet oxygen evolution and electron-transfer mechanisms, Appl. Catal. B: Environ., 321 (2023) 122034. https://doi.org/10.1016/j.apcatb.2022.122034

[4] A. Ouedrhiri, M. Ennabely, Y. Lghazi, M. Chafi, S. Alougayl, B. Youbi, A.K. Halabi, M. Khoukhi, I. Bimaghra, Adsorption of anionic and cationic dyes in aqueous solution by a sustainable and low-cost activated carbon based on argan solid waste treated with H3PO4, Environ. Sci. Pollut. Res., (2023). https://doi.org/10.1007/s11356-023-26550-z

[5] A.A. Mana, A. Allouhi, K. Ouazzani, A. Jamil, Feasibility of agriculture biomass power generation in Morocco: Techno-economic analysis, J. Clean. Prod., 295 (2021) 126293. https://doi.org/10.1016/j.jclepro.2021.126293

[6] M.H. Sedra, Date Palm Status and Perspective in Morocco, in: J.M. Al-Khayri, S.M. Jain, D.V. Johnson (Eds.), Date Palm Genetic Resources and Utilization: Volume 1: Africa and the Americas, Springer Netherlands, Dordrecht, pp. 257–323, 2015. https://doi.org/10.1007/978-94-017-9694-1_8

[7] B. Moumni, M. Achik, H. Benmoussa, A. Oulmekki, A. Touache, N. El Moudden, M. Charroud, D. Eliche-Quesada, O. Kizinievic, V. Kizinievic, A. Infantes-Molina, G. Gonzalez

Álvaro, F. Guitián Rivera, Recycling argan nut shell and wheat straw as a porous agent in the production of clay masonry units, Constr. Build. Mater., 384 (2023) 131369. https://doi.org/10.1016/j.conbuildmat.2023.131369

[8] A. Onder, H. Ozay, Highly efficient removal of methyl orange from aqueous media by amine functional cyclotriphosphazene submicrospheres as reusable column packing material, Chem. Eng. Process., 165 (2021) 108427. https://doi.org/10.1016/j.cep.2021.108427

[9] M.A. Dutt, M.A. Hanif, F. Nadeem, H.N. Bhatti, A review of advances in engineered composite materials popular for wastewater treatment, J. Environ. Chem. Eng., 8 (2020) 104073. https://doi.org/10.1016/j.jece.2020.104073

[10] Q. Liu, Z. Zheng, X. Yang, X. Luo, J. Zhang, Effect of factors on decolorization of azo dye methyl orange by oxone/natural sunlight in aqueous solution, Environ. Sci. Pollut. Res., 19 (2012) 577–584. https://doi.org/10.1007/s11356-011-0591-4

[11] M. Saeed, A. Mansha, ZnO catalyzed degradation of methyl orange in aqueous medium, Chiang Mai J. Sci., 44 (2017) 1646-1653. https://www.thaiscience.info/journals/Article/CMJS/10987608.pdf

[12] V.I. Pet'kov, E.A. Asabina, A.V. Markin, K.V. Kir'yanov, Calorimetric study of sodium-rich zirconium phosphate, Thermochim. Acta, 403 (2003) 185–196. https://doi.org/10.1016/S0040-6031(02)00656-1

[13] A. Önder, Preparation of cationic composite hydrogel improved by activated carbon and its use in removal of anionic dye, J. Inst. Sci. Tech., 13 (2023) 1902–1915. https://doi.org/10.21597/jist.1243905

[14] V.K. Gupta, D. Pathania, S. Sharma, S. Agarwal, P. Singh, Remediation and recovery of methyl orange from aqueous solution onto acrylic acid grafted Ficus carica fiber: Isotherms, kinetics and thermodynamics, J. Mol. Liq., 177 (2013) 325–334. https://doi.org/10.1016/j.molliq.2012.10.007

[15] H. ait Hmeid, M. Akodad, M. Baghour, A. Moumen, A. Skalli, G. Azizi, A. Anjjar, M. Aalaoul, I. Daoudi, Adsorption of a basic dye, methylene blue, in aqueous solution on bentonite, Mor. J. Chem., 9 (2021) 416-433. https://doi.org/10.48317/IMIST.PRSM/morjchem-v9i3.23303

[16] D. Saetta, K. Buddenhagen, W. Noha, E. Willman, T.H. Boyer, Ultraviolet/visible absorbance trends for beverages under simulated rinse conditions and development of data-driven prediction model, Food Control, 146 (2023) 109530. https://doi.org/10.1016/j.foodcont.2022.109530

[17] G.L. Arueya, T.M. Oyewale, Effect of varying degrees of succinylation on the functional and morphological properties of starch from acha (Digitaria exilis Kippis Stapf), Food Chem., 177 (2015) 258–266. https://doi.org/10.1016/j.foodchem.2015.01.019

[18] M.F. Mohamad Yusop, A.Z. Abdullah, M.A. Ahmad, Malachite green dye adsorption by jackfruit based activated carbon: Optimization, mass transfer simulation and surface area prediction, Diam. Relat. Mater., 136 (2023) 109991. https://doi.org/10.1016/j.diamond.2023.109991

[19] S. Ramola, T. Belwal, C.J. Li, Y.Y. Wang, H.H. Lu, S.M. Yang, C.H. Zhou, Improved lead removal from aqueous solution using novel porous bentonite - and calcite-biochar composite, Sci. Total Environ., 709 (2020) 136171. https://doi.org/10.1016/j.scitotenv.2019.136171

[20] Y.-Z. Wu, J. Xu, H.-X. Li, Y.-H. Tong, Z.-L. Xu, C. Lian, H. Liu, Enhanced steric effect and desolvation process on organic solvent nanofiltration: A mechanism study for removing anionic dyes, Chem. Eng. J., 446 (2022) 137360. https://doi.org/10.1016/j.cej.2022.137360

[21] W. Pan, H. Xie, Y. Zhou, Q. Wu, J. Zhou, X. Guo, Simultaneous adsorption removal of organic and inorganic phosphorus from discharged circulating cooling water on

biochar derived from agricultural waste, J. Clean. Prod., 383 (2023) 135496. https://doi.org/10.1016/j.jclepro.2022.135496

[22] A.A. Alghamdi, A.-B. Al-Odayni, W.S. Saeed, M.S. Almutairi, F.A. Alharthi, T. Aouak, A. Al-Kahtani, Adsorption of azo dye methyl orange from aqueous solutions using alkali-activated polypyrrole-based graphene oxide, Molecules, 24 (2019) 3685. https://doi.org/10.3390/molecules24203685

[23] M. Husaini, B. Usman, M.B. Ibrahim, Kinetic and thermodynamic evaluation on removal of anionic dye from aqueous solution using activated carbon derived from agricultural waste: equilibrium and reusability studies, Appl. J. Environ. Eng. Sci., 9 (2023) 9–138. https://doi.org/10.48422/IMIST.PRSM/ajees-v9i3.40418

[24] K. Singh, S.K. Azad, H. Dave, B. Prasad, D.M. Maurya, M. Kumari, D. Dubey, A.K. Rai, D. Singh, M. Sillanpää, M.P. Sah, K.S. Prasad, A mechanistic insight into chromium (VI) ion adsorption onto pristine, UCB as well as Al-modified Neolamarckia cadamba wood biochar, Biomass Conv. Bioref., (2022). https://doi.org/10.1007/s13399-022-03620-9

[25] H.N. Tran, Improper estimation of thermodynamic parameters in adsorption studies with distribution coefficient K_D (q_e/C_e) or Freundlich constant (K_F): considerations from the derivation of dimensionless thermodynamic equilibrium constant and suggestions, Adsorpt. Sci. Technol., 2022 (2022) e5553212. https://doi.org/10.1155/2022/5553212

[26] M.B.H. Abadi, Air pollution control: The evaluation of TerphApm@ MWCNTs as a novel heterogeneous sorbent for benzene removal from air by solid phase gas extraction, Arab. J. Chem., 13 (2020) 1741-1751. https://doi.org/10.1016/j.arabjc.2018.01.011

[27] M. Osanloo, Nobel method for toluene removal from air based on ionic liquid modified nano-graphene, Int. J. Occup. Hyg., 6 (2014) 1-5. http://ijoh.tums.ac.ir

[28] C. Jamshidzadeh, A new method for removal of hazardous toluene vapor from air based on ionic liquid-phase adsorbent, Int. J. Environ. Sci. Technol., 16 (2019) 2797-2808. https://doi.org/10.1007/s13762-018-1975-5

[29] C. Jamshidzadeh, A new analytical method based on bismuth oxide-fullerene nanoparticles and photocatalytic oxidation technique for toluene removal from workplace air, Anal. Methods Environ. Chem. J., 2 (01) (2019) 73-86. https://doi.org/10.24200/amecj.v2.i01.55

[30] W. Qu, D. He, H. Huang, Y. Guo, Y. Tang, R.-J. Song, Characterization of amino-crosslinked hypromellose and its adsorption characteristics for methyl orange from water, J. Mater. Sci., 55 (2020) 7268–7282. https://doi.org/10.1007/s10853-020-04517-6

[31] N. Kütük, S. Arslan, Biosorption of methyl orange from aqueous solution with hemp waste, investigation of isotherm, kinetic and thermodynamic studies and modeling using multigene genetic programming, Chem. Papers, 76 (2022) 1–16. https://doi.org/10.1007/s11696-022-02411-w

[32] J. Fan, Z. Zhao, W. Liu, Y. Xue, S. Yin, Solvothermal synthesis of different phase N–TiO_2 and their kinetics, isotherm and thermodynamic studies on the adsorption of methyl orange, J. Colloid Interface Sci., 470 (2016) 229–236. https://doi.org/10.1016/j.jcis.2016.02.045

[33] A. Ouedrhiri, Y. Lghazi, J. Bahar, M. Ait Himi, C. El Haimer, B. Youbi, M. Khoukhi, Y. Bimaghra, Adsorption of the methylene blue dye in environmental water samples by biochar obtained from the valorization of argan shells, Phys. Chem. Res., 10 (2022) 301–313. https://doi.org/10.22036/pcr.2021.303554.1968

[34] E.D. Revellame, D.L. Fortela, W. Sharp, R. Hernandez, M.E. Zappi, Adsorption kinetic modeling using pseudo-first order and pseudo-second order rate laws: A review, Clean. Eng. Technol., 1 (2020) 100032. https://doi.org/10.1016/j.clet.2020.100032

Anal. Methods Environ. Chem. J. 7 (2) (2024) 74-88

AMECJ

Research Article, Issue 2
Analytical Methods in Environmental Chemistry Journal
Journal home page: www.amecj.com/ir

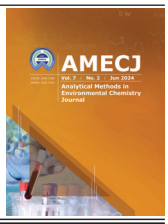

Dolomite utilization for removal of Zn^{2+} and Cu^{2+} ions from wastewater before determination by flame atomic absorption spectroscopy

Firas Fadhel Ali[a], Ahmed S. Al-Rawi[b], Abdulsalam M. Aljumialy[c], and Mohammed Oday Ezzat[*,a]

[a] *Department of Chemistry, Education College for Women, University of Anbar, Ramadi, Iraq*
[b] *Department of Chemistry, College of Science, University of Anbar, Ramadi, Iraq*
[c] *Department of Applied Chemistry, College of Applied Sciences, University of Fallujah, Fallujah, Iraq*

ARTICLE INFO:

Received 12 Feb 2024
Revised form 16 Apr 2024
Accepted 15 May 2024
Available online 30 Jun 2024

Keywords:
Flame atomic absorption spectroscopy
Adsorption
Dolomite
Wastewater
Heavy metal ions

ABSTRACT

This study aims to use dolomite to remove Zn^{2+} and Cu^{2+} from wastewater. The adsorption process of the Zn^{2+} and Cu^{2+} was performed using the batch method at various factors (such as the amount of adsorbent, contact time, particle size, pH media, temperature, and initial concentration) to investigate the optimum removal conditions. The flame atomic absorption spectroscopy (F-AAS) was used to determine Zn^{2+} and Cu^{2+} after removal steps. The LOD of Zn^{2+} and Cu^{2+} were 0.05 mg L^{-1} and 0.08 mg L^{-1}, respectively. Results showed that the adsorbent dolomite efficiently removed Zn^{2+} and Cu^{2+} with up to 98 % when 0.4 g of dolomite was used. The smaller dolomite particle size had higher removal efficiency for Zn^{2+} and Cu^{2+} ions. The results showed the removal of Zn^{2+} and Cu^{2+} was the maximum in the basic medium. Also, the removal of ions reached the maximum when dolomite had been in contact for 30 minutes with the wastewater. The experimental results of Langmuir and Freundlich adsorption isotherms show linearity where R^2 is more than (0.998 and 0.978) and (0.9915 and 0.9996) for Zn^{2+} and Cu^{2+}, respectively. The maximum monolayer capacities (q_{max}) were obtained at 91.74 mg g^{-1} for Cu^{2+} and 44.24 mg g^{-1} for Zn^{2+}.

1. Introduction

The decrease in the amount of rain around the world caused todecreasein the level of freshwater. On the other side, global freshwater demand is estimated to increase due to population growth and industrial development[1]. Therefore, it is very important to keep the water resources as clean as possible, whereby the contamination of resource water can lead to reducing accessible freshwater. The pollution of freshwater resources has become a serious problem that needs quick action before it is too late to handle[2–5]. Developing current and new industries including but not limited to batteries, paper mills, board mills, fertilizers, petrochemicals, inorganic chemicals, basic steel works, basic non-ferrous metal works, motor vehicles, steam generation power plants, plating and painting has resulted in the release a significant amount of heavy metal ions such as lead, cadmium, chromium, copper and zinc that end up in the environment, especially in the water resource[6–8]. The increasein pollutants discharged into the water resource affects the amount of usable water and the ecosystem because of their high toxicity[9]. These pollutants must be removed from wastewater before they are released into the surface water.

*Corresponding Author: Mohammed Oday Ezzat
Email: edw.mohamed_oday@uoanbar.edu.iq
https://doi.org/10.24200/amecj.v7.i02.311

The researchers aim to find a way to reduce the release of pollutants into water resources[6,10]. Copper and zinc ions are considered toxic heavy metals. At the health-based guideline, copper and zinc concentrations in surface watersthat arebelow 2 mg L^{-1} and 3 mg L^{-1} respectively are deemed acceptable [9,11]. Thus, the concentration of heavy metals in wastewater should not exceed the maximum allowable concentration (MAC) before it is discharged to meet water quality guidelines. It is crucial to address the treatment of wastewater contaminated with heavy metals, which poses a significant challenge for industries[12]. Removal of heavy metal ions from wastewater can be accomplished by a variety of treatment methods including chemical methods such as precipitation, complexation, ion exchange, solvent extraction, and adsorption process by activated carbon and clay, and sieve process by membranes[1, 13, 14]. The use of an adsorption process to remove heavy metal ions from wastewater has recently achieved significant interest because it mainly depends on using environmentally friendly and economically effective materials as their adsorbents[3,15]. The heavy metal removal can be achieved by an adsorption process using minerals, which have essential properties that make them excellent adsorbents.The heightened capability to adsorb due to their high surface area, pores, and cavities are among these properties[16]. The minerals could also act as ion exchangers replacing the ions contained in their structure with the heavy metal ions in the wastewater[17,18]. These minerals can beeasily collected as waste or side products from numerous industries atzero value, and they have to be an effective adsorbent. Minerals like dolomite powder,which is regarded as waste from the residual of the build processes. Furthermore, it can be a viable choice to be used as an adsorbent for the removal of heavy metalsfrom wastewater[3,19].

This study aims to evaluate the potentialability of dolomite powder for removing of Zn^{2+} and $Cu^{2+}$from wastewater. Dolomite powder is naturally occurring rockproduced in large amounts as a byproduct withlow cost. So,the dolomite powder is used as an adsorbent for removing Zn^{2+} and Cu^{2+}ions in water samples before being determined by F-AAS.

2. Materials and Methods

2.1. Materials

Both Zn^{2+} and Cu^{2+}stock solutions were prepared by dissolving 3.8019 g of $Cu(NO_3)_2.3H_2O$(CAS N.: 10031-43-3, Sigma, Germany) and 2.0849 g $ZnCl_2$ (CAS N.: 7646-85-7, Sigma, Germany) in 1 L of deionized water to get 1000 mg L^{-1}as stock solutions. Hydrochloric acid (37%, CAS N.: 7647-01-0), Nitric acid (HNO_3, CAS N.: 7697-37-2), Ammonia-ammonium chloride buffer(CAS N,: 16052-06-5), sodium acetate -acetic acid buffer (pH 3.7-5.6, CAS N.:126-96-5), Na_2HPO_4-NaH_2PO_4 buffer (pH 5.8-8.0, CAS N.: 7558-79-4) purchased from Sigma, Germany.

2.2. Preparation of adsorbent

The dolomite was obtained from the residual of the building processes. The dolomite was firstly dried overnight, milled, and sieved to unify particles size of three sizes of 150, 250, and 300 μm[19].

2.3. Apparatus

Field emission scanning electron emission with Energy dispersive spectroscopy (FE-SEM with EDX) was utilized for screening of the morphology of dolomite and component analysis using HITACHI S4500. The X-ray diffraction (XRD) was achieved on a Bruker D8 Advance (Cu Kα radiation, λ = 1.5406 nm) to study the structure of dolomite. Thermal gravimetric analysis (TGA) was achieved using a Rheometric Scientific STA 1500 instrument to measure water contents and thermal stability. Flame atomic absorption spectroscopy (FAAS) (Phoenix 986 AAS, USA) was used to determine the remaining concentration of Zn^{2+} and Cu^{2+} in the solution after the adsorption process was conducted.

2.4. Adsorption Procedure

The adsorption experiment was accomplished usingthe batch method. 0.4 g of dolomite was mixed with 50 mL of Zn^{2+} and Cu^{2+}solutions in a 100 mL polyethylene tube. The samples were shaken under

controlled conditions for a specific time between 15-120 min. The adsorption process was achieved at pH between 2 - 10, temperatures between 293 - 323°K, and initial concentrations between 50-100 mg L^{-1}[17, 19]. By separating,the dolomitewas separated from the mixture via centrifugation.The last remainingconcentration of Zn^{2+} and Cu^{2+}in the solution after the adsorption process wasevaluated by flame atomic absorption spectroscopy (FAAS) by standard concentration between 0.1 and 1 mg L^{-1} for both ions Zn^{2+} and Cu^{2+}. The FAAS has a low detection limits (LOD) value, a limit of quantification (LOQ) value,and high selectivity, which make it the perfect apparatus for determining most heavy metal concentrations (Fig.1). The LOD of Zn^{2+} and Cu^{2+}were 0.05 mg L^{-1} and 0.08 mg L^{-1}, respectively. The LOQ of Zn^{2+} and Cu^{2+}were evaluated at 0.18mg L^{-1} and 0.25mg L^{-1}, respectively. The whole average relative standarddeviation (RSD) was 3.6% and 5.6% for Zn^{2+} and Cu^{2+}, respectively.

2.5. Adsorption Isotherms:

The relationship between the amount value of removed ions adsorbed and the amount value of dolomite at equilibrium conditionswas calculatedusing Equation 1which was published byVanderborght and Van Griekenm[20]. The Hanes–Woolf as Equation 2 was applied to express the Langmuir isotherms at equilibrium conditions[2, 17, 18]. The Freundlich adsorption modelwas used as another absorption model (Eq. 3). This model is useful to indicate that the adsorption energy value on a homogeneous surface is independent of surface coverage, according to the Equation 3[17].The Temkin model has been shown by the Equations 4 and 5 [21].

$$q_e = (C_o - C_e) * {}^{V}/_{m}$$

(Eq.1)

Where q_e=Quantity (mg g^{-1}) of ion adsorbed on the dolomite at equilibrium conditions, C_o=Initial concentration (mg L^{-1}) of the ion, C_e=Concentration (mg L^{-1}) at equilibrium conditions, m = Mass (g) of adsorbent and V=Volume of the solution

$${}^{C_e}/_{q_e} = {}^{1}/_{(K_L * q_m)} + ({}^{1}/_{q_m}) * C_e$$

(Eq.2)

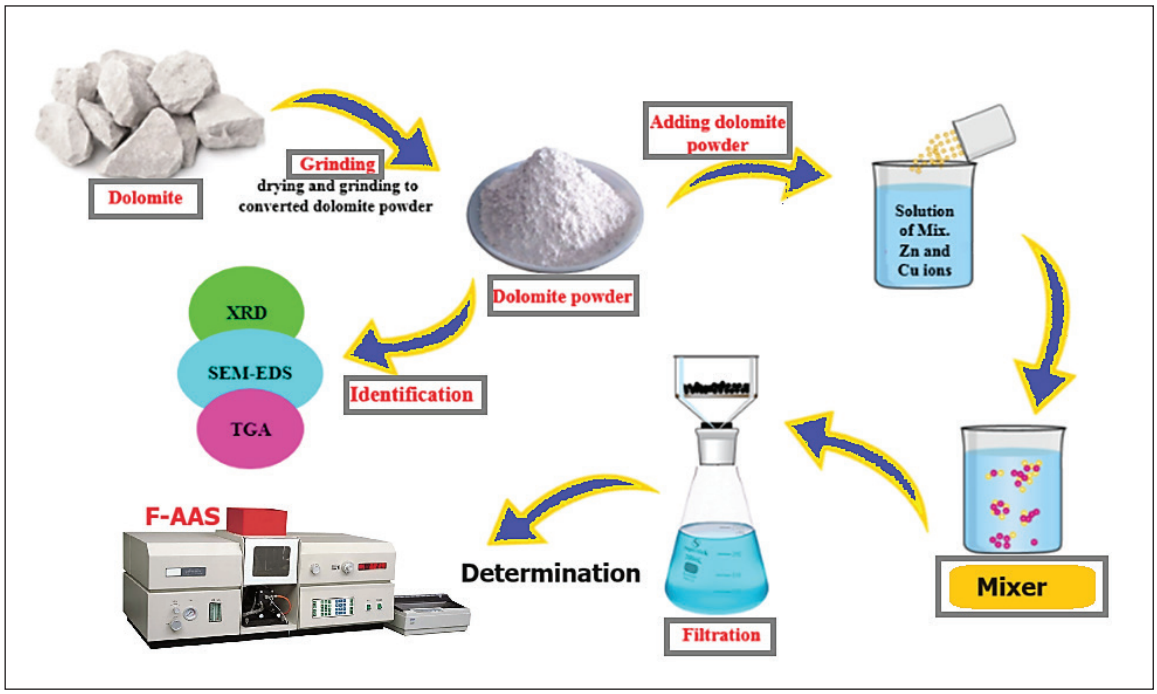

Fig. 1. The Zn^{2+} and Cu^{2+} removal/adsorption based on dolomite before determined by F-AAS

where q_{max} (mg g^{-1}) =The maximum amount value of ions adsorbed on the dolomite surface, leading to creating amonolayer of ions on the surface of dolomite, and K_L=The Langmuir constant corresponding to the adsorption energy value. The value of q_{max} was calculated from the slope and K_L was calculated from the crossing intercept of the plot of C_e/q_e against C_e.

$$q_e = K_f \, C_e^{1/n} \qquad \text{(Eq. 3)}$$

where K_f =Freundlich model constant (mg g^{-1}), n=Adsorption intensity, C_e=The remaining concentration (mg L^{-1}) at equilibrium, q_e = The quantity (mg g^{-1}) of ion adsorbed onto dolomite at equilibrium [17,18].

$$q_e = B \; In \; A_T + B \; In \; C_e \qquad \text{(Eq. 4)}$$

$$b_T = {}^{RT}/_{B} \qquad \text{(Eq. 5)}$$

where B=Constant related to heat of sorption ($Jmol^{-1}$), b_T = Temkin model constant, A_T =Temkin modelequilibrium binding constant (L g^{-1}), q_e = the quantity (mg g^{-1}) of ion adsorbed onto dolomite at equilibrium, R=Universal gas constant (8.314 $Jmol^{-1}K^{-1}$) and T= Temperature at 298°K.

3. Results and Discussion

3.1. Characterization of the synthesized materials

Scanning electron microscopy (SEM) was used to image the morphology of the dolomite. From the SEM images of dolomite shown in Figure 2, it was observed that the morphology of dolomite consists of irregularly shaped particles with rough surfaces[22]. The XRD patterns of dolomite powder are shown in Figure3. The results indicate that dolomite powder mainly consists of dolomite[23]. These results are consistent with the EDX spectrum shown in Table 1. EDX spectrum was used to study the components of dolomite. The results illustrated in Table 1 show that the dolomite is dominated by oxygen at ~ 41%, calcium at ~ 36%, and carbon at 22%[22].

The TGA (Fig. 4) shows weight loss at ~ 600°Csuggesting the release of CO_2 from the decomposition of dolomite ($CaCO_3$)[23].The reaction can be described by by Equation 6.

$MgCa(CO_3)_2 \grave{e} MgCaO_2 + CO_2$ (Eq.6)

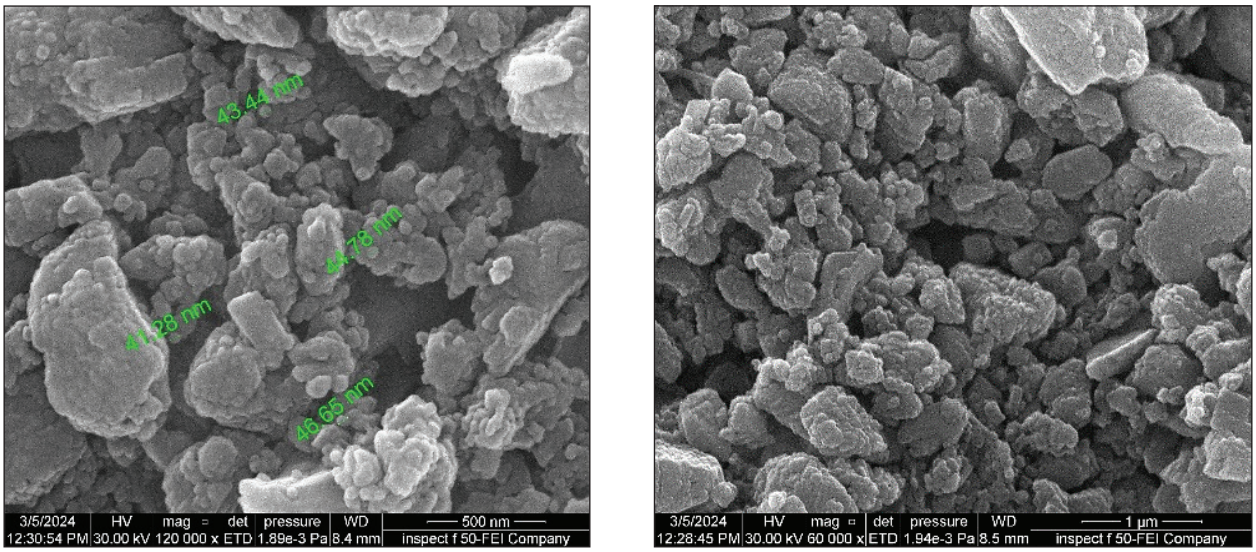

Fig. 2.SEM images of dolomite

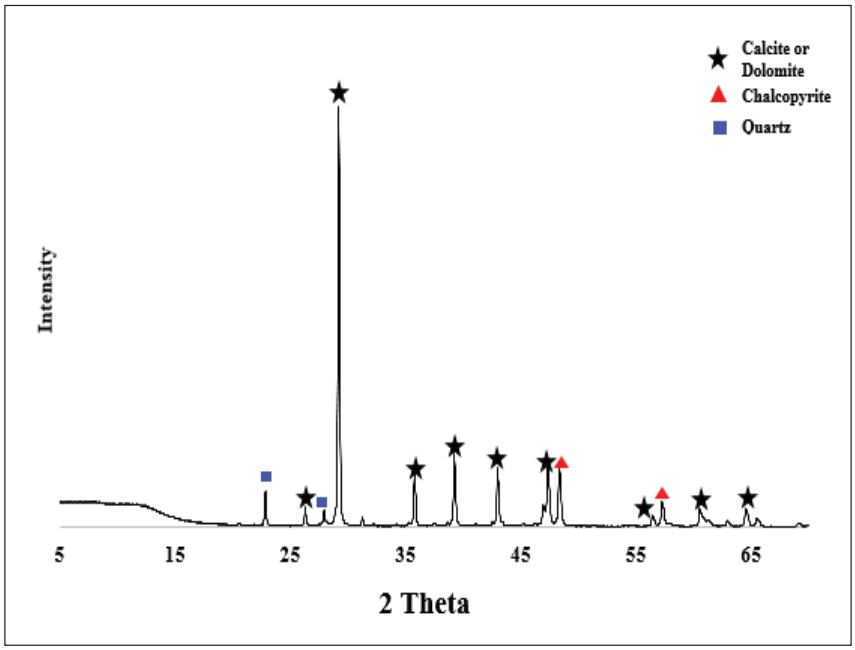

Fig.3.XRD of the dolomite

Table 1. The elemental analysis of dolomite

Element	Weight %
C	14.4
O	47.37
Mg	0.51
Al	0.25
Si	0.55
Ca	36.93
Total	100.00

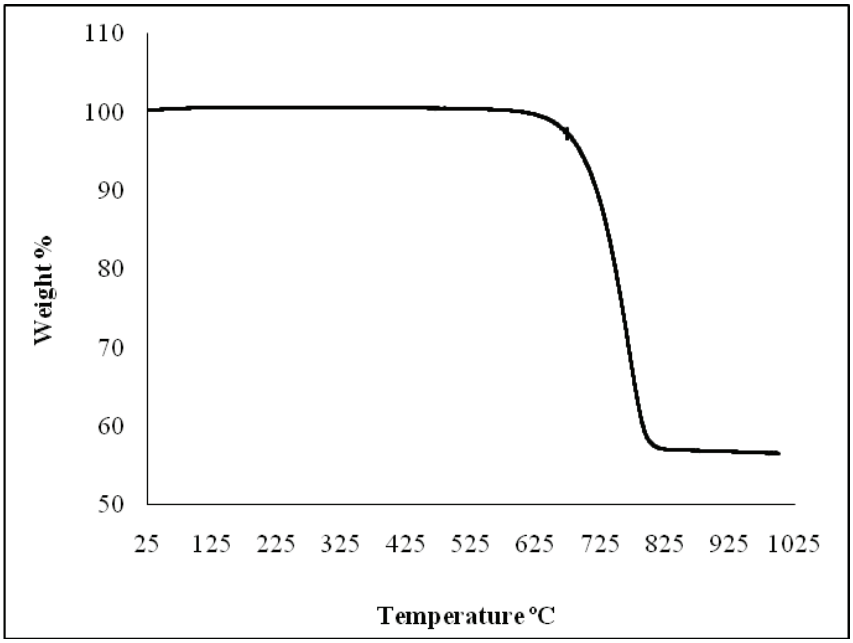

Fig.4.TGA of the dolomite

3.2. Adsorption study

3.2.1.Effect of dolomite amounts

A variety of dolomite amounts at 0.2, 0.4, 0.6, 0.8, and 1 g were used toremove of Zn^{2+} and Cu^{2+}as shown in Figure 5. The dolomite adsorption capacity for the removal of Zn^{2+} was around 82% when an amount of 0.2 g of dolomite was used. The adsorption capacity sharply increases up to 98% when the dolomiteamountisincreased to 0.4 g. On the other side, the adsorption capacity for the removal of Cu^{2+} was around 86% when 0.2 g of the dolomite was used. This adsorption capacity for the removal of Cu^{2+} was increased to 98% when the dolomite amount was increased to 0.4 g. The adsorption capacity for the removal of Zn^{2+} and Cu^{2+}showed no noticeable increase when the dolomite amount increased up to 1.0 g. According to these results, the 0.4 g of dolomite amount would be used to investigate other adsorption factors[24].

3.2.2.Contact time effect

The adsorption capacity for Zn^{2+} and $Cu^{2+}$was measured as an indicator for determining the optimum contact time for the removal of Zn^{2+} and $Cu^{2+}$by dolomite.The adsorption results obtained at 25°C for Zn^{2+} and Cu^{2+}have the same trend as shown in Figure 6. The results implicate that the adsorption on the dolomiteincreased rapidly when the time was increased from 15 min to 30 min after the adsorption became almost constant.The maximum removal of Zn^{2+} and Cu^{2+}, around 98.5%, was achieved after 30 min, and so, equilibrium was reached, where no noticeable change in the adsorption was observed. The contact time was kept to 120 min[24, 25].

3.2.3.Effect of pH

The pH of solution at which the adsorption process would take place is an important factor that affects the efficiency of adsorption. The pH can influence the solubility of the ions to be removed. It can also affect the charge of function group onto the surface of the adsorbent. This study investigated the adsorption at a range of pH between 2 and 10, time of 30 min, weight of adsorbent of 0.4 g, and size of particles of 150 µm. The removal percentage of Zn^{2+} and Cu^{2+}at the chosen range of pH is illustrated in Figure7.At a lower pH of 2, the removal percentage of the Zn^{2+} was 80% because metal ions were hindered by hydrogen ions that occupied active sites available on the adsorbent surface and competedwith the metal ions.

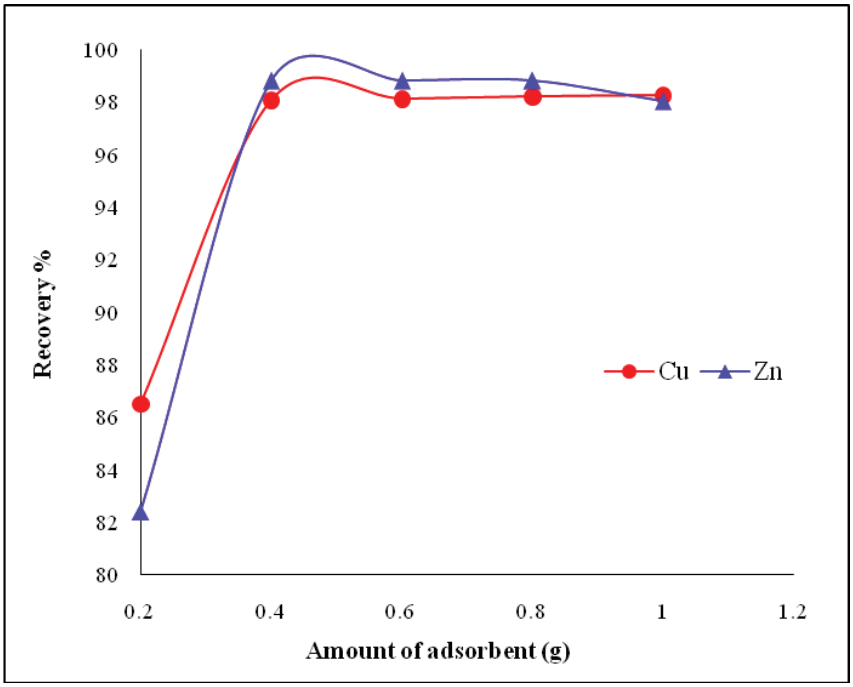

Fig. 5. The effect of dolomite amounts onZn^{2+} and Cu^{2+}removal

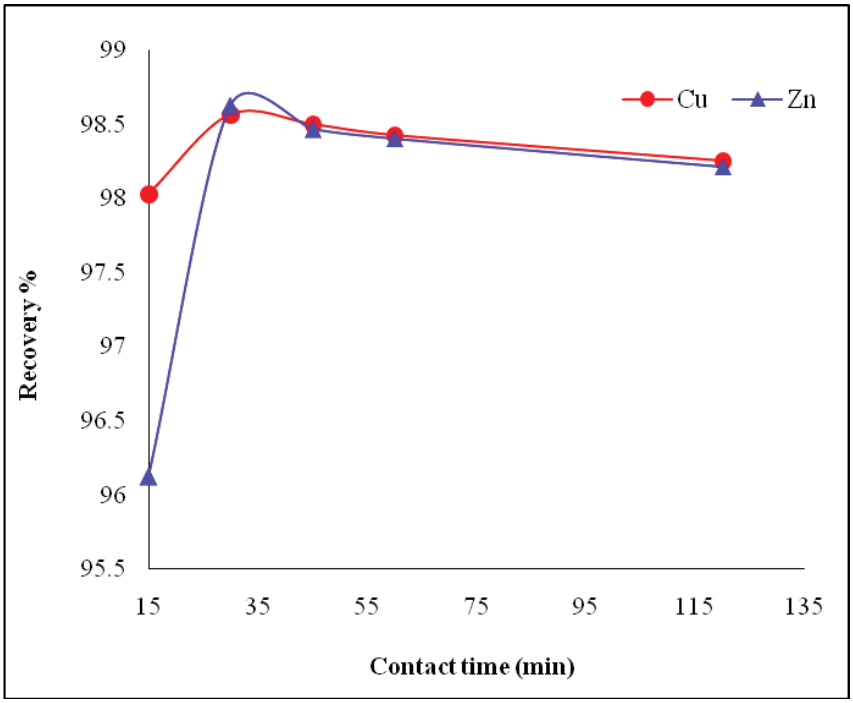

Fig. 6.The effect of time on the removal ofZn^{2+} and Cu^{2+}at 293K using dolomite as adsorbent

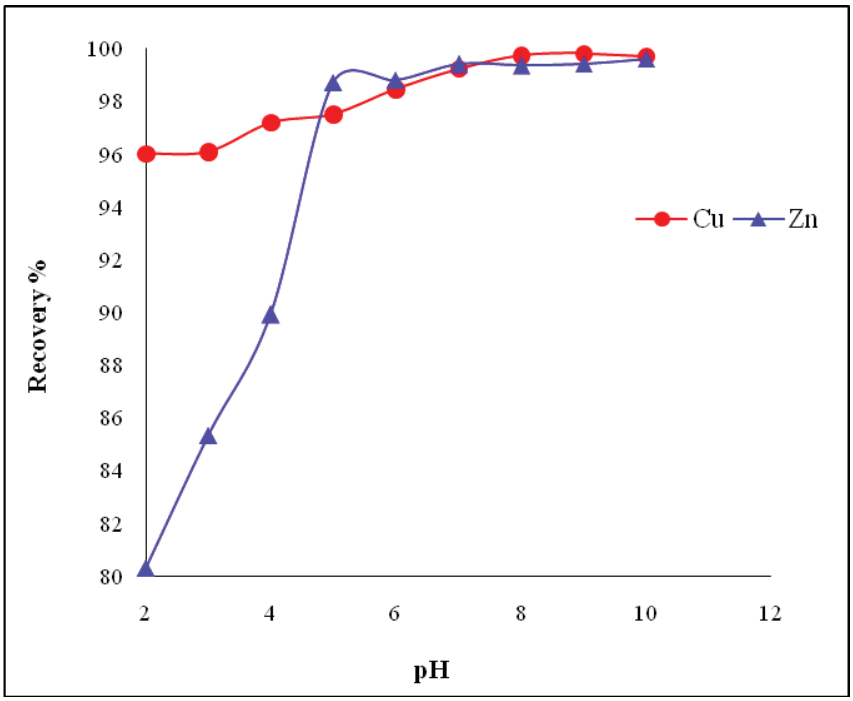

Fig. 7. The effect of pH on the removal ofZn^{2+} and Cu^{2+}using dolomite as adsorbent

As the pH increased, the removal percentage of the Zn^{2+} increased due to reducing the concentration of hydrogen ions in the solution and setting free the active site onto the adsorbent surface. The removal percentage reached 98.7% at a pH of 5, and no significant increase in the removal was observed at higher pH. The change of pH showed a slight effect on the removal of Cu^{2+} whereby the removal percentage also increased as the pH increased from 96% at a pH of 2 to 99.3% at a pH of 8[10, 24, 26].

3.2.4.Effect of dolomiteparticle size

The effect of dolomite particles size was studied, and thus three sizes of the dolomite were investigated 150, 250 and 300 µm., andthe results are illustrated in Figure 8. It can be noticed that the adsorption capacity of Zn^{2+} and Cu^{2+}did not change when the particle size increased from 150 to 250µm for both ions (Zn^{2+} and Cu^{2+}). On the other side, using dolomite at 300 µm showed a slight decrease in the adsorption capacity for Cu^{2+} owing to the reduction of the surface area of the dolomite. This result confirmed that decreasing the particle size leads to an increase in the surface area of the dolomite powder and simultaneously increases the removal capability of ions[10, 27].

3.2.5.Effect of adsorption temperature

The effect of solution temperature (293, 303, 313, and 323°K)on the adsorption process was studied and shown in Figure 9. Temperature was shownto have a noticeable effect on the adsorption capacity of the Zn^{2+} and Cu^{2+}. The adsorption capacity of dolomite for Zn^{2+} showeda slight decrease from 98.6% to 98.3% as the temperature increased from 293 to 323°K. On the other hand,the dolomite adsorption capacity for Cu^{2+} decreased from 98.4% to 97.3% when the temperature increased from 293 to 323^{0}K. These results confirmed that the adsorption is an exothermic process[28, 29].

3.2.6.Effect of initial concentration

The adsorption capacities ofZn^{2+} and Cu^{2+}onto the dolomite at various initial concentrations of the ions between 50–100 mg $L^{-1}$are shown in Figure10. It can be noticed that the adsorption capacity of Zn^{2+} and Cu^{2+}did not change and the adsorption capacity was almost the same for both ions. During the adsorption process, the initial concentration of targeted ions in the solution played a key role that limited the capacity of the adsorbent[30, 31]. Using the dolomite as an adsorbent for the removal of Zn^{2+} and Cu^{2+}showedthat the adsorption capacity waskept constant as high as 98.6% for Zn^{2+} and $Cu^{2+}$with a very slight decrease for the adsorption capacity of Zn^{2+} to 97.8% when the initial concentration increased from 50 to 100 mg L^{-1}.Increasing the initial concentration from 50 to 100 mg L^{-1}while the adsorption capacity was maintained as high as 98.8% confirms that the adsorbent did not reach the saturation point, and the initial concentration can be increased, where the adsorption capacity of $Cu^{2+}$was retained at 98.6% even though the concentration raised to 100 mg L^{-1}[30, 31].

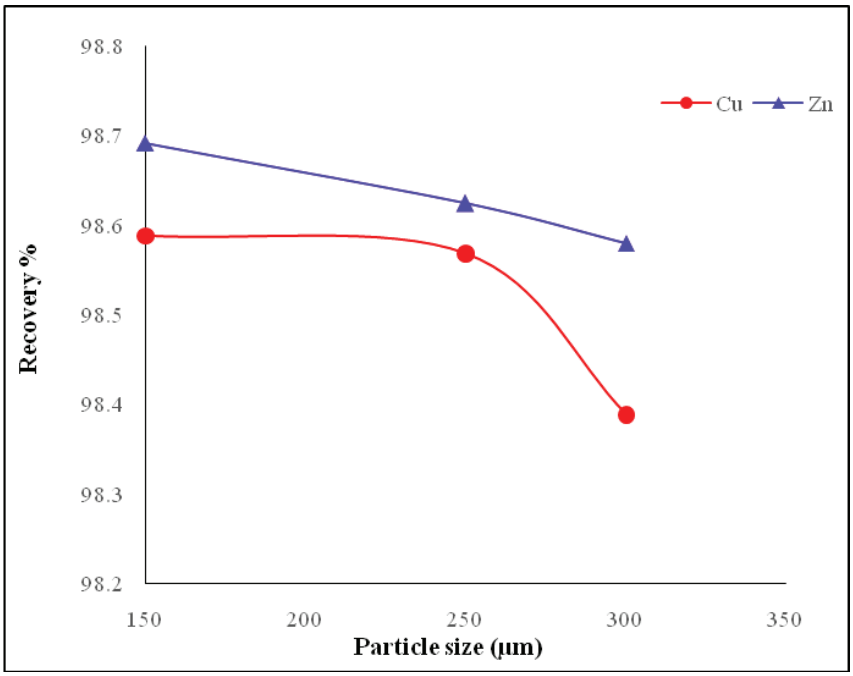

Fig. 8. The effect of dolomiteparticle size on the removal ofZn^{2+} and Cu^{2+}

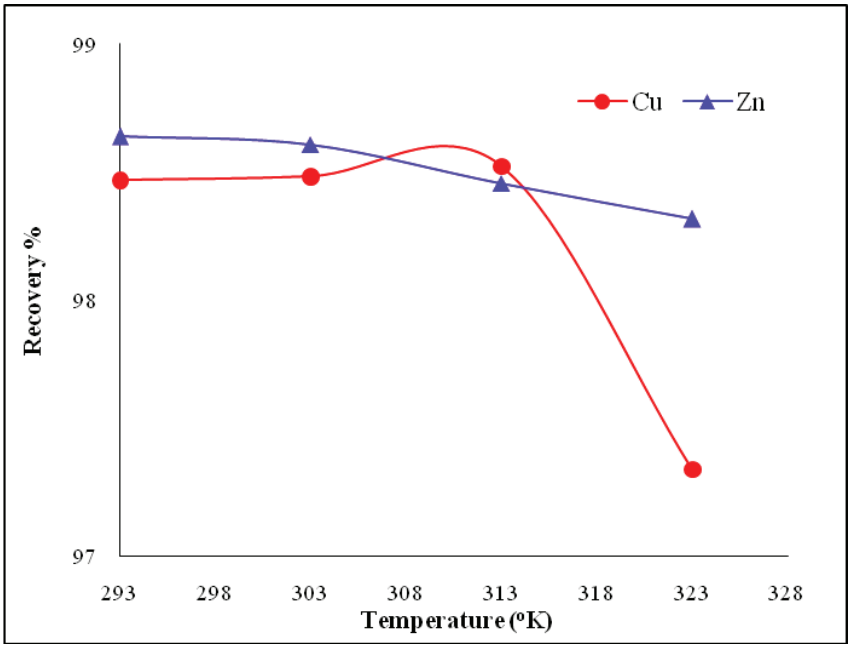

Fig. 9.The effect of temperature on the removal of Zn^{2+} and Cu^{2+}

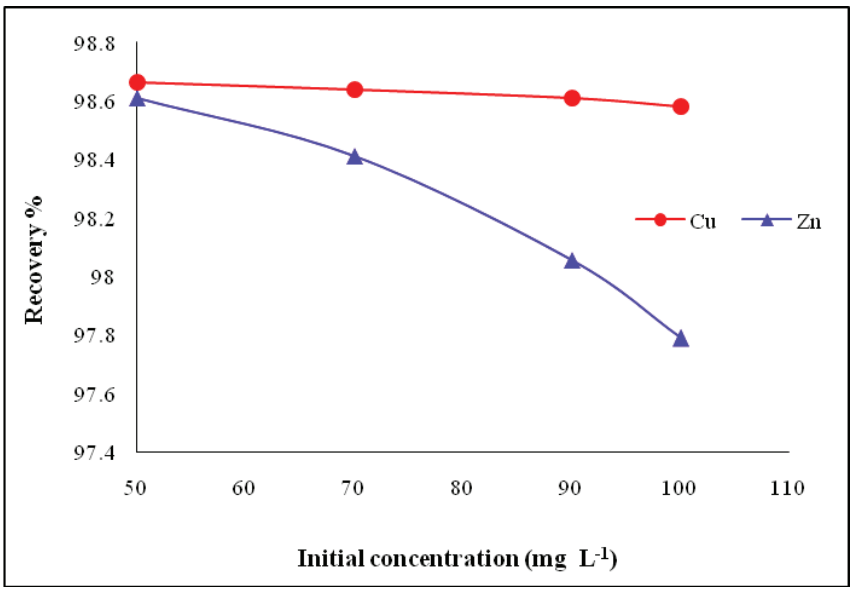

Fig. 10. The effect of initial concentration on the removal of Zn^{2+} and Cu^{2+}

3.2.7.Isotherm model

The adsorption experiments were conducted to determine the extent of corresponding with Langmuir, Freundlich, and Timken models at optimum conditions of (dolomite amount 0.4 g, time 30 min, initial Zn^{2+} and Cu^{2+}concentration 50, 70, 90, and 100 mg $L^{-1}$and pH 8). The association between the amounts of ions removed by the dolomite at equilibrium conditions was determined using the procedure illustrated in the experiment and materials section[17], [32–35]. According to the Langmuir isotherm models; the Hanes–Woolf equation has been used and the results are shown in Figure11. The correlation coefficient value summarized in Table 2 and obtained via this equation was up to 0.998 and 0.978 for Zn^{2+} and Cu^{2+}respectively.This suggests that the adsorption process is conformable with the Langmuir model and the Zn^{2+} and Cu^{2+}adsorbed onto

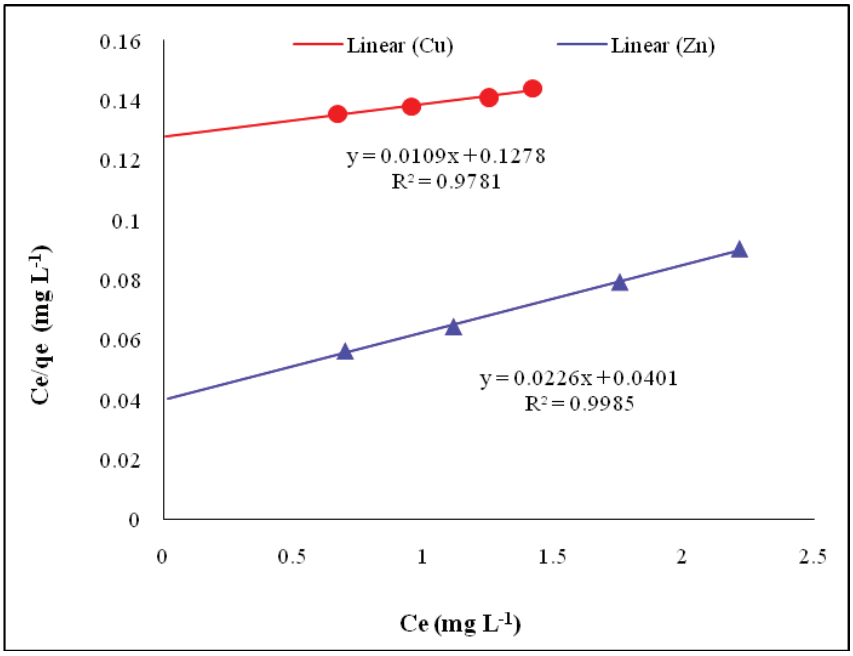

Fig. 11. Langmuirmodel at 293°K

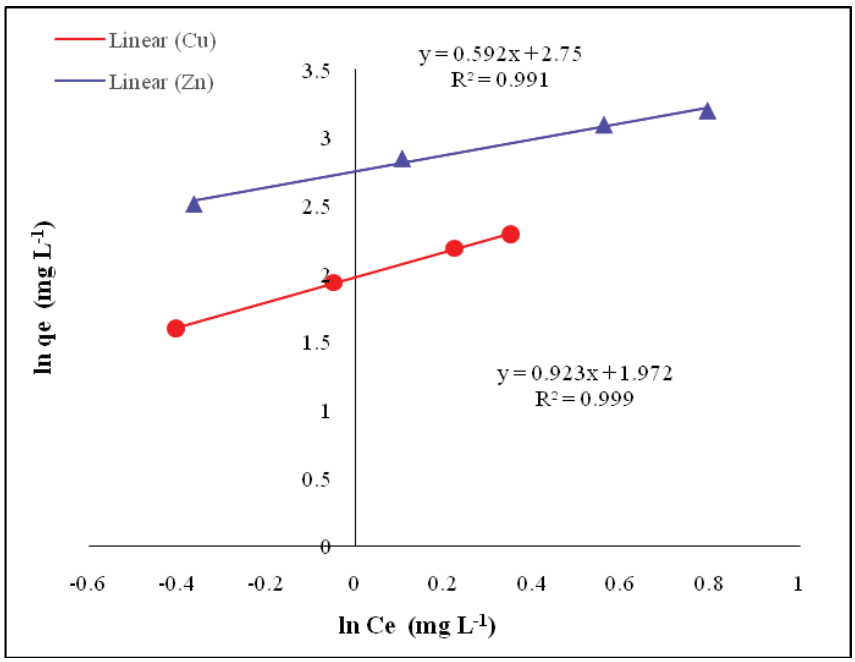

Fig.12.Freundlich model at 293°K

the dolomite surface initially formed a monolayer[32], [35]. The maximum monolayer capacities of Zn^{2+} and Cu^{2+}adsorbed onto the dolomite obtained by the Langmuir model are 44.24 and 91.74 (mg g^{-1}), respectively, as summarized in Table2.

The Freundlich isotherm model obtained using equation 3 is shown in Figure 12. The Freundlich isotherm showedgood linearity where the correlation coefficient (R^2) was 0.9915 and 0.9996 for Zn^{2+} and Cu^{2+},respectively,as summarized in Table 2. This confirms the multilayer adsorption of removed ions onto the dolomite surface and the obtained adsorption results agree with the Freundlich adsorption isotherm model[21,36–38]. The K_f is an estimated indicator for the adsorption capacity, while 1/n refers to the adsorption strength.

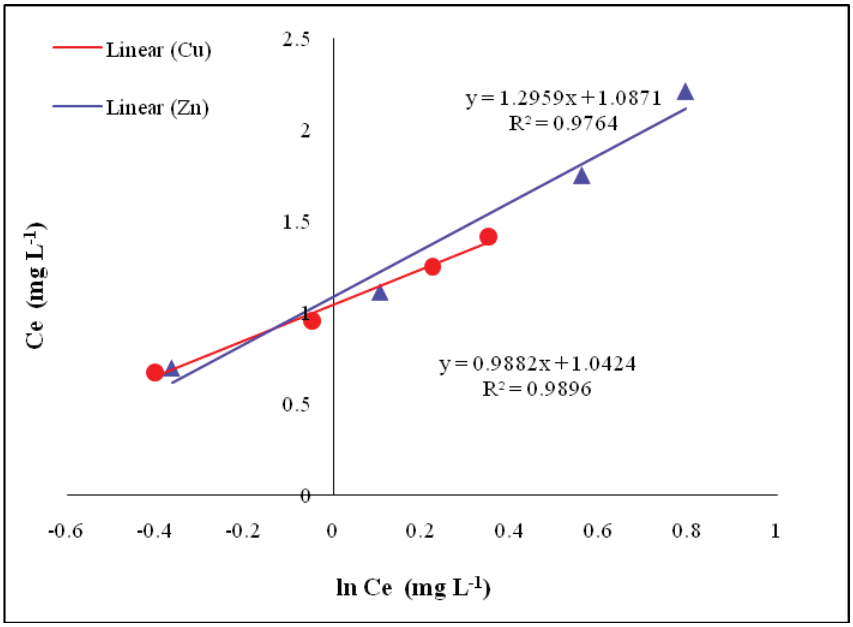

Fig. 13.Timken model at 293 K

Table 2. Adsorption models of Zn^{2+} and Cu^{2+} onto the dolomite

Ion	Model	Equation	Constant	Value
Cu	Langmuir	$C_e/q_e = 1/(K_L\, q_{max}) + (1/q_m)\, C_e$	R^2	0.997
			q_{max} (mg g^{-1})	91.743
			K_L (L mg^{-1})	0.085
	Freundlich	$q_e = K_f\, C_e^{1/n}$	R^2	0.999
			n	1.082
			1/n	0.923
			K_f (mg g^{-1})	-0.679
	Timken	$q_e = B \ln A_T + B \ln C_e$ $b_T = RT/B$	R^2	0.989
			B J mol^{-1}	0.988
			A_T (L g^{-1})	2.871
			b_T	2507.66
Zn	Langmuir	$C_e/q_e = 1/(K_L\, q_{max}) + (1/q_m)\, C_e$	R^2	0.999
			q_{max} (mg g^{-1})	44.247
			K_L (L mg^{-1})	0.563
	Freundlich	$q_e = K_f\, C_e^{1/n}$	R^2	0.991
			n	1.687
			1/n	0.592
			K_f (mg g^{-1})	-1.011
	Timken	$q_e = B \ln A_T + B \ln C_e$ $b_T = RT/B$	R^2	0.976
			B J mol^{-1}	1.295
			A_T (L g^{-1})	2.313
			b_T	1911.85

When 1/n is equal to 1, the separation between the two phases is independent of the concentration. If the value of 1/n is higher than 1, this indicates normal adsorption. When 1/n is lower than 1, this implies cooperative adsorption. According to the adsorption results summarized in Table 2, the value of 1/n of Zn^{2+} and Cu^{2+}=0.592 and 0.923 while n=1.687 and 1.082 respectively, indicating that the sorption of Zn^{2+} and Cu^{2+}onto dolomite is favorable[21, 36–38].

The R^2 values summarized in Table 2 were 0.976 and 0.989 for Zn^{2+} and Cu^{2+}, respectively. They wereobtained by fitting the adsorption experimental results to the Temkin model. Figure 13 shows that not all the plotted points of both ions were linear together. These findings suggest that the Langmuir and Freundlich models are highly convenient for predicting Zn^{2+} and Cu^{2+}adsorption onto the dolomite surface in comparison with the Timken model. From the Temkin plot, the following values were estimated for Zn^{2+} and Cu^{2+}: A_T= 2.313 Lg^{-1}, B=1.295 $Jmol^{-1}$, and A_T = 2.871 Lg^{-1}, B=0.988 $Jmol^{-1}$ respectively which represents the heat of adsorption suggesting a physisorption process[33, 35, 39,40].

4. Conclusion

In this paper, an investigation of the removal of Zn^{2+} and $Cu^{2+}$was carried out using dolomite as an adsorbent. This adsorption capacity was up to 98% when the amount of dolomite was 0.4 g. The amount of adsorption onto dolomite powder was slightly higher for Cu^{2+} compared to Zn^{2+} from wastewater, where the maximum monolayer capacities (q_{max}) was 91.74 mg g^{-1} for Cu^{2+} ion and 44.24 mg $g^{-1}$for Zn^{2+}. The value of 1/n and n for zinc and copper was obtained (0.592, 0.923) and (1.687, 1.082), respectively, indicating that the adsorption of zinc and copper onto dolomite is favorable. The experimental results agreed with the Langmuir, Freundlich, and Temkin model. The comparison between the three models shows that the Langmuir and Freundlich models have the highest correlation coefficient value of 0.998 compared with the Temkin model. It could be concluded that dolomite is an active adsorbent for the removal of Zn^{2+} and $Cu^{2+}$from wastewater.

5. Acknowledgment

The authors appreciate the support of the University of Anbar/College of Science and College of Education for Women andthe University of Fallujah/ College of Applied Sciences. The authors wish to thank the service research lab in the Chemistry Department, College of Science.

6. References

[1] N. Abdullah, N. Yusof, W. J. Lau, J. Jaafar, A. F. Ismail, Recent trends of heavy metal removal from water/wastewater by membrane technologies, J. Ind. Eng. Chem., 76 (2019) 17–38. https://doi.org/10.1016/j.jiec.2019.03.029

[2] S. Ahmadi, C. A. Igwegbe, Adsorptive removal of phenol and aniline by modified bentonite: adsorption isotherm and kinetics study, Appl. Water Sci., 8 (2018)170. https://doi.org/10.1007/s13201-018-0826-3

[3] F. F. Ali, A. S. Al-Rawi, A. M. Aljumialy, Limestone residues of sculpting factories utilization as sorbent for removing Pb (II) ion from aqueous solution, Results Chem., 4 (2022) 100621. https://doi.org/10.1016/j.rechem.2022.100621

[4] M. Karnib, A. Kabbani, H. Holail, Z. Olama, Heavy metals removal using activated carbon, silica and silica activated carbon composite, Energy Procedia, 50(2014) 113–120. https://doi.org/10.1016/j.egypro.2014.06.014

[5] K. Atkovska, K. Lisichkov, G. Ruseska, A. T. Dimitrov, A. Grozdanov, Removal of heavy metal ions from wastewater using conventional and nanosorbents: a review, J. Chem. Technol. Metall., 53 (2018) 202-219. https://journal.uctm.edu/node/j2018-2/7_17-59_A_Grozdanov_p_202_217.pdf

[6] M. Yari, Removal of Pb (II) ion from aqueous solution by graphene oxide and functionalized graphene oxide-thiol: effect of cysteamine concentration on the bonding constant, Desalin.Water Treat., 57 (2016) 11195–11210. https://doi.org/10.1080/19443

994.2015.1043953

[7] O. Moradi, M. Aghaie, K. Zare, M. Monajjemi, H. Aghaie, The study of adsorption characteristics Cu2+ and Pb2+ ions onto PHEMA and P (MMA-HEMA) surfaces from aqueous single solution, J. Hazard. Mater., 170 (2009) 673–679.https://doi.org/10.1016/j.jhazmat.2009.05.012

[8] A. S. Al-Rawi, A. M. Aljumialy, W. M. Saod, E. A. Al-Heety, Pollution Level and Sources of Heavy Metals in Indoor Dust from College of Science, University of Anbar Campus, Iraq, in IOP Conference Series: Earth Environ. Sci., IOP Publishing, 1300 (2024) 012019.https://doi.org/10.1088/1755-1315/1300/1/012019

[9] WHO, Guidelines for drinking-water quality, World Health Organization, 2022.https://www.who.int/publications/i/item/9789240045064

[10] H. Çelebi, G. Gök, O. Gök, Adsorption capability of brewed tea waste in waters containing toxic lead (II), cadmium (II), nickel (II), and zinc (II) heavy metal ions, Sci. Reports, 10 (2020) 17570. https://doi.org/10.1038/s41598-020-74553-4

[11] F. Edition, Guidelines for drinking-water quality, 4th ed, World Health Organization, 38 (2011) 104–108.https://www.scirp.org/reference/referencespapers?referenceid=3088676

[12] T. Zhang, Removal of heavy metals and dyes by clay-based adsorbents: From natural clays to 1D and 2D nano-composites, Chem. Eng. J., 420 (2021) 127574.https://doi.org/10.1016/j.cej.2020.127574

[13] A. Khaligh, F. Golbabaei, A Vahid, On-line micro column preconcentration system based on amino bimodal mesoporous silica nanoparticles as a novel adsorbent for removal and speciation of chromium (III, VI) in environmental samples, J. Environ. Health Sci. Eng., 13 (2015) 47. https://doi.org/10.1186/s40201-015-0205-z

[14] A.A.M. Beigi, MM Eskandari, B Kalantari, Dispersive liquid-liquid microextraction based on task-specific ionic liquids for determination and speciation of chromium in human blood, J. Anal. Chem., 70 (2015) 1448-1455. https://doi.org/10.1134/ S1061934815120072

[15] M.K. Abbasabadi, F Hosseini, Nanographene oxide modified phenyl methanethiol nanomagnetic composite for rapid separation of aluminum in wastewaters, foods, and vegetable samples by microwave dispersive magnetic micro solid-phase extraction, Food Chem., 347(2021)129042. https://doi.org/10.1016/j.foodchem.2021.129042

[16] MM Eskandari, Cloud point assisted dispersive ionic liquid-liquid microextraction for chromium speciation in human blood samples based on isopropyl 2-[(isopropoxycarbothiolyl) disulfanyl] ethane thioate, Anal. Chem. Res., 10 (2016) 18-27 .https://doi.org/10.1016/j.ancr.2016.10.002

[17] S. Sen Gupta, K. G. Bhattacharyya, Interaction of metal ions with clays: I. A case study with Pb (II), Appl. Clay Sci., 30 (2005) 199–208. https://doi.org/10.1016/j.clay.2005.03.008

[18] A. A. El-Bayaa, N. A. Badawy, E. Abd AlKhalik, (2009)Effect of ionic strength on the adsorption of copper and chromium ions by vermiculite pure clay mineral, J.Hazard. Mater., 170 (2009) 1204–1209.https://doi.org/10.1016/j.jhazmat.2009.05.100

[19] A. S. Yahya, Study affecting factors on the recovery of some heavy metal ions from aqueous solutions using natural clay, J.Univ. Anbar Pure Sci., 10 (2016)76-82.https://doi.org/10.37652/JUAPS.2016.135145

[20] B. M. Vanderborght, R. E. Van Grieken, Enrichment of trace metals in water by adsorption on activated carbon, Anal. Chem., 49 (1977) 311–316. https://doi.org/10.1021/ac50010a032

[21] B. Abbou, Kinetic and thermodynamic study on adsorption of cadmium from aqueous solutions using natural clay, J. Turk. Chem.

Soc. Section A: Chem., 8 (2021) 677–692. https://doi.org/10.18596/jotcsa.882016

[22] H. Yang, Calcined dolomite: an efficient and recyclable catalyst for synthesis of α, β-unsaturated carbonyl compounds, Catal. Lett., 149 (2019) 778–787.https://doi.org/10.1007/s10562-018-2632-9

[23] S. Medina-Carrasco, J. M. Valverde, In situ XRD analysis of dolomite calcination under CO_2 in a humid environment, Cryst. Eng. Comm., 22 (2020) 6502–6516. https://doi.org/10.1039/D0CE00974A

[24] H. Gebretsadik, A. Gebrekidan, L. Demlie, Removal of heavy metals from aqueous solutions using Eucalyptus Camaldulensis: An alternate low cost adsorbent, Cogent Chem., 6 (2022) 1720892. https://doi.org/10.1080/23312009.2020.1720892

[25] H. Hernández-Cocoletzi, Natural hydroxyapatite from fishbone waste for the rapid adsorption of heavy metals of aqueous effluent, Environ. Technol. Inno., 20 (2020) 101109. https://doi.org/10.1016/j.eti.2020.101109

[26] Z. Deng, Modification of coconut shell-based activated carbon and purification of wastewater, Adv. Compos. Hybrid Mater., 4 (2021) 65–73.https://doi.org/10.1007/s42114-021-00205-4

[27] B. Yu, Y. Zhang, A. Shukla, S. S. Shukla, K. L. Dorris, The removal of heavy metal from aqueous solutions by sawdust adsorption—removal of copper, J. Hazard. Mater., 80 80 (2000) 33–42. https://doi.org/10.1016/S0304-3894(00)00278-8

[28] S. Wadhawan, A. Jain, J. Nayyar, S. K. Mehta, Role of nanomaterials as adsorbents in heavy metal ion removal from waste water: A review, J. Water Process Eng., 33 (2020) 101038. https://doi.org/10.1016/j.jwpe.2019.101038

[29] G. Sarojini, S. Venkateshbabu, M. Rajasimman, Facile synthesis and characterization of polypyrrole-iron oxide–seaweed (PPy-Fe3O4-SW) nanocomposite and its exploration for adsorptive removal of Pb (II) from heavy metal bearing water, Chemosphere, 278 (2021) 130400. https://doi.org/10.1016/j.chemosphere.2021.130400

[30] Z. A. Alothman, Low cost biosorbents from fungi for heavy metals removal from wastewater, Sep. Sci. Technol., 55 (2020) 1766–1775. https://doi.org/10.1080/01496395.2019.1608242

[31] F. Almomani, R. Bhosale, M. Khraisheh, T. Almomani, Heavy metal ions removal from industrial wastewater using magnetic nanoparticles (MNP), Appl. Surf. Sci., 506 (2020) 144924. https://doi.org/10.1016/j.apsusc.2019.144924

[32] S. Bahah, S. Nacef, D. Chebli, A. Bouguettoucha, B. Djellouli, A new highly efficient algerian clay for the removal of heavy metals of Cu (II) and Pb (II) from aqueous solutions: characterization, Fractal, kinetics, and isotherm analysis, Arab. J. Sci. Eng., 45 (2020) 205–218. https://doi.org/10.1007/s13369-019-03985-6

[33] E. C. Nnadozie, P. A. Ajibade, Data for experimental and calculated values of the adsorption of Pb (II) and Cr (VI) on APTES functionalized magnetite biochar using Langmuir, Freundlich and Temkin equations, Data brief., 32 (2020)106292. https://doi.org/10.1016/j.dib.2020.106292

[34] T. C. Umeh, J. K. Nduka, K. G. Akpomie, Kinetics and isotherm modeling of Pb (II) and Cd (II) sequestration from polluted water onto tropical ultisol obtained from Enugu Nigeria, Applied Water Sci., 11(2021) 65. https://doi.org/10.1007/s13201-021-01402-8

[35] S. Tonk, L. E. Aradi, G. Kovács, A. Turza, E. Rápó, Effectiveness and characterization of novel mineral clay in Cd^{2+} adsorption process: Linear and non-linear isotherm regression analysis, Water, 14 (2022) 279. https://doi.org/10.3390/w14030279

[36] K. S. Obayomi, M. Auta, A. S. Kovo,

Isotherm, kinetic and thermodynamic studies for adsorption of lead (II) onto modified Aloji clay, Desalin. Water Treat., 181(2020) 376–384. https://doi.org/10.5004/dwt.2020.25142

[37] A. Benmessaoud, D. Nibou, E. H. Mekatel, S. Amokrane, A comparative study of the linear and non-linear methods for determination of the optimum equilibrium isotherm for adsorption of Pb^{2+} ions onto Algerian treated clay, Iran. J. Chem. Chem. Eng., 39 (2020) 153–171. https://doi.org/10.30492/IJCCE.2019.35116

[38] A. Samad, M. I. Din, M. Ahmed, Studies on batch adsorptive removal of cadmium and nickel from synthetic waste water using silty clay originated from Balochistan–Pakistan, Chin. J. Chem. Eng., 28 (2020)1171–1176. https://doi.org/10.1016/j.cjche.2019.12.016

[39] M. Osanloo, Validation of a new and cost-effective method for mercury vapor removal based on silver nanoparticles coating on micro glassy balls, Atmos. Pollut. Res., 8 (2017) 359-365. https://doi.org/10.1016/j.apr.2016.10.004

[40] A. Samad, M. I. Din, M. Ahmed, S. Ahmad, Synthesis of zinc oxide nanoparticles reinforced clay and their applications for removal of Pb (II) ions from aqueous media, Chin. J. Chem. Eng., 32 (2021) 454–461. https://doi.org/10.1016/j.cjche.2020.09.043

Anal. Methods Environ. Chem. J. 7 (2) (2024) 89-106

AMECJ

Research Article, Issue 2
Analytical Methods in Environmental Chemistry Journal
Journal home page: www.amecj.com/ir

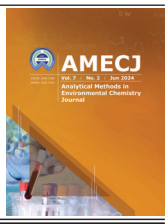

Hydrothermal synthesis of zinc borate as photocatalyst for efficient removal and determination of Congo red dye from aqueous solution by UV-Vis spectroscopy

Hasan Jasim Mohammad [a,*], and Zaki Naser Kadhim [a]
[a] *University of Basra, College of Science, Chemistry Department, Basra, Iraq*

ARTICLE INFO:
Received 26 Jan 2024
Revised form 23 March 2024
Accepted 7 May 2024
Available online 29 Jun 2024

Keywords:
Zinc borate adsorbent
Adsorption
Congo red day
UV-Vis Spectroscopy
Isotherm model

ABSTRACT
This study synthesized zinc borate ($Zn_2BO_3(OH)$, ZB) through one-step precipitation from nano zinc oxide and boric acid. FTIR, XRD, SEM, EDX, and Zeta potential characterized the product. Due to the photocatalyst properties Congo Red Day (CRD) was removed from the aqueous solution. Effective factors on the adsorption efficiency are studied (time, amount of adsorbent, concentration, pH, and temperature). Results of the study indicated that the best amount of adsorbent was obtained at 0.1 g which was used against dye when adsorption capacities equal 6.034 mg g^{-1}. Also, the adsorption capacities [$q_{(mg/g)}$] were obtained at 35.556 mg g^{-1} in the CRD concentration of 50 mg L^{-1}, and [$q_{(mg/g)}$] was equal to 20.154 mg g^{-1} in 100 mL sample at pH 5.5. All adsorption processes using distilled water (DW) were analyzed using UV-Vis spectroscopy. The adsorption capacity was calculated by using Langmuir and Freundlich isotherm models, and results showed that the maximum adsorption capacity (q_{max}) in the Langmuir model was achieved at 212.7 mg g^{-1} for $Zn_2BO_3(OH)$. The R-squared (R^2) or the low coefficient of determination for Langmuir and Freundlich isotherms adsorption were obtained at 0.98 and 0.89, respectively. The kinetic adsorption based on the first-order and second-order pseudo coefficients were achieved at R^2=0.89 and R^2=0.99, respectively. The thermodynamics values (ΔS, ΔG, ΔH) are measured and the results indicate that the adsorption process is spontaneous and endothermic.

1. Introduction

Zinc borates one of the most important materials of the first row in the world [1]. ZB is used for various industries due to their specific properties such as smoke suppressant, synergistic effect, flame retardant, corrosion inhibitors, anti-bacterial properties, good mechanical properties, and high surface area [2]. Colors are among the important chemicals that can be involved in industrial processes in various fields, as they occupy an important commercial place. These colors have multiple sources according to their nature, natural or artificial. The industrial type usually has a dye or pigment source [3]. Substances that work to exclude colors belonging to the dye family are superior to those materials that work to exclude pigment colors because of their high solubility in solvents and do not require additional stages of dispersion. The processes involved in painting fibers and fabrics annually release a lot of harmful waste into river water, causing pollution [4], Where 15 % of the dyes used in industrial painting processes leak into river canals and streams, causing major water

*Corresponding Author: Hasan Jasim Mohammad
Email: Jasiem33@gmail.com
https://doi.org/10.24200/amecj.v7.i02.319

pollution [5]. Therefore, this water must be treated and rid of these chemical pollutants, whether they are dyes or organic or inorganic materials. It is possible that these materials negatively affect the health and safety of humans, threatening the human body with some serious diseases. These risks may be carcinogenic or toxic, and these dyes and chemicals may pose a real danger to the aquatic environment and the living organisms that live in it [6]. Treating and purifying this water from pollutants is neither easy nor simple, as there are many purification theories and many practical principles, as in removal benzene vapor from air by a simple and efficient method based on the triphenyl(3-sulfopropyl)phosphonium *p*-toluene sulfonate as TSIL was coated on multi-walled carbon nanotubes ([TPhPP][SUTO]–MWCNTs) [7], and remove the formaldehyde from the air by a photocatalytic degradation–adsorption process (PC-DAP) by using Bismuth oxide and titanium oxide nanoparticles [8], and toluene removal from air by liquid–gas-phase extraction method by using five ionic liquids were pasted on micro glassy balls [9] , and remove toluene in water and air samples by using new methods based on adsorption, desorption, biodegradation, catalytic process, UV photo irradiation-adsorption, and mixture filtration/adsorption [10], and benzene removal from artificial air after loaded in Robson quartz tubes (RGT) by using A new and efficient method based on solid phase gas extraction (SPGE) with Schiff base immobilized [11], extraction of styrene from water samples by ultra-assisted dispersive cyclic conjugation-micro-solid phase extraction procedure by using (BF_4) [12]. One of the most important applied and practical theories in water purification and filtration is the adsorption process, where the principle of this theory is based on the clinging of molecules of adsorbate substance to molecules of adsorbent substance [13]. This clinging is either based on Van der Waals forces, and thus it is physical adsorption, or based on chemical bonds, and is called chemical adsorption [14]. The two adsorptions used to extract dyes from water are easy to apply, cheap, safe, and harmless to the environment. When dealing with physical adsorption, has some characteristics, including the nature of the forces bonding between molecules of the adsorbate and the adsorbent material, which are weak forces known as Van der Waals forces. Also, this type of adsorption is multi-layered and can be considered a reversible process, as the adsorption process can be reversed by raising the ambient temperature or by changing the conditions of the process, the reverse process of adsorption is called desorption. Chemical adsorption is characterized by the nature of cohesion between adsorbate molecules and adsorbent surface by chemical bonds that are very strong and cannot be separated through certain methods. Therefore, this adsorption is irreversible, this type of adsorption is characterized by its high efficiency in extracting a wide range of impurities and heavy metals from the water to be purified. The dye can be removed from river and lake water by the adsorption process, which is easy and relatively inexpensive and does not cause waste or harm to life in the river environment. It has a relatively large ability to remove pollutants over a wide range and good selectivity, and it can be used at different pollutant concentrations (high or low concentration). What enhances the use of adsorption in removing dyes from water is the diversity and abundance of adsorbent materials of all types, organic, inorganic, and polymeric, especially nano-types, which have a large surface area due to the presence of pores and holes. Activated carbon can be classified as one of the most important types of materials used for the adsorption of dyes from solutions. This is due to its chemical stability, low density, and the soft nature of its composition. Natural or synthetic clay can also be considered a good example of adsorbent material due to its abundance, ease of preparation, and high effectiveness against the molecules desired to be removed from solutions. This is due to its chemical stability, low density, and the soft nature of its composition. Natural or synthetic clay can also be considered a good example of adsorbent material due to its abundance, ease of preparation, and high effectiveness against the

molecules desired to be removed from solutions. Among the dyes that fall within the azo dyes is CR dye which can be considered one of the important colored dyes in many industries, including leather, fiber, paper, and many paint fields (Schema 1). However, the CR dye is toxic and carcinogenic, and this toxicity increases with increasing of the dye concentrations. The surplus of this dye when used, which is usually no less than 15%, as well as poor storage, leaks from factories and textile factories into river streams and lakes, causing pollution of the aquatic environment of the rivers, which leads to harm to living organisms, whether plants, animals, and humans. Leakage of CR dye causes a highly persistent red color to the water that is difficult to set aside [15]. The accumulated concentrations of this dye in living organisms cause health damage, and the most important damage to humans is skin and urinary system problems, liver cirrhosis, and cancer. The study aims to prepare (Zn_2BO_3) and the ability to act as a photocatalyst to remove CRD from an aqueous solution by adsorption method.

2. Material and Methods

2.1. Prepare adsorbent

Zinc borate (Zn_2BO_3) was synthesized by one-single-step precipitation by mixing zinc oxide NP and boric acid with a molar ratio varying from (4:1) in 200 mL of distilled water under a stirrer at 500 rpm at mixing time 10 hours at 60°C, after that the mixture was filtered, then washed for several times with distilled water to remove excess boric acid (Fig.1). The product dried in an oven for 24 hours at 70 C^0 [16].

2.2. Preparing Adsorbate

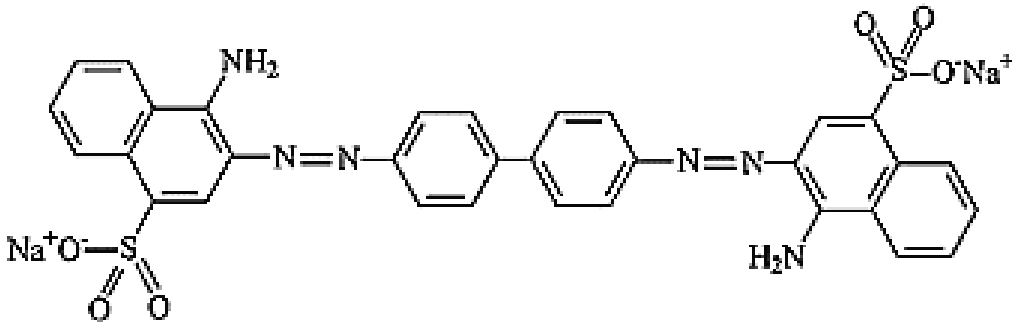

Schema 1. Structure of Congo red dye

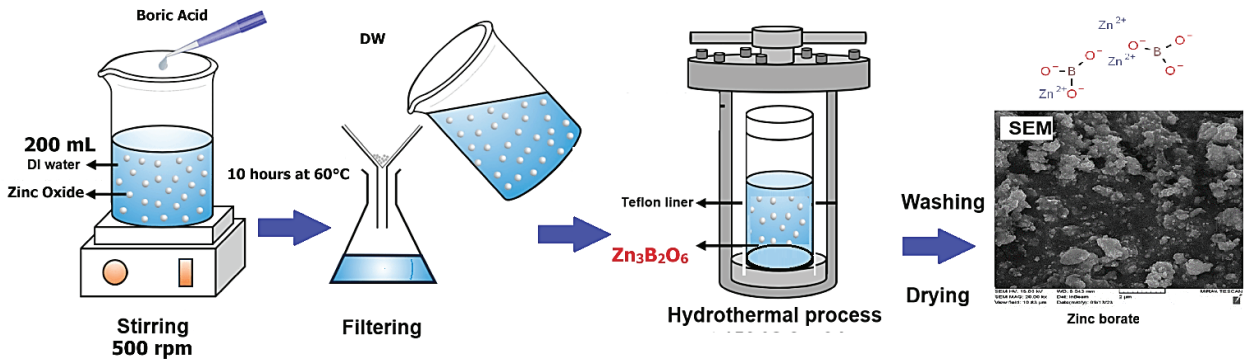

Fig.1. Synthesis of zinc borate (ZB, Zn_2BO_3) by mixing zinc oxide and boric acid

Congo Red dye solution was prepared by dissolving 1.0 g of dye in 1000 mL of distilled water, after that different concentrations of dye were prepared.

2.3. Photocatalyst Procedure

The different dye concentrations were prepared by dissolving solid CR dye at pH 5.5 of 100 mL volume and at the required temperature and placing it in a test tube. After that, an adsorbent (Zn_2BO_3) loaded with a weight of 0.1 g was placed in a shaker and exposed to sunlight for some time, then transported to a centrifuge device to be centrifuged to separate the aqueous solution, which contained the remaining concentration of CR dye that did not adsorb on the adsorbent surface. After that, carefully set aside the solution with a pipette and transfer it to glass cells to place the solution containing the unadsorbed dye into the UV-VIS device to measure the remaining dye concentration. The measurement process was carried out at a wavelength of 495 nm (Fig, 2).

3. Result and Discussion

3.1. FTIR spectra

FTIR spectra of (Zn_2BO_3) obtained are shown in (Fig.3). The peak at 3387.11 cm^{-1} is due to O–H groups in zinc borate [17]. The peak at 1508.38 cm^{-1} and the peak at 1388.79 cm^{-1} belong to the asymmetric stretching of B (3)–O and in-plane bending of B–O–H, respectively. The peaks at 1041.6 and 837.31 cm^{-1} are for asymmetric and symmetric stretching vibrations of B (4)–O, respectively. The peak at 551.66 cm^{-1} is attributed to the in-plane bending of B (3)–O. The peak at 470 cm^{-1} is due to the bending of Zn–O.

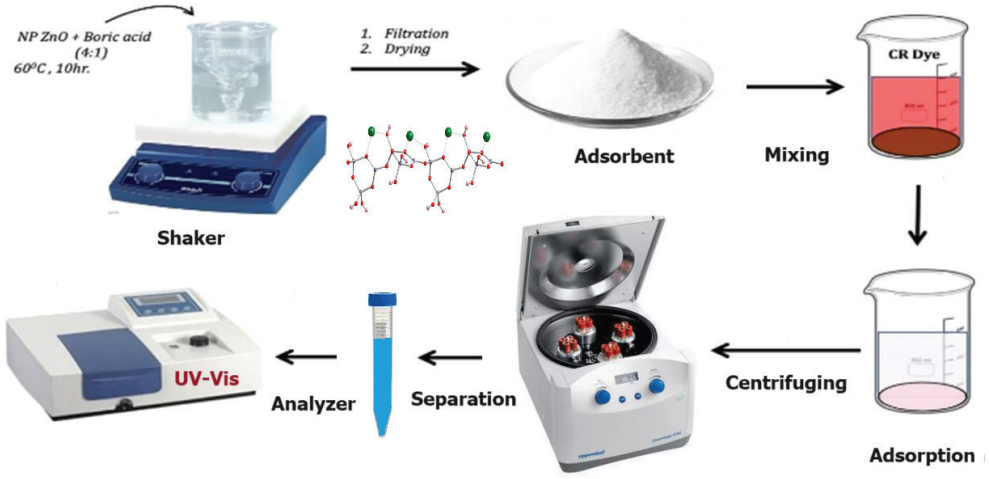

Fig. 2. Schematic diagram of the adsorption process with Zn_2BO_3

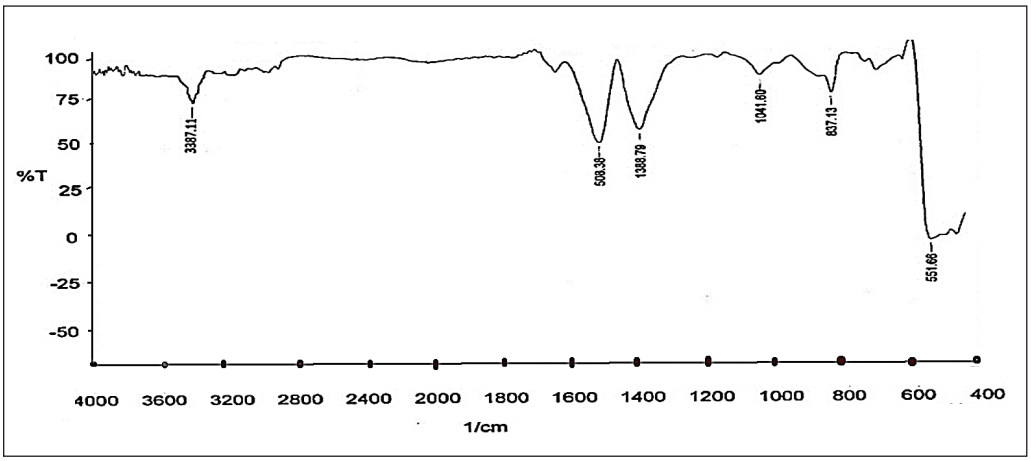

Fig. 3. FTIR spectra of Zn_2BO_3

3.2. XRD analysis

XRD pattern of (Zn_2BO_3) shown in Figure 4 values of (2θ) for the main peaks of zinc borate were reported as 19.0°, 21.03°, 23.0°,25.11°, 29.0°,31.22°,32.16° and 37.0° [18]. It is completely consistent with the XRD pattern explained in the literature [19].

3.3. SEM analysis

The shapes represent images of the scanning electron microscope with a field of light emission of the prepared compound, the figures of the compound showed semi-spherical shapes as well as an image that took the presence of a conglomerate in the prepared compound and that the surface of the compound contains holes and pores [20], and that the presence of these pores increases the surface area of the compound and therefore these holes will play an important role in increasing adsorption as shown in Figure 5a-f that crystals of the compound fall within the nanoscales of Zn_2BO_3.

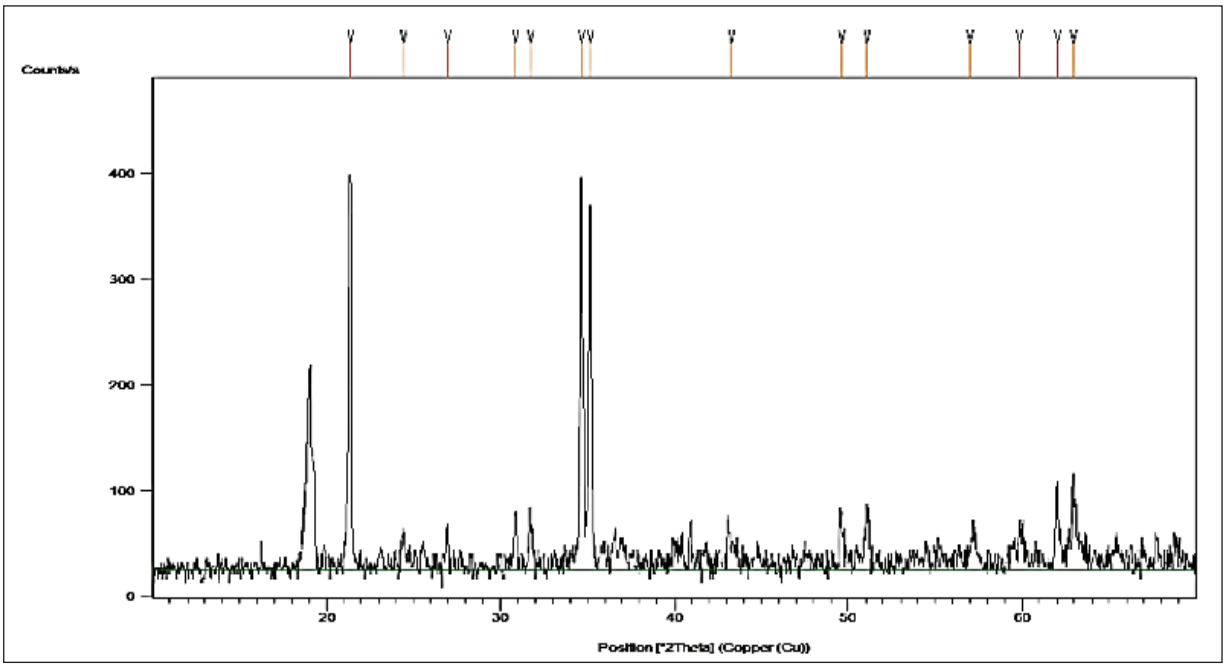

Fig.4. XRD Patterns of Zn_2BO_3

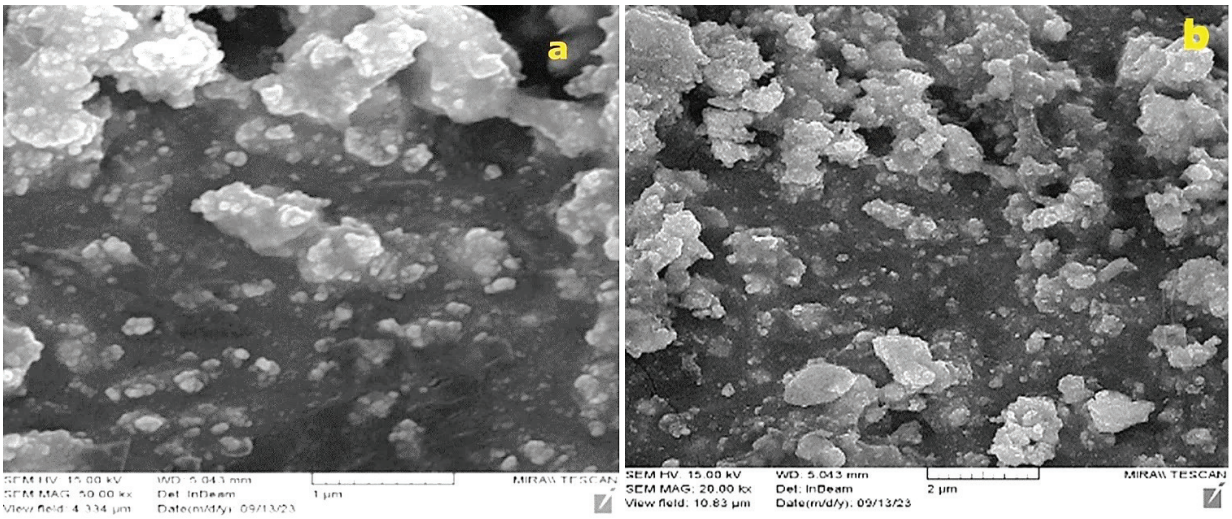

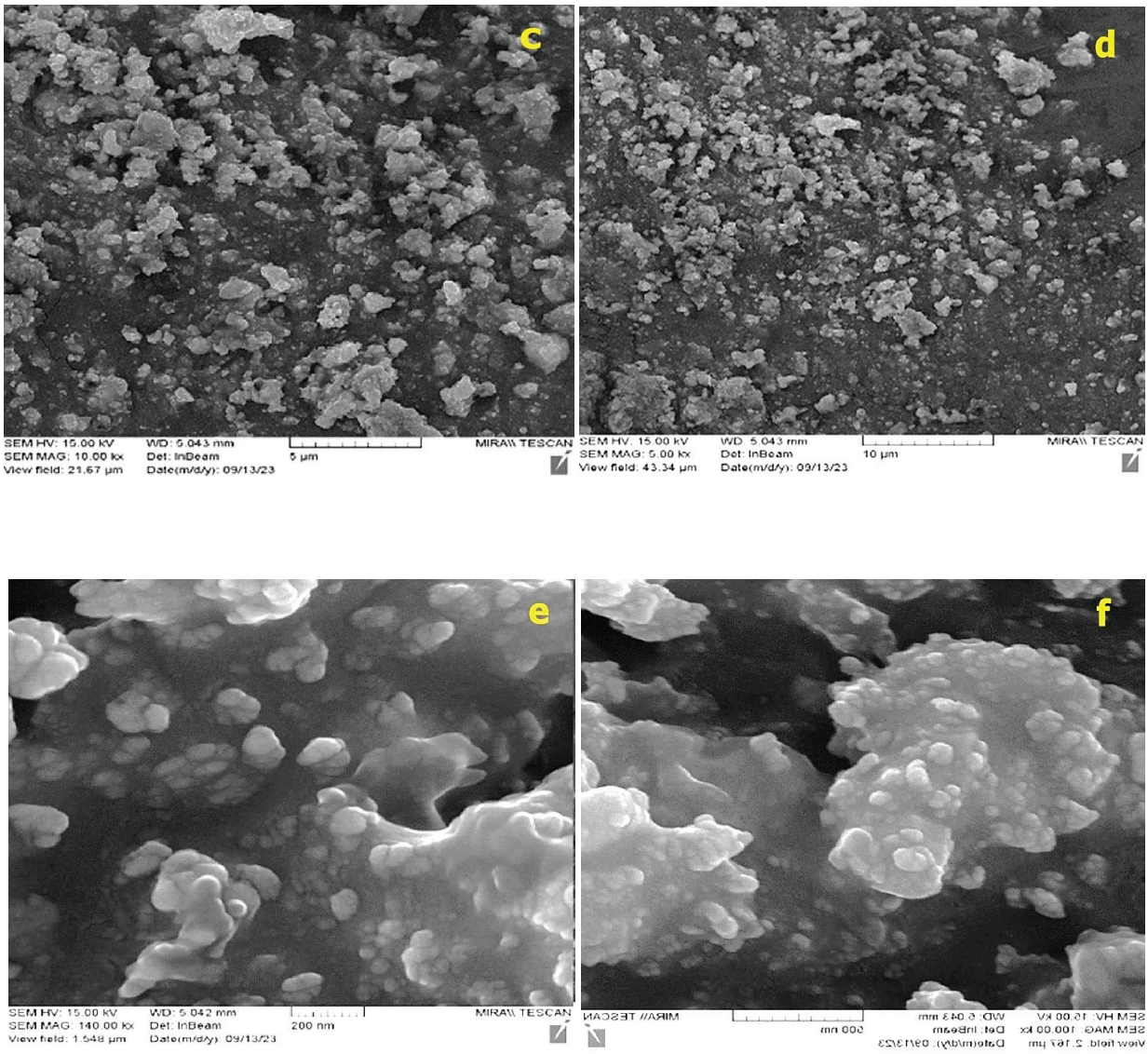

Fig. 5a-f. SEM of nanoscales of Zn_2BO_3

3.4. EDX analysis

EDX analysis of Zn_2BO_3 is shown in Table 1 and Figure 6. The theoretical composition of zinc borate is 63.31% zinc, 30.97% oxygen, and 5.23%. The chemical composition of the (Zn_2BO_3) sample was determined as 65.67% zinc, 29.01% oxygen, and 5.32% boron by data EDX analysis. While the experimental and theoretical composition values of Zn and O are near each other, the value of B is completely different as the boron element has low atomic mass [21].

3.5. Zeta Potential Analysis

There are many different ways of calculating zeta potential. In this study, the method of calculating zeta potential is electrophoretic (Table 2).

As shown in Figure 7 and Table 3, the value of the zeta potential of zinc borate (-36.0 mv) means the surface of the product has a negative charge, it is stable [22], and it is good to use to adsorb CR from aqueous solution. Zinc borate product is too difficult to make colloid with a solution so it was easy to isolate it from an aqueous solution to measure the amount of adsorption.

Table 1. EDX values of Zn_2BO_3 composition.

Composition	W %	A %
B	5.32	14.87
O	29.01	54.78
Zn	65.67	30.35
Total	100.00	100.00

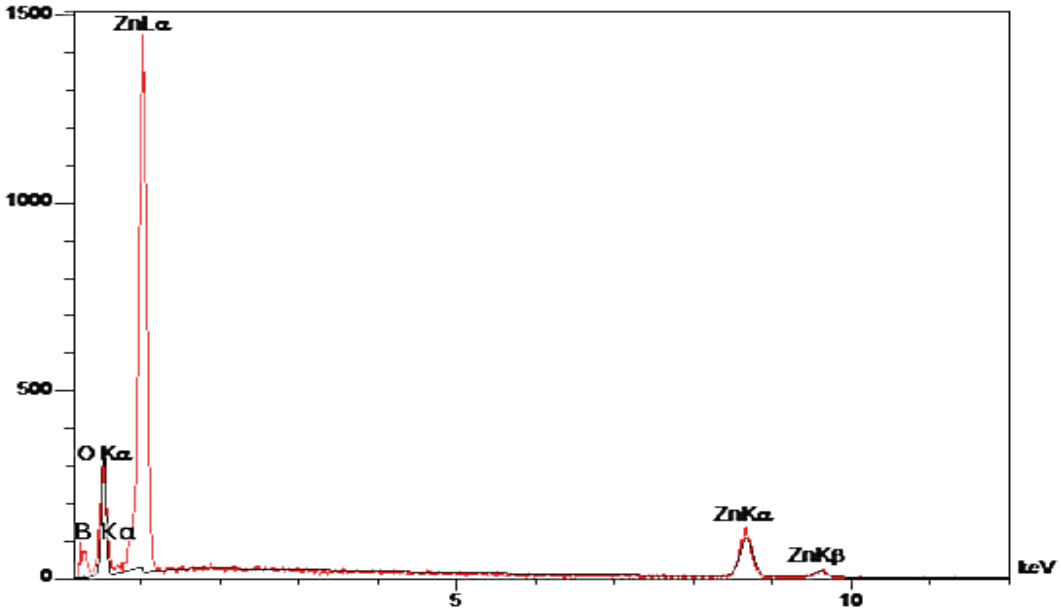

Fig. 6. The EDX positions of the (Zn_2BO_3) compound

Table 2. The range of stability according to Zeta potential analysis

Stability behavior of the particles	Zeta Potential (mV)
Rapid Coagulation or Flocculation	0 to ±5
Incipient Instability	±10 to ±30
Moderate Stability	±30 to ±40
Good Stability	±40 to ±60
Excellent Stability	More than ±61

Table 3. The zeta potential of Zn_2BO_3

Peak NO:	zeta potential	Electrophoretic
1	-36.0 mV	- 0.000186

3.6. Determination of the calibration curve

The calibration curve of the dye was calculated by preparing different concentrations of 5,10,15,20,25 mg L^{-1} at pH = 8 and the absorption was measured at the highest wavelength 495 nm by plotting concentration versus absorption, where $R^2 = 0.9973$ represents the linear equation as in Figure 8

3.7. Adsorption Studies

3.7.1.Study of equilibrium time

The factor affecting adsorption efficiency is the equilibrium time between the adsorbent (Zn_2BO_3) and CR dye [23]. The equilibrium time for adsorption of CR dye by 0.1 g of Zn_2BO_3 adsorbent was studied between 1-100 min in a dye

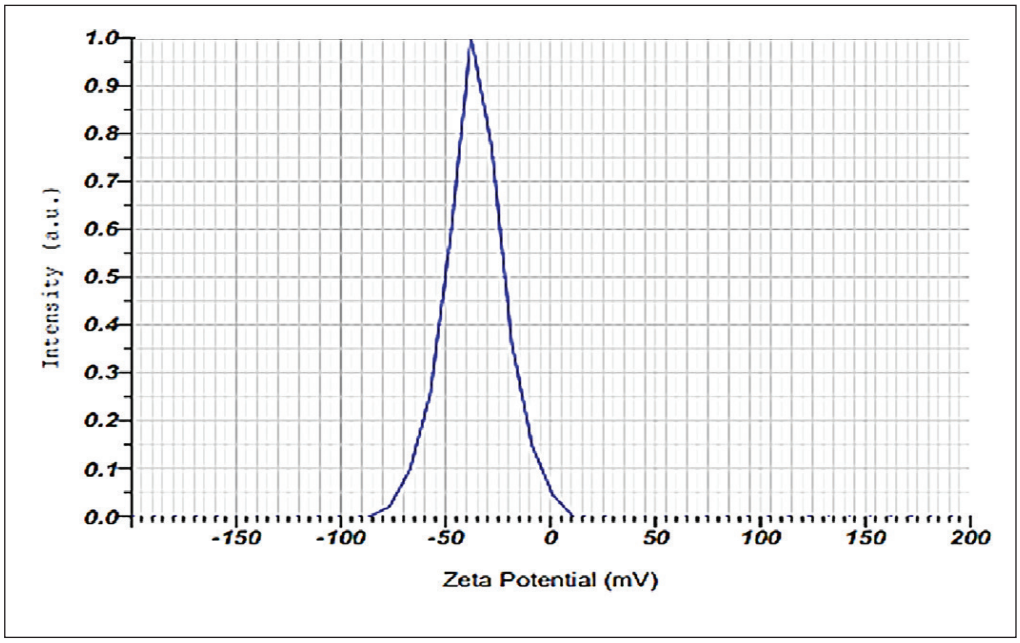

Fig.7. Zeta potential position of Zn_2BO_3 surface

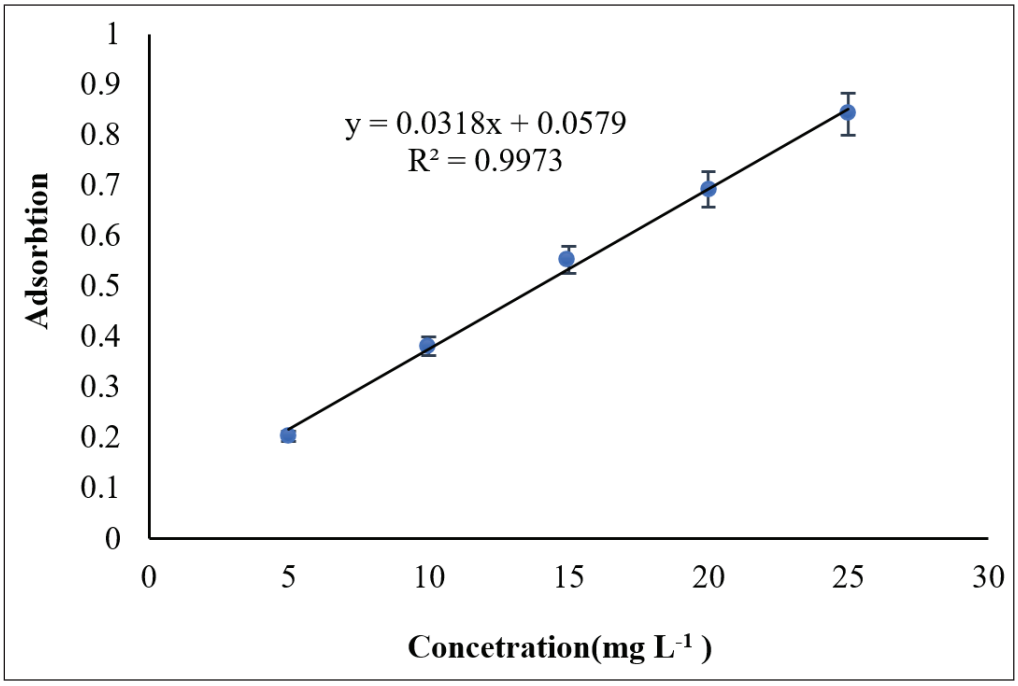

Fig. 8. The calibration curve of CR dye at pH 8

Table 4. Equilibrium time of adsorption Cr dye on Zn_2BO_3 adsorbent

Time (min)	5	10	15	30	45	60
q (mg g^{-1})	9.61949	13.2673	16.411	17.355	17.4811	17.669

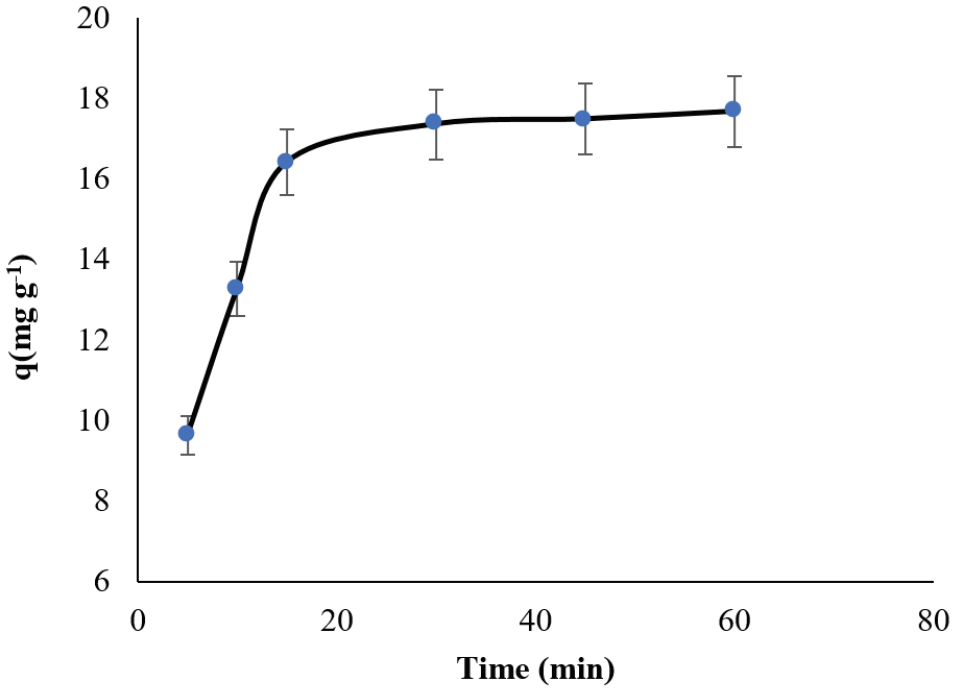

Fig. 9. The effect of time on adsorption of CR dye by Zn_2BO_3 adsorbent

concentration of 25 mg L^{-1} and 300 K^0. According to Figure 9 and Table 4, The equilibrium time of 30 minutes is the best time for the adsorption process. The absorption capacity was obtained at 17.355. The amount of adsorbate on Zn_2BO_3 adsorbent (qe =mg g^{-1}) is calculated by Equation 1.

$$q = \frac{(C_o - C_e)V}{M} \qquad \text{(Eq.1)}$$

C_0: initial concentration of CR in solution
C_e: Remaining concentration of CR in solution
V: Volume of solution
M: Wight of adsorbent ZB

3.7.2. Optimization parameters

Due to previous research main parameters such as adsorbent amount, pH, effect of initial concentration, the effect of temperature, sample volume, and capacity absorption for the extraction or removal of various organic materials based on different nanoparticle adsorbents (carbon nanotube, bismuth oxide nanoparticles) must be analyzed [24-26].

3.7.2.1. Effect of adsorbent amount

The effect of altering the adsorbent amount on the CR dye adsorption was studied using different amounts of Zn_2BO_3 adsorbent (0.1,0.0.2,0.03,0.06 g) in 60 min, the dye concentration of 25 mg L^{-1}, and sample volume of 100 mL at wavelength 495 nm. It was found that the adsorption of CR dye was increased by increasing catalyst weight due to the high surface area and active sites [27] as shown in Table 5 and Figure 10.

Table 5. amount of CR dye adsorbed on (Zn_2BO_3) adsorbent in (mg g^{-1})

Amount of ZB (g)	0.06	0.1	0.2	0.3
$q_{(mg/g)}$	2.261	6.034	8.77	11.82

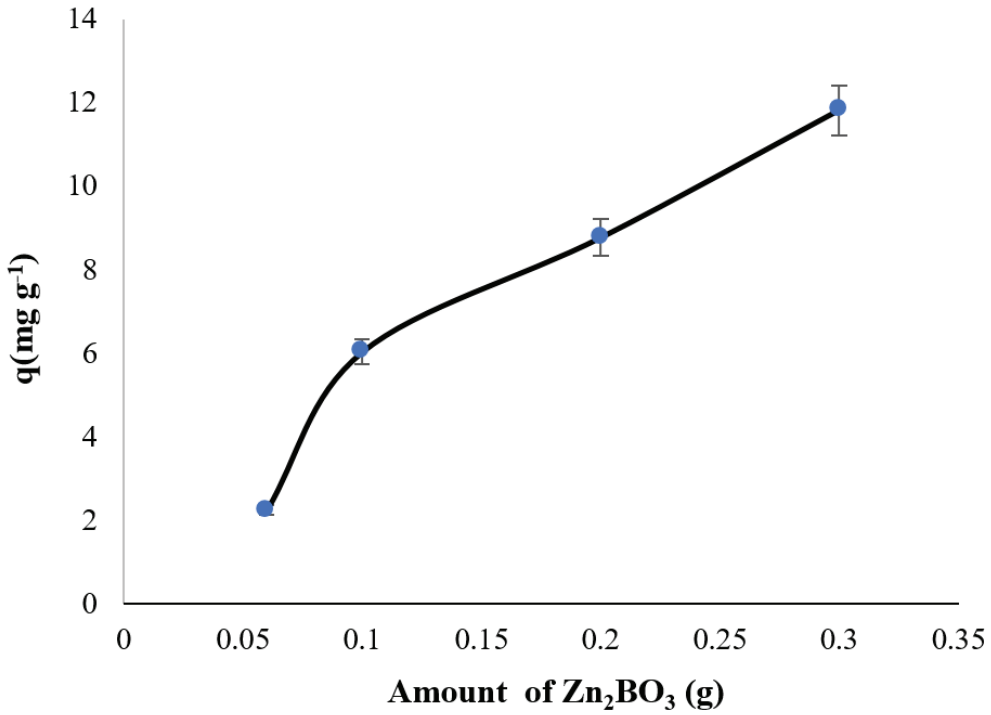

Fig. 10. The effect of the amount of Zn_2BO_3 adsorbent on the adsorption of CR dye

3.7.2.2. Effect of pH

The removal efficiency of CR dye using 0.1 g of Zn_2BO_3, 100 mL of sample, and 25 mg L^{-1} CR dye was evaluated in different pH (3,5,7,9,11) at 60 min. The adsorption of the dye in an acidic medium is greater than in a base medium as shown in Table 6 and Figure 11. It is related to the ability of dye tendency to bind in an acidic medium with the catalyst more than its tendency to bind with solvent molecules. The removal processing of dye by photocatalysis is subject to several mechanisms, including direct reduction by electrons in the conduction beam, direct oxidation through gaps in the valence beam, and finally, hydroxy radical attack [28]. These mechanisms mentioned depend on the nature of the material and the pH function of the medium in which the adsorption process takes place has an effect on both adsorbate and adsorbent. However, it should be noted that this dye is deposited at pH=2 and also changes the color of dye at acid function pH=3 causing a difference in wavelength, so it was settled to use the pH = 5.5 in the next experiments.

Table 6. Effect pH on adsorption amount of CR dye on (Zn_2BO_3) adsorbent.

pH	3	5	7	9	11
Adsorbate (q)	24.525	20.154	9.933	17.292	17.732

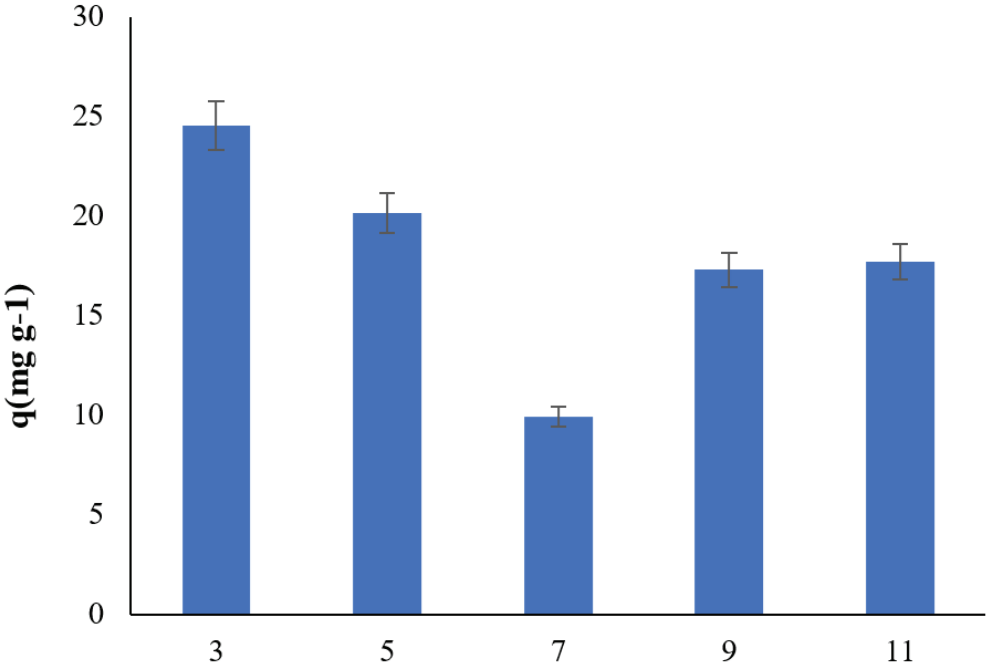

Fig. 11. The effect of pH solution on adsorption of CR dye

3.7.2.3. Effect of initial dye concentration

The dye concentration affects the adsorption process. So, in this study, different concentrations of red Congo dye were taken. At values of 50,75,100,125,150 mg L^{-1} with a constant amount of adsorbent of zinc borate, the adsorption efficiency was increased by increasing concentrations of dye where the highest adsorption value was recorded [29] as shown in Table 7 and Figure 12. This is because the largest amount of dye will be adsorbed on the adsorbent and the generation of free radicals for hydroxyl will decrease due to a lack of active sites of hydroxyl ions. The percentage of adsorption in high initial concentration of dye did not increase which hinders access of photons of light to the catalytic surface causing a decrease in absorption of photons and, consequently a decrease in decomposition rate. The maximum adsorption capacity of Zn_2BO_3 was obtained at 61.028 mg g^{-1} for 150 mg L^{-1} of CR dye.

Table 7. The effect of initial dye concentration on the adsorption amount of CR dye by Zn_2BO_3

C_0	50 mg L^{-1}	75 mg L^{-1}	100 mg L^{-1}	125 mg L^{-1}	150 mg L^{-1}
q (mg g^{-1})	35.556	48.026	48.292	54.896	61.028

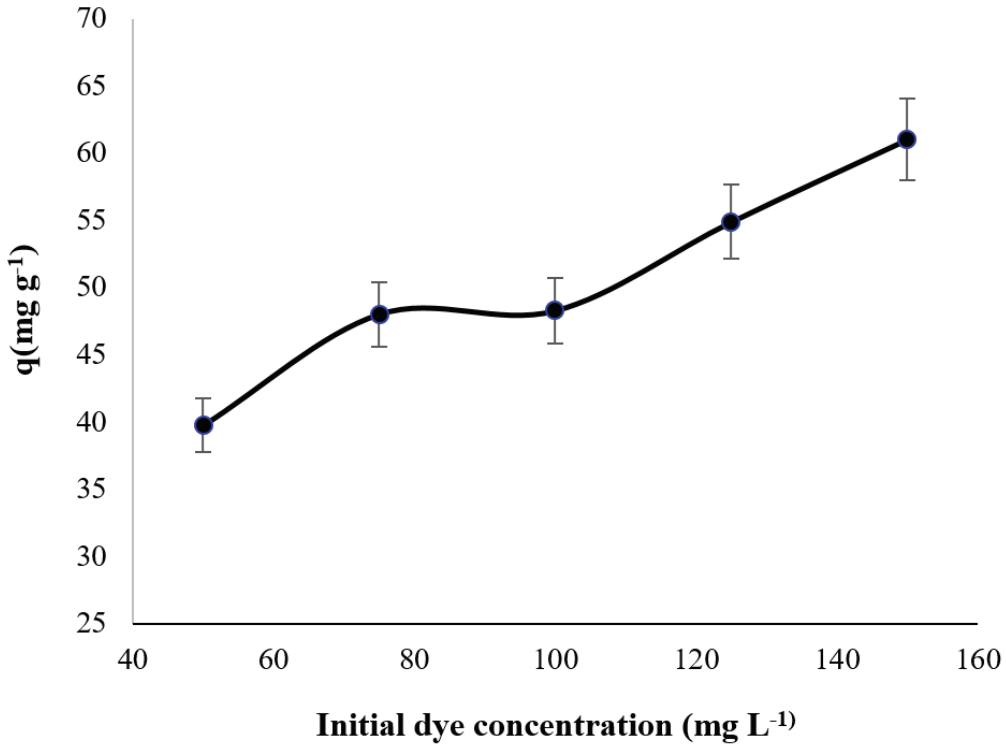

Fig. 12. The effect of initial dye concentration on adsorption of CR dye

3.7.2.4. Effect of Temperature

The temperature of the medium that occurs when adsorption is one of the factors affecting dye removal. In this study, the measurements were made within three temperatures (300^0K,318^0K,333^0K) where it was found that the efficiency of adsorption increases with increasing temperature degrees and accelerates access to equilibrium time [30], where the measurements made at a constant concentration and different times extended from (5-90 min). Also, the amount of adsorbent Zn_2BO_3 used to adsorb CR dye was 0.1 g and the adsorption efficiency increased due to obstruction of rearrangement electron-gap process. Due to increased temperature, this cycle proves that the adsorption process on this adsorbent is endothermic. In addition, the high temperature increases the oxidation rate of organic compounds and thus enhances decomposition capacity (Table 8 and Fig. 13).

Table 8. Effect of temperature on adsorption amount of CR dye on Zn_2BO_3 adsorbent in (mg g^{-1}).

Time(min)	300 K		318K		333K	
Zn_2BO_3	C_e	q	C_e	q	C_e	q
5	24.37	25.62	18.02	31.97	12.70	37.29
10	20.56	29.43	16.16	33.83	8.336	41.66
15	11.38	38.61	7.990	42.00	5.349	44.65
30	9.216	41.78	7.361	42.63	4.279	45.62
45	7.518	42.48	6.921	43.07	4.185	45.81
60	7.330	42.73	6.229	43.77	3.965	46.03

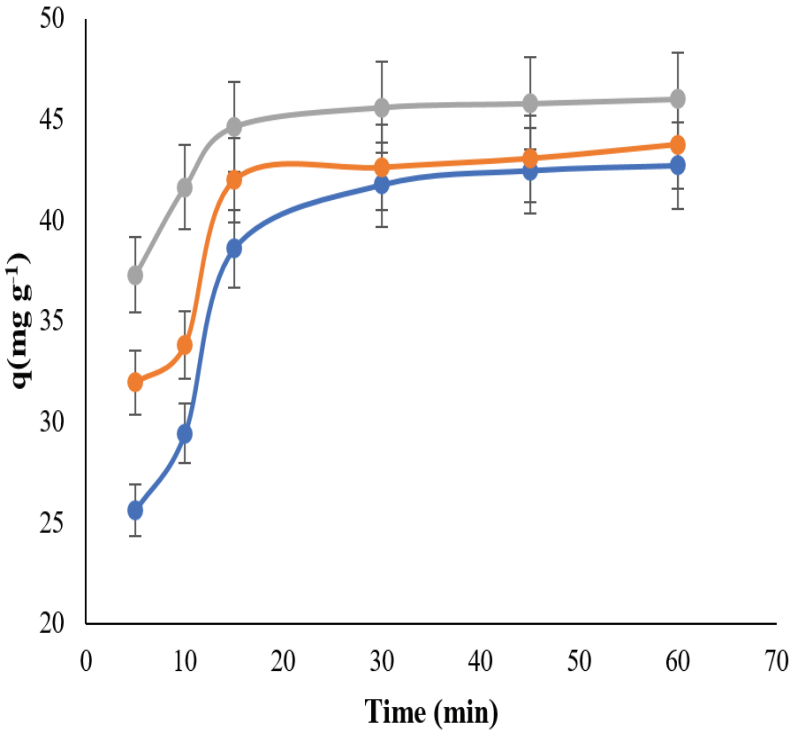

Fig. 13. The effect of temperature on adsorption of CR dye, blue line (300oK), orange line (318oK), and gray line (333oK)

3.8. Adsorption Isotherm

Calculations and study of adsorption isotherm, calculations of effect primary dye concentration at room temperature 300^{0}K was used to apply the mathematical equation of isotherm Langmuir by plotting linear equation of Langmuir equation based on values of C_e and C_e/q_e as shown in Table 9. and Figure 14. Langmuir constant (K_L=0.0525), values of maximum adsorption (Q_{max}=212.7), and correlation coefficient (R^2=98) were obtained for Zn_2BO_3. The linear relationship of the Freundlich equation based on values of log Ce versus log qe is shown in Table 10 and Figure 15. The Freundlich constants such as T=300^{o}K, R^2=0.8993, n=3.86, and Kf=3.556 were calculated. The R^2 value of Langmuir and Freundlich isotherm is 0.98 and 0.8993, respectively. So, the adsorption process flows by Langmeyer's isotherm model.

Table 9. Langmeyer isotherm study for adsorption amount of CR dye (mg g^{-1}).

C_0 (mg L^{-1})	C_e	q_e	C_e/q_e
50	14.443	35.556	0.1354
75	26.973	48.026	0.2246
100	51.707	48.292	0.3569
125	70.103	54.896	0.4256
150	88.971	61.028	0.4859

Table 10. Freundlich's adsorption Isotherm for adsorption amount of CR dye (mg g-1).

C_0	50	75	100	125	150
Log C_e	1.1596	1.4309	1.7135	1.8457	1.9492
Log q_e	1.9492	1.6814	1.7838	1.7395	1.7855

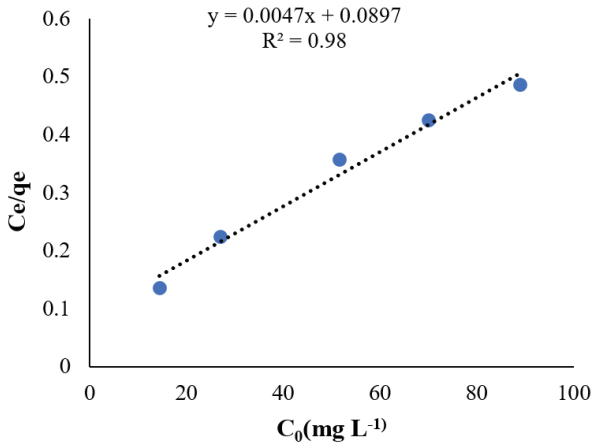

Fig. 14. Langmeyer adsorption Isotherm

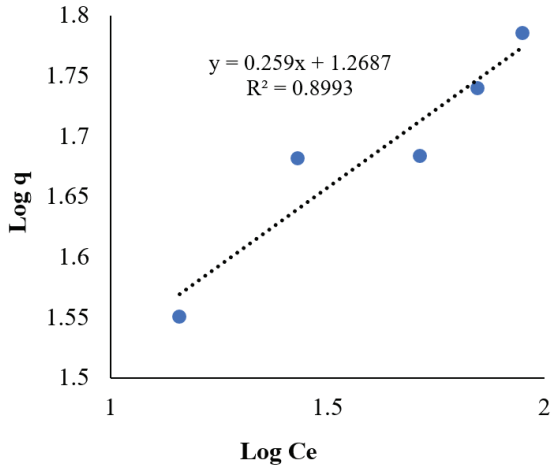

Fig. 15. Freundlich adsorption Isotherm

3.9. Thermodynamic study

Due to the temperature effect, the thermodynamic functions (ΔH enthalpy, ΔG free energy, and ΔS entropy) were calculated. For the adsorption of red Congo dye on adsorbent (Zn_2BO_3) the importance of these functions to understanding the adsorption process. Table 11 represents values of both ln k_c and values of temperature, while Figure 16 shows a relationship between ln K_c versus the inverse of time (1/T), from which the values of (ΔH, (ΔS) can be obtained that can be calculated through values of interception= (ΔH/R) and slop= (ΔS/R). Table 12 shows thermodynamic values.

Table 11. values of both (ln k_c) and values of Inverse temperature

T(K^0)	300	318	333
1/T * 10^{-3}	3.333	3.144	3.003
Ln K_c	1.5	1.66	2.122

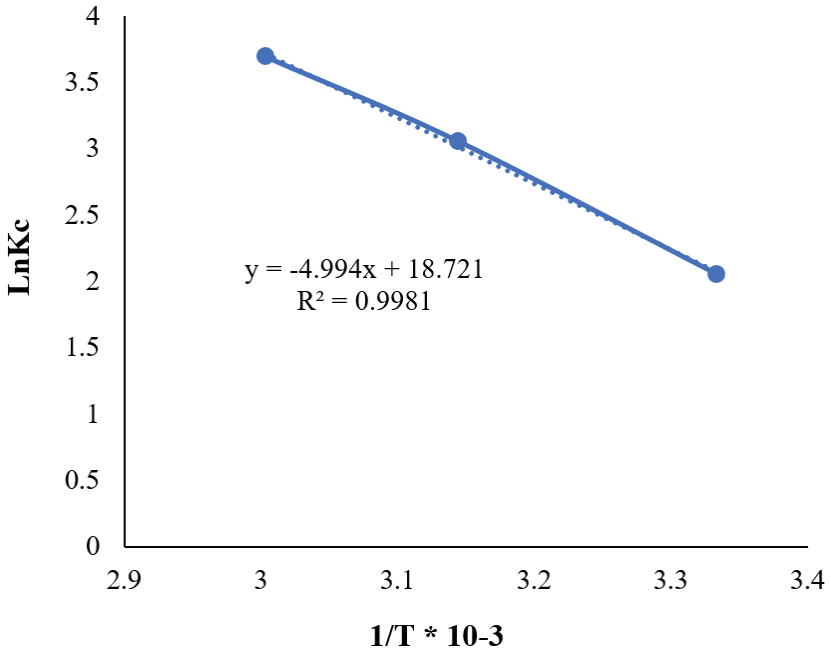

Fig. 16. Linear relationship between lnk_c vs. $1/T*10^{-3}$

Table 12. values of (ΔH enthalpy, ΔG free energy, ΔS entropy)

Compound	ΔG(KJ mol^{-1})			ΔS(KJ K^{-1} mol^{-1})	ΔH(KJ mol^{-1})
	300 K^0	318 K^0	333 K^0		
ZB	-(3.741)	-(4.388)	-(5.875)	62.65	15.2

From the values shown above in Table 13. we conclude, free energy value ΔG of adsorption all negative, which is evidence that adsorption process is spontaneous. Entropy value ΔS for the adsorption of CR dye on adsorbent (Zn_2BO_3) is positive, indicating that adsorbent molecules are in continuous motion on the surface of the adsorbent, causing an increase in system randomness. The value of adsorption temperature enthalpy ΔH is positive for adsorption indicating that the adsorption process is endothermic and that increased temperature leads to the increased rate of propagation speed of adsorbed particles on the adsorbent surface between pores in the adsorbent surface. The pseudo-first-order equation is called Lagergren, where experimental data is applied. The pseudo-second-order equation shows that the adsorption rate depends on the adsorption amplitude in the adsorption surface, (Lagergren Pseudo second order – equation).

Table 13. values of (ln qe-qt) versus the time values of the adsorption process

Time	5	10	15	30	45	60
q_e	42.7327	42.7327	42.7327	42.7327	42.7327	42.7327
q_t	34.619	38.267	41.411	42.353	42.481	42.732
$\ln(q_e-q_t)$	2.093	1.496	0.278	-0.974	-1.38	NUM

Table 13 shows the value of ln qe-qt and time values (t) of the adsorption process of CR on adsorbent Zn_2BO_3 and Figure 17 represents the linear relationship of the false first-order equation, from which the adsorption rate constant (K_1), the adsorption capacity (q_e) and the correlation coefficient shown in Table 14 were calculated. Values in Table 14 it clear that the process of adsorption of red Congo dye on Zn_2BO_3 adsorbent follows the second kinetic equation for the reasons, the large difference between values of adsorption capacity calculated according to the false first order equation qe(cal) is different from the experimental adsorption value qe(exp) obtained through this study. As shown in Figure 17, the linear axis of the false first-order equation does not pass through all points, unlike the linear axis of the false second-order equation, which passes exactly all points as shown in Figure 18. The correlation value R^2 of the false first-order equation is less than 0.8986 away from the value of 1, unlike the correlation value of R^2 of the false second-order equation, which is limited to 0.999.

4. Conclusion

Zinc Borate is successfully synthesized by one-step precipitation from nano zinc oxide and Boric acid. The absorption of CR Day based on Zn_2BO_3 adsorbent was determined by UV-Vis spectroscopy. FTIR spectra showed the position of active aggregates of the compound. It clearly showed their importance in the process of dye adsorption. XRD analysis position of 2Θ for crystal lattice patterns proved the formation of the desired compound and clarified the dimensions and size of the crystal. SEM analysis images of compound surface contain holes and pores, EDX analysis explained compassion component. Zeta potential analyses indicate (Zn_2BO_3) has a negative charge, and it is stable. All effective factors in the adsorption process have been studied and isotherm and kinetic have been explained.

Table 14. Adsorption capacity (qe) and the correlation coefficient of false first-order equation

Equation	Comp	$Q_{e,exp}$	K_1(min^{-1})	q_e (mg g^{-1})	R^2
False first-order equation	ZB	42.732	0.00146	8.483	0.8986
False second-order equation	ZB	42.732	0.20092	43.66	0.999

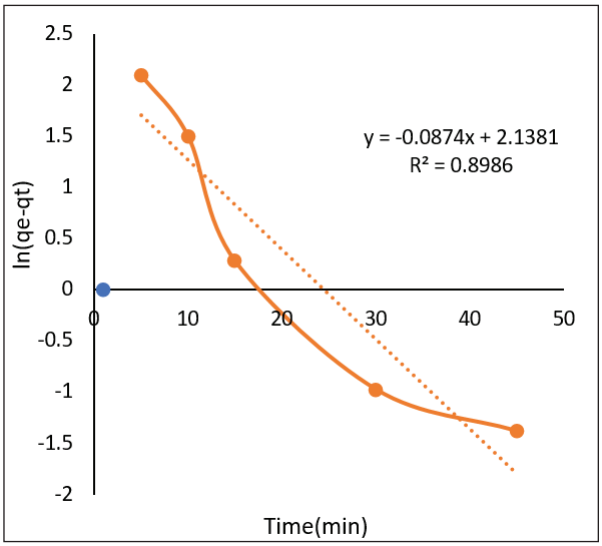

Fig. 17. Linear relationship of the first-order

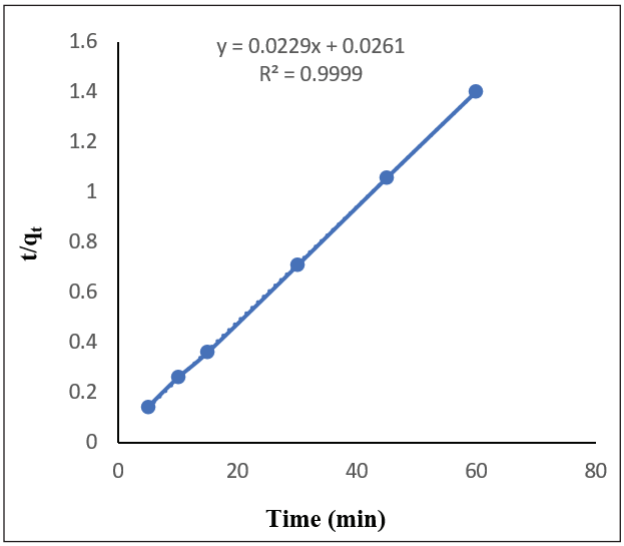

Fig. 18. L linear relationship of the second-order

5. References

[1] K. Shen, S. Kochesfahani, F. Jouffret, Zinc borates as multifunctional polymer additives, Polymer Adv. Technol., 19 (2008) 469-474. https://doi.org/10.1002/pat.1119

[2] D. M. Schubert, Hydrated zinc borates and their industrial use, Molecules, 24 (2019) 2419. https://doi.org/10.3390/molecules24132419

[3] M. Yusuf, S. Mohd, M. Faqeer, Natural colorants: Historical, processing and sustainable prospects, Nat. Prod. Bioprospect., 7 (2017) 123-145. https://doi.org/10.1007/s13659-017-0119-9

[4] A.K. Roy Choudhury, (2014). Environmental impacts of the textile industry and its assessment through life cycle assessment. In: Muthu, S. (eds) Roadmap to sustainable textiles and clothing. Textile Sci. Cloth. Technol., Springer, Singapore, 2014. https://doi.org/10.1007/978-981-287-110-7_1

[5] N. Akhtar, M.I Syakir Ishak, S.A. Bhawani, K. Umar, Various natural and anthropogenic factors responsible for water quality degradation, A review, Water, 13 (2021) 2660. https://doi.org/10.3390/w13192660

[6] M. Smail, K. Akhtar, M.I. Khan, T. Kamal, M.A. Khan, A. M Asiri, S.B. Khan, Pollution, toxicity, and carcinogenicity of organic dyes and their catalytic bio-remediation, Curr. Pharm. Des., 25 (2019) 3645-3663. https: // doi.org/10.2174/1381612825666191021142026

[7] R. Ashouri, Dynamic and static removal of benzene from air based on task-specific ionic liquid coated on MWCNTs by sorbent tube-headspace solid-phase extraction procedure, Int. J. Environ. Sci. Technol., 18 (2021) 2377-2390. https://doi.org/10.1007/s13762-020-02995-4

[8] M.M. Asl, Functionalized graphene oxide with bismuth and titanium oxide nanoparticles for efficiently removing formaldehyde from the air by photocatalytic degradation–adsorption process, J. Anal. Test., 7 (2023) 444-458. https://doi.org/10.1007/s41664-023-00272-0

[9] A. Faghihi-Zarandi, New method for removal of hazardous toluene vapor from air based on ionic liquid-phase adsorbent, Int. J. Environ. Sci. Technol., 16 (2019) 2797–2808. https://doi.org/10.1007/s13762-018-1975-5

[10] S. Teimoori, A.H. Hassani, M. Panahi, An immobilization of aminopropyl trimethoxysilane-phenanthrene carbaldehyde on graphene oxide for toluene extraction and separation in water samples, Chemosphere, 316 (2023) 137800. https://doi.org/10.1016/j.chemosphere.2023.137800

[11] M. Abadi, Air pollution control: The evaluation of TerphApm@ MWCNTs as a novel heterogeneous sorbent for benzene removal from air by solid phase gas extraction, Arab. J. Chem., 13 (2020) 1741-1751. https://doi.org/10.1016/j.arabjc.2018.01.011

[12] J. Rakhtshah, A rapid extraction of toxic styrene from water and wastewater samples based on hydroxyethyl methylimidazolium tetrafluoroborate immobilized on MWCNTs by ultra-assisted dispersive cyclic conjugation-micro-solid phase extraction, Microchem. J., 170 (2021) 106759. https://doi.org/10.1016/j.microc.2021.106759

[13] R. Liang, A. Hu, Robert, M. Hatat-Fraile, N. Zhou, Fundamentals on adsorption, membrane filtration, and advanced oxidation processes for water treatment, Nanotechnol. Water Treat. Purif., (2014) 1-45. https: /doi.org/10.1007/978-3-319-06578-6_1

[14] W. Liu, A. Tkatchenko, M. Scheffler, Modeling adsorption and reactions of organic molecules at metal surfaces, Acc. Chem. Res., 47 (2014) 3369-3377. https://doi.org/10.1021/ar500118y

[15] T.U.T Dao, H.T.T, D.T.C Nguyen, H.T. LE, H.T. Nguyen, S.T. Do, T.D Nguyen, Process optimization studies of Congo red dye adsorption onto nickel-iron layered double hydroxide using response surface methodology, Solid State Phenomena, 298 (2019) 83-88. https://doi.org/10.4028/www.scientific.net/SSP.298.83

[16] A. Yalçın, G. Mehmet, A novel approach for the production of zinc borate ($4ZnO{\cdot}B_2O_3{\cdot}H_2O$) using a single-step hydrothermal method, Main Group Met. Chem., 44 (2021) 1-8. https://doi.org/10.1515/mgmc-2021-0001

[17] Y.Y. Zhang, L. Ping, H.L. Zhi, Controllable synthesis and flame-retardant properties of bunch-, chrysanthemum-, and plumy-like $4ZnO{\cdot}B_2O_3{\cdot}H_2O$ nanostructures, Powder Technol., 210 (2011) 208-211. https://doi.org/10.1016/j.powtec.2011.03.018

[18] R. Stefan, P. Pascuta, A. Popa, O. Raita, E. Indera, E. Culea, XRD and EPR structural investigation of some zinc borate glasses doped with iron Ions, J. Phys. Chem. Solids, 73 (2012) 221-226. https://doi.org/10.1016/j.jpcs.2011.10.039

[19] X. Shi, M. Li, PEG-300 assisted hydrothermal synthesis of $4ZnO{\cdot}B_2O_3{\cdot}H_2O$ Nanorods, Materials Research Bulletin 42.9 (2007) 1649-1656. https://doi.org/10.1016/j.materresbull.2006.11.034

[20] M. Vayer, C. Serré, N. Boyard, C. Sinturel, R. Errer, Surface morphologies of composites based on unsaturated polyester pre-polymer, J. Mater. Sci. 37 (2002) 2043-2051. https://doi.org/10.1023/A:1015263618720

[21] C. Zhao, Y. Jiao, Y. K. Chen, G. Ren, The tribological properties of zinc borate ultrafine powder as a lubricant additive in sunflower oil, Tribol. Trans., 57 (2014) 425-434. https://doi.org/10.1080/10402004.2013.878776

[22] I. Mohammed, D. Al Shehri, M. Mahmoud, M. S. Kamal, O. S. Alade, A surface charge approach to investigating the influence of oil contacting clay minerals on wettability alteration, ACS Omega, 6 (2021) 12841-12852. https://doi.org/10.1021/acsomega.1c01221

[23] R. Labied, O. Benturki, A. Y. Eddine Hamitouche, A. Donnot, Adsorption of hexavalent chromium by activated carbon obtained from a waste lignocellulosic material (Ziziphus jujuba cores): Kinetic, equilibrium, and thermodynamic study, Adsorp. Sci. Technol., 36 (2018) 1066-1099. https://doi.org/10.1177/0263617417750739

[24] S. Teimoori, New extraction of toluene from water samples based on nano-carbon structure before determination by gas chromatography, Int. J. Environ. Sci. Technol., 20 (2023) 6589-6608. https://doi.org/10.1007/s13762-023-04906-9

[25] S. Teimoori, Rapid extraction of BTEX in water and milk samples based on functionalized multi-walled carbon nanotubes by dispersive homogenized-micro-solid phase extraction, Food Chem., 421 (2023) 136229. https://doi.org/10.1016/j.foodchem.2023.136229

[26] A. Faghihi-Zarandi, J. Rakhtshah, BB. Yarahmadi, A rapid removal of xylene vapor from environmental air based on bismuth oxide coupled to heterogeneous graphene/graphene oxide by UV photo-catalectic degradation-adsorption procedure, J. Environ. Chem. Eng., 8 (2020) 104193. https://doi.org/10.1016/j.jece.2020.104193

[27] G. Leofanti, M. Padovan, G. Tozzola, B. J. C. T. Venturelli, Surface area and pore texture of catalysts, Catal. Today, 41 (1998) 207-219. https://doi.org/10.1016/S0920-5861(98)00050-9

[28] B.K. Hashim, N. K. Zaki, Preparation and study photocatalytic properties of BiOX (X= Cl, Br, I), J. Kufa Chem. Sci., 2 (2022) 50-68. https://journal.uokufa.edu.iq/index.php/jkcs/article/view/11089

[29] C.H. Wu, Comparison of azo dye degradation efficiency using UV/single semiconductor and UV/coupled semiconductor systems, Chemosphere, 57 (2004) 601-608. https://doi.org/10.1016/j.chemosphere.2004.07.008

[30] L. Karimi, S. Zohoori, E.Y. Mohammad, Photocatalytic degradation of azo dyes in aqueous solutions under UV irradiation using nano-strontium titanate as the nano photocatalyst, J. Saudi Chem. Soc., 18 (2014) 581-588. https://doi.org/10.1016/j.jscs.2011.11.010